Pigment epithelium-derived factor (PEDF) alone or in combination with an anti-VEGF drug as a possible treatment of choroidal neovascularization and ischemic ocular diseases

Dissertation

Zur Erlangung des Grades eines

Doktors der Naturwissenschaften

der Mathematisch-Naturwissenschaftlichen Fakultät

und

der Medizinischen Fakultät

der Eberhard-Karls-Universität Tübingen

vorgelegt

von

Lei Xi

Aus Shandong, China

February – 2022

Tag der mündlichen Prüfung: 17/02/2022

Dekan der Math.-Nat. Fakultät	Prof. Dr. Thilo Stehle
Dekan der Medizinischen Fakultät	Prof. Dr. Bernd Pichler
1. Berichterstatter	Prof. Dr. Ulrich Schraermeyer
2. Berichterstatter	Prof. Dr. Frank Schaeffel
Prüfungskommission	Prof. Dr. Ulrich Schraermeyer
	Prof. Dr. Frank Schaeffel
	Prof. Dr. Michela Deleidi
	Prof. Dr. Stefan Liebau

Erklärung / Declaration:
Ich erkläre, dass ich die zur Promotion eingereichte Arbeit mit dem Titel:

“Pigment epithelium-derived factor (PEDF) alone or in combination with an anti-VEGF drug as a possible treatment of choroidal neovascularization and ischemic ocular diseases”

selbständig verfasst, nur die angegebenen Quellen und Hilfsmittel benutzt und wörtlich oder inhaltlich übernommene Stellen als solche gekennzeichnet habe. Ich versichere an Eides statt, dass diese Angaben wahr sind und dass ich nichts verschwiegen habe. Mir ist bekannt, dass die falsche Abgabe einer Versicherung an Eides statt mit Freiheitsstrafe bis zu drei Jahren oder mit Geldstrafe bestraft wird.

I hereby declare that I have produced the work entitled “Pigment epithelium-derived factor (PEDF) alone or in combination with an anti-VEGF drug in the treatment of choroidal neovascularization and ischemic ocular diseases”, submitted for the award of a doctorate, on my own (without external help), have used only the sources and aids indicated and have marked passages included from other works, whether verbatim or in content, as such. I swear upon oath that these statements are true and that I have not concealed anything. I am aware that making a false declaration under oath is punishable by a term of imprisonment of up to three years or by a fine.

Tübingen, den ..... 09/03/2022 .... Lei Xi .....
Datum / Date Unterschrift /Signature

Contents

List of figures

List of tables

Abbreviations

AAV: adeno-associated virus

Ad: adenoviral

AJs: adherens junctions

AMD: age-related macular degeneration

ATP: adenosine triphosphate

BM: Bruch’s membrane

BRVO: branch retinal vein occlusion

CCA: common carotid artery

CCl_4: carbon tetrachloride

CNV: choroidal neovascularization

$cPLA_2$: cytosolic phospholipase A_2

CRVO: central retinal vein occlusion

CTGF: connective tissue growth factor

DMEM: Dulbecco's modified eagle medium

DMI: Diabetic macular ischemia

DR: diabetic retinopathy

ECM: extracellular matrix

EM: electron microscopy

ERG: electroretinograms

ERK: extracellular regulated protein kinases

FA: fluorescein angiography

FasL: fas-ligand

GFAP: glial fibrillary acidic protein

HIF-1α: hypoxia-inducible transcription factor-1α

IAA: iodoacetic acid

ICG: indocyanine green angiography

IHC: immunohistochemistry

IOP: intraocular pressure

IVT: intravitreal injection

LE: Long Evans

MA: macular atrophy

MAPK: mitogen-activated protein kinase

NFκB: nuclear factor κB

mPTPs: mitochondrial permeability transition pores

OCT: optical coherence tomography

OIR: oxygen-induced retinopathy

OS: oxidative stress

PDGF: platelet-derived growth factor

PDR: proliferative diabetic retinopathy

PEDF: Pigment epithelium-derived factor

PPAR-γ: peroxisome proliferator-activated receptor gamma

PRP: pan-retinal photocoagulation

PDT: photodynamic therapy

RAO: retinal artery occlusion

RGCs: retinal ganglion cells

RNFL: retinal nerve fiber layer

ROS: reactive oxygen species

RP: retinitis pigmentosa

RPE: retinal pigment epithelial

RVO: retinal vein occlusion

STAT: signal transducers and activators of transcription

STZ: streptozotocin

TGF-β: Transforming growth factor-β

TJs: tight junctions

TNF: tumor-necrosis factor

TTT: transpupillary thermotherapy

TUNEL: terminal deoxynucleotidyl transferase dUTP nick end labeling

UCP2: upregulating protein 2

VEGF: vascular endothelial growth factor

1 Abstract

Ocular neovascular diseases such as choroidal neovascularization (CNV) and age-related macular degeneration (AMD) are today the most common causes of visual loss and blindness. Although intravitreal anti-vascular endothelial growth factor (VEGF) therapy has achieved major breakthroughs in the treatment of CNV and wet AMD, it does not always successfully suppress CNV, and no efficacious treatment is yet available to prevent photoreceptor degeneration. The formation of CNV is a compensatory response to ocular ischemia. If CNV can be stabilized, it may be helpful for photoreceptor survival and maintaining the normal physiological function of the retina. With a wide use of optical coherence tomography angiography (OCTA) in the clinic, quiescent CNVs without exudation are much more frequently found than previously assumed.

In this study, I examined the efficacy of a pigment epithelium derived factor (PEDF) protein alone or combined with a VEGF antagonist (Avastin) in the treatment of rat quiescent CNV *in vivo*. The rat quiescent CNV was established by subretinal injection of an adeno-associated viral (AAV)-VEGF-A^{165} vector, which expresses VEGF and leads to vascular growth from the choroid into the subretinal space. The fluorescein angiography (FA), indocyanine green angiography (ICG) and optical coherence tomography (OCT) were performed at the third week, fourth week, sixth week and seventh week after subretinal injection of the AAV-VEGF-A^{165} vector. The maximal thickness of CNV was measured in the OCT images. Picrosirius red stain was used to quantify mature and immature collagen content in the formalin-fixed, paraffin-embedded quiescent CNV samples. The collagen Ⅳ, VEGF and PEDF were examined in the quiescent CNV samples by immunohistochemistry (IHC), and the percentage of positive staining area to the total CNV area was calculated by ImageJ software. To analyze the effect of PEDF on retinal photoreceptor cells, the outer nuclear layer (ONL) area as a percentage of the corresponding CNV area was quantified. The apoptosis of ONL cells above the CNV area was detected by TUNEL staining.

PEDF combined with anti-VEGF therapy significantly inhibits VEGF expression in quiescent CNV. The ONL area as a percentage of the corresponding CNV area is increased in the PEDF treatment group (92.29, 120.27) and decreased in the Avastin treatment group (55.11, 75.59) ($P < 0.001$, Wilcoxon test with Kruskal-Wallis test). The apoptosis of ONL cells above the CNV area is reduced in the PEDF treatment group (0.95 ± 0.60, n/1000μm) compared to the vehicle treatment group (2.26 ± 0.95, n/1000μm) ($P < 0.001$, one-way ANOVA test). Thus, PEDF shows a neuroprotective

effect for the retinal photoreceptor cells. In this *in vivo* experiment, a VEGF antagonist (Avastin) can significantly inhibit the formation of CNV in this rat quiescent CNV model and reduce its thickness. However, quiescent CNV can supply oxygen to the photoreceptor cells and protect photoreceptor cells from degeneration, thus maintaining vision. Although anti-VEGF (Avastin) treatment alone inhibits CNV, it also accelerates photoreceptor cell degeneration in this *in vivo* quiescent CNV model. In the clinic, development of macular geographic atrophy and fibrosis are found in patients with wet AMD under long term anti-VEGF treatment. PEDF has no effect on mature and immature collagen in this quiescent CNV model. The information on the therapeutic effect is shown in Table 1. PEDF is a potential vascular stabilizing and neuroprotective factor for stabilizing CNV and maintaining vision.

Ischemic/hypoxic retinopathy is a common condition that can cause visual impairment and blindness. However, the changes of the choroidal blood vessels under ischemic/hypoxic conditions are not clearly known. The apoptosis of retinal ganglion cells (RGCs) and the retinal degeneration under ischemic/hypoxic conditions cannot be treated.

In this study, I established an ischemic/hypoxic *ex vivo* eye model by incubating the freshly enucleated rat eyes in Dulbecco's modified eagle medium (DMEM) at 4 °C for 14 hours. After 14 hours, eyes (including control eyes, eyes intravitreally injected with vehicle or PEDF protein) were fixed for electron microscopy (EM) and immunohistochemistry (IHC) respectively. The area of lumen ($\mu m^2/\mu m$ of Bruch's membrane) and the area of the whole vessel ($\mu m^2/\mu m$ of Bruch's membrane) were analyzed and immunohistochemical staining for VEGF and PEDF in the retina and choroidal vessels was performed. The effects of PEDF on the choriocapillaris and retinal neural cells under ischemia/hypoxia were investigated. In addition, the oxygen concentration within the vitreous was measured by an oxygen-sensitive microsensor in both the ischemic/hypoxic *ex vivo* eye model and the living rats under anesthesia. TUNEL staining was performed and the apoptosis of retinal neural cells was analyzed.

In the living rats, the concentration of oxygen within the vitreous was on average 16.4 % of the oxygen concentration in the air. In the ischemic/hypoxic *ex vivo* eyes, the oxygen concentration within the vitreous was gradually decreased and the concentration was about 50% of the value in the eyes immediately after enucleation after about 400 minutes of incubation, indicating mild hypoxia during this process. After 14 hours of ischemia/hypoxia, the endothelial cells of the

choroidal vessel were ultra-structurally similar with respect to cell organelles compared to the immediately fixed control eyes, but the morphology of the choroidal vessels changed dramatically. In the ischemic/hypoxic eyes, filopodia-like projections filled out the choroidal vessel lumen and appeared identical to the labyrinth-capillaries found in surgically extracted choroidal neovascular membranes from patients with wet AMD. The structural changes within the choriocapillaris in this ischemic/hypoxic eye model can mimic early changes in the process of pathological angiogenesis as observed in patients with CNV or wet AMD. This *ex vivo* eye model can be used to investigate short term drug effects on the choriocapillaris after ischemia/hypoxia. PEDF inhibited the filopodia-like projection formation and kept the choroidal lumen open as *in vivo*. The area of lumen is significantly reduced in the ischemic/hypoxic group (0.308±0.087μm^2/μm) compared to the PEDF-treated group (1.034±0.077μm^2/μm) ($P < 0.001$, t test). The area of vessel is significantly reduced in the ischemic/hypoxic group (0.675±0.048 μm^2/μm) compared to the PEDF-treated group (1.583±0.094μm^2/μm) ($P < 0.001$, t test). The intravitreally injected PEDF protein located in the whole retina and the choroidal vessels, indicating that PEDF protein can penetrate the retina and is transported into the choroid. The apoptosis of RGCs (2.36, 2.89; percentage of positive cells per 100μm) and inner nuclear cells (15.81, 22.89; number of positive cells per 1000μm) was significantly reduced in the PEDF-treated eyes compared to the ischemic/hypoxic eyes [RGCs (3.14, 3.75; percentage of positive cells per 100μm) ($P = 0.015$), inner nuclear cells (33.69, 45.22; number of positive cells per 1000μm) ($P = 0.001$) Wilcoxon test]. The detailed information is shown in Table 2. Thus, PEDF is a promising candidate for treating ischemic/hypoxic retinopathy or human CNV alone or combined with other drugs.

In short, PEDF protected retinal neural cells in both the *in vivo* quiescent CNV model and the *ex vivo* ischemic/hypoxic eye model. PEDF inhibits the formation of filopodia-like projections and keeps the choroidal vessel lumen open in this *ex vivo* ischemic eye model.

Table 1. The treatment effect for each group in the *in vivo* experiment

	Control group	Vehicle-treated group	PEDF-treated group	Avastin-treated group	PEDF/Avastin-treated group
Inhibition of CNV thickness			★ (the 7th week)	★★ (the 7th week)	★ (the 6th week)
Inhibition of					★

VEGF					
ONL-area/CNV-area			★★		★
Reduction of the apoptosis of ONL cells			★★	★	★
Inhibition of mature and immature collagen					
Inhibition of collagenⅠ/Ⅴ		★	★	★	★

CNV: choroidal neovascularization; ONL: outer nuclear layer; PEDF: pigment epithelial derived factor.

★: weak effect, ★★: strong effect.

Table 2. The treatment effect for each group in the *ex vivo* experiment

	Control group	Ischemic/hypoxic alone group	Vehicle-treated group	PEDF-treated group
VEGF level in the neural retina			↑↑	↑↑
VEGF level in the RPE layer				
VEGF level in the choroid				
Labyrinth capillaries in the choriochepillaris		↑↑		↓↓
The area of lumen		↓↓		
The area of vessel		↓↓		
PEDF in the RPE layer			↓	↑↑
PEDF in the choroid				↑↑
Neural protective for the RGCs		↓↓	↓↓	↑
Neural protective for the INL		↓↓	↓↓	↑
Neural protective for the ONL		↓	↓	

VEGF: vascular endothelial growth factor, PEDF: pigment epithelial derived factor, RPE: retinal pigment epithelium, INL: inner nuclear layer, ONL: outer nuclear layer.

↑: weak effect; ↑↑: strong effect; ↓: weak reduction; ↓↓: strong reduction.

2 Introduction

2.1 Choroidal neovascularization

Choroidal neovascularization (CNV) is a sight-threatening disease and is characterized by the invasion of neovessels originating from the choroid which breach Bruch's membrane (BM) and extend into the subretinal space (Figure 1). CNV is one of the leading causes of severe vision loss in the elderly population and pathological myopia patients (Coelho et al., 2021). The new blood vessels leak easily because of the incomplete development of the vessel walls. Hemorrhage and exudation are two main features of the CNV lesion (Kim et al., 2016; Costa et al., 2005). In severe cases, hemorrhage and exudation eventually result in scar formation and chorioretinal atrophy (Daniel et al., 2018), which can lead to permanent loss of vision.

The detailed mechanisms of the formation of CNV are not well understood. A primary cause of CNV pathogenesis is the imbalance between pro-angiogenic factors and anti-angiogenic factors. The increased production of vascular endothelial growth factor (VEGF), a potent proangiogenic factor, is identified as an essential factor in the development of CNV (Farnoodian et al., 2017). For the pathogenesis of CNV, the primary source of VEGF is thought to be the retinal pigment epithelial (RPE) cells (Zhao et al., 2021; Grossniklaus et al., 2002), which are a major source of ocular angio-regulatory proteins. Several studies have proposed the hypothesis of choroidal ischemia or hypoperfusion, based on the concept that loss of choroidal blood flow or choriocapillaris dysfunction causes ischemia which triggers pathologic neovascularization in the choroid as compensation (Nesper et al., 2021; Coleman et al., 2013). However, the attenuation of choroidal blood flow and choriocapillaris dysfunction are presented in dry age-related macular degeneration (AMD) (Seddon et al., 2016; Lutty et al., 2020), but the evidence of ischemia or hypoxia for the development of CNV is still without pathologic evidence. Thus, the effect of choroidal ischemia or hypoperfusion on CNV formation is still uncertain.

The evolution of CNV begins with a break or defect in Bruch's membrane. The disruption or degradation of Bruch's membrane facilitates the invasion of endothelial cells into the surrounding micro-environment and allows neovascular tissue from the choroid to enter the subretinal space (Martinez and Peplow, 2021; Grossniklaus et al., 2010). Inflammation (Sung et al., 2019), matrix

metalloproteinase (Kim et al., 2021), complement cascade (Tan et al., 2015), and macrophages (Yang et al., 2016) are also involved in CNV formation.

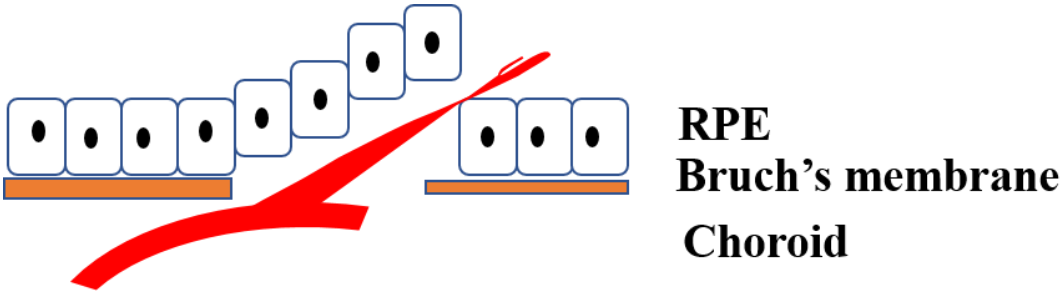

Figure 1: Schematic representation of choroidal neovascularization (CNV). CNV is the neovascularization which originates from the choroidal vessels and could stretch into Bruch's membrane or the retinal pigment epithelium (RPE) layer.

2.2 Quiescent choroidal neovascularization

Quiescent CNV was first introduced by Querques et al and is sub-RPE CNV secondary to AMD, showing absence of intraretinal/subretinal exudation on repeated optical coherence tomography (OCT) examinations over at least six months (Querques et al., 2013). Quiescent CNV is likely to be a compensatory form of vessel that grows in response to an ischemic outer retina. Nowadays, quiescent CNV is much more frequent than previously assumed due to a wide use of OCT angiography (OCTA) in the clinic (Matysik-Woźniak et al., 2021). OCTA is a non-invasive device and is fast and sensitive in the detection of quiescent CNV.

After one year of follow-up, 6.6% of quiescent CNV changes to exudative CNV (Carnevali et al., 2018), and approximately 30% of the eyes with quiescent CNV will develop exudation during a mean two-year follow-up period (Fukushima et al., 2021). Whether asymptomatic quiescent CNV could be left untreated until the development of subretinal/intraretinal exudation on OCTA is not completely established (Serra et al., 2020). However, because the exudation can occur, a close follow-up should be recommended. The predictive factors for exudation for quiescent CNV are an increase in retinal thickness, increase in pigment epithelial detachment size (height or width) and enlargement of the quiescent CNV on OCT-A (Solecki et al., 2021).

The quiescent CNV may provide oxygen and nutrients to the outer retina and there is a potential protective effect of quiescent CNV on the RPE and overlying neurosensory retina (Pfau et al., 2020). The current therapeutic concept is to achieve complete regression of the CNV. However, quiescent

CNV may protect against RPE cells and photoreceptor degeneration. So, treatment will be needed when the exudative signs develop in the quiescent CNV. Maintaining the stability of quiescent CNV and avoiding leakage of the exudative CNV may be the best strategies to protect vision.

2.3 Current therapeutic options for CNV

At present, several approaches have been tried in the clinic to treat CNV, including resection of the subretinal neovascular membrane, focal thermal laser photocoagulation, photodynamic therapy with verteporfin, and intravitreal anti-VEGF therapy. However, these approaches have their own limitations. Currently, anti-VEGF therapy is the first-line treatment option for CNV (Toto et al., 2021), especially for myopic CNV (El et al., 2015), based on the notion that VEGF over-expression is the main reason for CNV (Reid et al., 2018).

2.3.1 Anti-vascular endothelial growth factor

The importance of VEGF for the development of CNV led to the anti-VEGF therapeutic strategy. Anti-VEGF treatment targets key mediators of the angiogenic cascade. While intravitreal anti-VEGF therapy is currently the standard of care for treatment of CNV, and its effectiveness delays disease progression and restores vision in most patients, there are, however, still many therapeutic limitations with our current therapy regimens (Mettu et al., 2020). A significant proportion of eyes develop visually adverse pathology including fibrotic scar, thinner retina, and CNV lesion growth despite long-term anti-VEGF therapy (Daniel et al., 2014; Jaffe et al., 2019). In addition, many patients suffer from incomplete response or non-response to anti-VEGF treatment (Romdhane et al., 2020; Krebs et al., 2013), and the outcomes are different between patients.

The efficacy and safety of anti-VEGF therapy have been shown in many studies (Bakri et al., 2019; Thulliez et al., 2018). Anti-VEGF therapy also raises drug associated side effects, such as retinal artery or vein occlusion (Mansour et al., 2010), retinal pigment epithelial (RPE) atrophy (Cho et al., 2020), macular atrophy (MA) (Zarubina et al., 2017), acute coronary syndrome and stroke (Weinstein et al., 2020), and thrombotic microangiopathy and acute kidney injury (Hanna et al., 2020). Many patients do not respond to anti-VEGF treatment or become refractory to anti-VEGF treatment during the treatment (Ehlken et al., 2014). Thus, anti-VEGF treatment is not completely suitable for all patients, and care should be taken with elderly patients with underlying diseases,

such as diabetes, myocardial infarction, cardiovascular and cerebrovascular diseases.

The physiological amount of VEGF plays a critical role in survival and maintenance of RPE integrity (Ford et al., 2011). VEGF released at the basal side of the RPE monolayer is important in maintaining the choroidal fenestrations (Marneros et al., 2005), which allow macromolecules to be transported into the retina. The knock-out of VEGF in the RPE results in choriocapillaris damage (Kurihara et al., 2012). This confirms that the physiological level of VEGF is a survival factor for the RPE and choriocapillaris. Thus, sustained suppression of VEGF through intravitreal anti-VEGF agents should be cautious. A reduction in VEGF under the required level can induce choroidal vessel collapse.

2.3.2 Photodynamic therapy

Photodynamic therapy (PDT) with verteporfin targets the vascular components and selective thrombosis of new vessels with relative preservation of adjacent structures. Before anti-VEGF treatment, photodynamic therapy was an established treatment for sub-foveal CNV for many years, but PDT does not restore visual acuity and is associated with long-term chorioretinal atrophy (Kang et al., 2017). A long follow-up period of PDT treatment of CNV secondary to pathologic myopia showed a significantly decreased visual acuity because of the development of chorioretinal atrophy (Giansanti et al., 2012). However, many studies reported that a combination of PDT and intravitreal anti-VEGF therapy for myopic CNV can result in better visual outcomes (Rishi et al., 2016; Smretschnig et al., 2016), but this combined therapy is not suitable for a larger size of CNV, and the loss of vision due to chorioretinal atrophy remains unresolved. To date, which therapy regimen is superior remains controversial.

PDT therapy has many limitations. PDT achieves neovascularization occlusion, but it has little effect on the angiogenic process, thus factors that promote angiogenesis are not suppressed (Koh et al., 2011; Bhuvaneswari et al., 2007). PDT treatment decreases the retinal and choroidal blood flow (Eris et al., 2019), and increases the risk of severe choroidal ischemia (Lee et al., 2009), thus stimulating the regeneration of VEGF. Many side effects such as severe retinal vascular infarction (Koizumi and Hatanaka, 2010), transient reduction in retinal function (Lai et al., 2004) and choroidal ischemia (Isola et al., 2006) after PDT treatment have been reported. Therefore, PDT can

delay the CNV lesions, but it cannot decrease the VEGF level and improve visual acuity.

2.4 Chorioretinal ischemia disease

The retina is a high nutrients and oxygen consumption tissue with a high metabolic activity. This high requirement of oxygen needs a properly developed and maintained vascular system (Alves et al., 2020). There are two blood sources for the neurosensory retina: the central retinal artery and the posterior ciliary arteries. The central retinal artery supplies the inner two-thirds of the retina and the choriocapillaris supplies the outer retina, consisting of retinal photoreceptor cells and the retinal pigment epithelium (RPE) (Pournaras et al., 2008). The retinal blood supply is complex and any factor that reduces blood supply to the retina and choroid and affects normal retinal metabolism can cause ischemic retinopathies.

Retinal ischemia is a disease in which retinal vessels or the choriocapillaris are damaged resulting in retinal nonperfusion and ischemia. The loss of oxygen supply, accumulation of metabolic substrates, and removal of waste products in the retina will initially lower homeostatic responses and with time will induce injury to the tissue (Osborne et al., 2004). Retinal ischemia can cause visual impairment and blindness. Retinal vein occlusion (RVO), retinal artery occlusion (RAO) and diabetic retinopathy (DR) are the most common ischemic retinopathies in the clinic. RVO and RAO are related to systemic diseases including hypertension and arteriosclerosis, and both RVO and RAO can lead to considerable vision loss and further complications, such as retinal detachments, macular edema and retinal neovascularization (Hajdu et al., 2020). DR is one of the most common retinal microangiopathies and is a leading cause of blindness and visual impairment disease. DR develops vascular changes over time, especially in the small capillaries. In the retina, capillary occlusion causes retinal nonperfusion (RNP), which leads to local retinal ischemia (Liu et al., 2021; Russell et al., 2021). If the ischemia occurs at the macular area, it is visually devastating. Diabetic macular ischemia (DMI) is an irreversible complication of diabetic retinopathy (Tsai et al., 2021). One study reported that 41.8% of DR patients had evidence of DMI, and 16.6% of eyes had evidence of moderate to severe DMI (Sim et al., 2013).

2.4.1 *In vivo* animal models of retinal ischemia

To investigate the pathogenesis of ischemic retinopathy, many animal models have been developed

to mimic retinal vascular occlusion. These include raised intraocular pressure (IOP) (Bermudez and Gonzalez, 2020), laser-induced occlusion of the retinal artery or vein (Wen et al., 2019; Neo et al., 2020), bilateral or unilateral common carotid artery occlusion (CCA) (Lee et al., 2020; Lee et al., 2020), and occlusion of the retinal circulation by a probe (Alder et al., 1990). Although a broad range of methods have previously been utilized, they all have their own limitations. Increased IOP may result in both vascular occlusion-induced retinal ischemia and mechanical injury to the retinal tissue and the optic nerve (Oz et al., 2005). Laser-induced retinal vessel occlusion is noninvasive to the retinal tissue, but reperfusion of the occlusion is likely to occur (Vestergaard et al., 2019). This should be validated by fundus angiography. Bilateral or unilateral CCA also interrupts blood supply to the brain and can lead to animal death. Occlusion of the retinal circulation by a probe seems to avoid damage to the retina, however, the success of occlusion is diverse, and the comparison between individuals is difficult. Therefore, establishing a preferable retinal ischemic model should imitate the human disease as closely as possible with less damage to other ocular tissues.

2.4.2 *Ex vivo* models of retinal ischemia/hypoxia

Ex vivo organ cultures can mimic the *in vivo* situations and raise minimal ethical concerns. Organ culture cannot replace *in vivo* animal experiments entirely, but they can reduce the number of animals used for experiments. It is a good alternative to animal experiments. To establish a retinal ischemic/hypoxic model, many studies tried to use N_2-saturated PBS containing iodoacetic acid (IAA) in airtight vials (Catalani et al., 2007), PBS containing iodoacetic acid and sodium cyanide (Mastrodimou et al., 2005), and cobalt chloride ($CoCl_2$) (Tsai et al., 2020) to simulate neurodegenerative ischemic/hypoxic mechanisms in the retinal explants culture. Among these chemical solutions, $CoCl_2$ is considered as a suitable hypoxia-mimetic agent and has been commonly used *in vitro* to mimic the ischemic/hypoxic condition. However, the effect of $CoCl_2$ is not restricted to retinal neurons, it also inhibits mitochondria function (Ingavale et al., 2008), increases the generation of oxygen radicals (Karovic et al., 2007), induces reactive oxygen species (ROS) (Fung et al., 2016), and damages certain retinal cell types, especially microglia (Hurst et al., 2020). The retinal explants cultured by $CoCl_2$ only partly mimic the hypoxic condition. $CoCl_2$-induced hypoxia cannot completely simulate the ischemia/hypoxia during the process of retinal

disease. Furthermore, chemical solution cultures cannot mimic the physiological micro-environment and the retinal explants are not in their natural state. During the process of making retinal explants, there are various degrees of trauma to the retina, leading to the apoptosis of retinal ganglion cells. Therefore, a new ocular ischemic/hypoxic model similar to the physiological microenvironment needs to be established.

2.5 Current therapeutic options for retinal ischemic disease

Ischemic retinopathies are characterized by microvascular changes that result in ischemia, followed by ischemia-induced abnormal neovascularization which ultimately leads to retinal detachment and blindness (Rivera et al., 2017). DR and RVO are the two most frequent macro and microvascular diseases which can cause retina ischemia and the release of VEGF. Neovascularization is one of the major complications in retinal ischemic diseases. To date, the most effective therapies for this complication are laser photocoagulation and intravitreal injection of anti-VEGF agents.

2.5.1 Intravitreal anti-VEGF therapy

With the advancements in research, several studies have identified a high level of VEGF in the aqueous humor of patients with central retinal vein occlusion (CRVO) and branch retinal vein occlusion (BRVO) (Boyd et al., 2002; Noma et al., 2014). VEGF is found to be elevated in the vitreous fluid of patients with ischemic CRVO and macular edema (Noma et al., 2009). Upregulation of VEGF expression increases endothelial cell proliferation and neovascularization formation, results in the breakdown of the blood-retina barrier and increases vascular permeability, which leads to the development of macular edema (Rogers et al., 2010). These results suggested that retinal ischemia in RVO causes an increase in VEGF, disrupts the blood-retina barrier, and causes macular edema. Intravitreal anti-VEGF therapy has become the first-line therapy for RVO patients with macular edema. A marked improvement was observed in the RVO patients with macular edema after intravitreal anti-VEGF therapy. The aggressive blockade of VEGF reduced progression of retinal nonperfusion and promoted reperfusion (Campochiaro et al., 2013). Patients with RVO who underwent intravitreal anti-VEGF treatment gained visual recovery which was maintained throughout the entire follow-up (Costa et al., 2021). Several other studies suggest that anti-VEGF therapy can be used for both ischemic and nonischemic forms of RVO (Khayat et al.,

2020), and anti-VEGF at an early stage of RVO may achieve good results.

Despite intravitreal anti-VEGF therapy resulting in success in some patients with RVO, other patients, however, continue to suffer from recurring macular edema or are resistant to anti-VEGF therapy (Noma et al., 2020). The pathogenesis of RVO with macular edema may be more complex and the disease process may involve factors related to inflammation or ischemia other than VEGF. In one present study, the aqueous levels of inflammatory cytokines were increased in the patients with BRVO (Ryu et al., 2021). Local inflammation may be implicated in the pathogenesis of RVO. One animal experiment showed that inhibition of inflammatory cells delayed retinal degeneration in RVO in mice (Jovanovic et al., 2020). In addition, there was a significant decrease in the retinal nerve fiber layer (RNFL) thickness in BRVO (Kim et al., 2014), and this indicated neuro atrophy. Anti-VEGF for patients with RVO and macular edema can reduce macular thickness by a 2-year follow-up, and the retinal sensitivity was not improved (Sharief et al., 2020). Therefore, for the treatment of retinal ischemic disease, a combination of neuroprotective and anti-VEGF therapy seems to be necessary.

Based on the role of VEGF in the pathogenesis of diabetic macular edema, intravitreal anti-VEGF agents were applied to treat diabetic retinopathy (DR) with macular edema (Simó et al., 2014). Intravitreal anti-VEGF therapy can effectively reduce retinal neovascularization and macular edema and improve visual activity. Anti-VEGF treatment was also found to be beneficial in patients with proliferative diabetic retinopathy (PDR), especially in cases with vitreous hemorrhage, neovascular glaucoma, and before vitrectomy (Osaadon et al., 2014). In the clinic, some patients with DR respond poorly to intravitreal anti-VEGF treatment, and anti-VEGF fails to solve the ischemic condition in the retina (Jalilian et al., 2020). In some cases, the laser photocoagulation as an additional treatment is also needed for the treatment of DR. The half-life of the anti-VEGF agents is short and frequent treatment should be performed to maintain the therapeutic efficacy. In fact, anti-VEGF therapy cannot fully substitute the laser photocoagulation treatment, which is the first line therapy for DR.

2.5.2 Laser photocoagulation therapy

Laser photocoagulation is an important treatment approach for the complications of retinal vascular

diseases, such as retinal ischemia and retinal neovascularization. The retinal ischemia (non-perfusion area) accelerates the expression of VEGF, which is the underlying cause of the neovascularization formation and macular edema (An and Jeong, 2020). Early-scatter laser photocoagulation to the non-perfusion area in BRVO promotes the formation of collateral vessels, which helps subretinal fluid resorption, reduces macular edema, and improves visual acuity (An and Jeong, 2020). Selective laser photocoagulation of the peripheral non-perfusion areas in the CRVO may improve visual outcomes (Rehak et al., 2014). Laser photocoagulation has many benefits in the treatment of retinal ischemic diseases. The effect of laser photocoagulation lasts longer than anti-VEGF. If laser photocoagulation is combined with anti-VEGF therapy, the frequency of intravitreal anti-VEGF injection can be reduced.

Laser photocoagulation is also associated with some complications. Decreased corneal sensation and signs of dry eye are common after pan-retinal photocoagulation (PRP) for diabetic retinopathy (Jamali et al., 2021). The thermal effect of the laser can damage the adjacent normal retina. Multifocal electroretinograms (mf-ERGs) recorded the transient increase in the amplitude following laser photocoagulation for diabetic macular edema. The transient increase in the amplitude likely resulted from a biological amplification of the partially damaged cells adjacent to the photocoagulation spots (Shimada et al., 2021). Another study also reported a reduced retinal function recorded by ERG following PRP for PDR, and the ERG showed an absolute amplitude reduction and delay latency (Khojasteh et al., 2020). Thus, the amount of retinal laser treatment and the therapeutic effect on the retinal ischemic area or regression of retinal neovascularization should be balanced. PRP treatment causes a decrease in retinal blood flow (Chew et al., 2003), reduces the choroidal luminal area and the sub-foveal choroidal thickness (Kim et al., 2020). PRP may potentially cause a decrease in macular pigment density, and macular pigment plays an important role in antioxidant and protective properties (Doğan and Kutluksaman, 2021). All the above changes may lead to the occurrence of macular disease. So, the post-PRP macular disease should be taken into consideration.

2.6 Pigment epithelial derived factor (PEDF)

Pigment epithelium-derived factor (PEDF) is a 50-kDa protein and is a member of the serine protease inhibitor supergene family. A previous study reported that RPE-conditioned medium

induced neuronal differentiation of Y79 human retinoblastoma cells, and then PEDF was purified from RPE cells as a factor that can induce neuronal differentiation (Tombran-Tink and Johnson, 1989). Now, it has been recognized that PEDF is a multifunctional protein, and has anti-angiogenesis, neurotrophic and neuroprotective functions. PEDF is a potential antiangiogenic agent in the treatment of ocular neovascularization diseases.

2.6.1 Location of PEDF in the retina

RPE cells secrete PEDF in a polarized fashion towards the neural retina, and the interphotoreceptor matrix around the RPE microvilli is a major location of PEDF (Maminishkis et al., 2006). PEDF in the RPE cells can antagonize the VEGF-induced choroidal neovessel breakdown of the RPE. In fact, PEDF is found not only in the apical side of the RPE cells but also in Bruch's membrane (Becerra et al., 2004). PEDF has both a neuroprotective and an anti-angiogenesis function. The polarity of PEDF production and its location in Bruch's membrane play a role in preventing the pathogenesis of retinal neuron degeneration and choroidal neovascularization formation.

2.6.2 Protective effect of PEDF on RPE cells

The retinal pigment epithelium (RPE) is essential in the outer segment of photoreceptor renewal and function, and it protects the retina from light-induced damage. RPE cells secrete protective agents as well as growth factors to maintain retinal homeostasis. PEDF is one of the factors secreted by RPE cells. This factor has a protective effect on RPE cells. It was found that PEDF induced oxidative stress (OS)-damaged RPE cell regeneration by regulating the oxidative status and improving the mitochondrial activities (Kim et al., 2021). One study demonstrated that PEDF protected human ARPE-19 cells against H_2O_2-induced oxidative stress via upregulating protein 2 (UCP2) (Wang et al., 2019). Human RPE cells transfected with a gene for PEDF are more resistant to the harmful effects of H_2O_2 (Bascuas et al., 2020). Therefore, PEDF may be effective in treating oxidative stress induced retinal neurodegenerative diseases. In normal conditions, VEGF is required for choriocapillaris development and is secreted at the basolateral side of RPE cells (Blaauwgeers et al., 1999). VEGF reduces RPE barrier properties, and VEGF secretion occurred in the RPE cells under oxidative stress. PEDF is effective in protecting the RPE barrier function and preventing the VEGF-induced RPE permeability (Ablonczy et al., 2009).

2.6.3 Protective effect of PEDF on retinal photoreceptor cells

PEDF is a promising neuroprotective protein for photoreceptor cells but the mechanisms mediating its effects are still not well understood. Calcium ions play a critical role in neuronal cell death. One study reported that intravitreal injection of PEDF protein in *retinal degeneration* (*rd1*) mutant mice attenuated calpain activation photoreceptors. PEDF protected the degenerating retina by decreasing intracellular calcium (Comitato et al., 2018). Another study found that intravitreal injection of PEDF protein attenuated photoreceptor degeneration and reduced inflammatory molecules in the mouse model of progressive focal retinal degeneration (Wang et al., 2013). This result means that PEDF slows photoreceptor degeneration via suppression of both apoptotic and inflammatory pathways. Similarly, intravitreal injection of purified PEDF protein into the mouse model of retinitis pigmentosa (RP), the *rd* mutant mice, resulted in a significant reduction of photoreceptor cell death (Cayouette et al., 1999). The mechanism by which PEDF could prevent apoptosis in photoreceptor cells is unknown. However, the result indicated that PEDF was required for the development of photoreceptors. Before the rat retina exposure to constant light-damage, a single intravitreal injection of PEDF rescued the morphology and function of photoreceptor cells from light-damage (Cao et al., 2001). In short, PEDF is useful for the survival of photoreceptors.

2.6.4 Protective effect of PEDF on retinal ganglion cells

PEDF is mainly expressed by RPE cells and is also expressed in Müller glia and retinal astrocytes. Müller cells are an important source of PEDF. The immunohistochemical analysis of the mouse retina showed that the PEDF signal is maximal in Müller glial end-feet. PEDF synthesized by Müller glial cells may be secreted at the end-feet which is around the RGC (Unterlauft et al., 2012). This result underlines that the PEDF originated from Müller glial cells and contributes to the neuroprotective effect of RGC. Müller glial cells co-cultured with retinal ganglion cells (RGCs) increased the number of viable RGCs (Unterlauft et al., 2014). The exact mechanism by which PEDF transduces survival-promoting signals into ganglion cells is not clear. One study reported that PEDF promotes retinal ganglion cell (RGC) survival via activation of signal transducers and activators of transcription (STAT) 3 pathway by the PEDF receptor (Eichler et al., 2017). PEDF induced an increased STAT3 activation in RGCs. In the glutamate-induced toxicity of cultured adult

rat RGCs, PEDF protected the survival of cultured adult rat RGCs via the activation of the nuclear factor κB (NFκB) and extracellular regulated protein kinases (ERK)1/2 pathways (Pang et al., 2007). Similarly, in the $CoCl_2$-mimetic hypoxia-induced apoptosis of rat RGCs, PEDF protected RGC from hypoxia-induced mitochondrial dysfunction by inhibiting the opening of mitochondrial permeability transition pores (mPTPs), suppressing the decrease of membrane potential, and inhibiting the cellular adenosine triphosphate (ATP) level (Tian et al., 2017). Under different conditions, PEDF protects RGCs by different mechanisms. It is unclear whether RGCs can directly respond to the PEDF stimulus by PEDF-receptor or are mediated by another cell type.

2.6.5 Anti-angiogenic effect of PEDF

PEDF is a potent angiogenic inhibitor, and VEGF is an angiogenic stimulator. In normal ocular tissues, there is a balance between angiogenic stimulators and angiogenic inhibitors. In the ischemia-induced retinal neovascularization rat model, there was an increased VEGF level and decreased PEDF level in the retina. An imbalance between PEDF and VEGF contribute to retinal neovascularization (Gao et al., 2001). The interactions between PEDF and VEGF are largely unclear. In the oxygen-induced retinopathy (OIR) rat, PEDF inhibited mitogen-activated protein kinase (MAPK)-mediated nuclear translocation of HIF-1, a major VEGF transcriptional factor, and competed with VEGF binding to VEGF-receptor 2 (VEGFR2) (Zhang et al., 2006). The detailed interaction between PEDF and VEGFR2 remains to be elucidated. PEDF may promote VEGFR2 internalization and/or degradation to limit VEGF function, and thereby block angiogenetic activity (Johnston et al., 2015).

The anti-angiogenic effects of PEDF are partially mediated through the induction of endothelial cell apoptosis. However, the underlying pathway by which PEDF induces apoptosis is not fully understood. Many studies tried to investigate the mechanisms and obtained some preliminary results. PEDF blocks VEGF-mediated survival of primary cultures of human umbilical vein endothelial cells (HUVECs) by activation of p38 followed by cleavage of caspases 3, 8, and 9 (Chen et al., 2006). Cytosolic phospholipase A_2 ($cPLA_2$) is a rate-limiting enzyme. PEDF induces apoptosis of endothelial cells through $cPLA_2$ by activation of P38 MAPK. The activated $cPLA_2$ promotes peroxisome proliferator-activated receptor gamma (PPAR-γ) activity, p53 overexpression, and endothelial cell apoptosis (Ho et al., 2009). Fas is a member of the tumor-necrosis factor (TNF)

receptor superfamily, and induces apoptosis of the receptor-bearing cell. PEDF induces an increase of Fas-Ligand (FasL) on the surface of immature endothelial cells. Fas/FasL-mediates endothelial apoptosis and blocks angiogenesis (Volpert et al., 2002). Therefore, PEDF action on endothelial cells is likely by different pathways.

2.6.6 Antifibrotic Effect of PEDF

PEDF has multiple functions, including an anti-angiogenic effect, neurotrophic activity and a neuroprotective effect. Many studies have reported that PEDF has an antifibrotic effect, such as antifibrotic cytokine in ethanol feeding and cerulein-induced pancreatitis (Schmitz et al., 2011), antifibrotic activity in an in vivo mouse model of carbon tetrachloride (CCl_4)-induced hepatic fibrosis (Tsai et al., 2014) and attenuating the fibro-inflammatory reaction in human pancreatic cancer (Principe et al., 2016).

Transforming growth factor-β (TGF-β)1 is a profibrotic cytokine and is recognized as a modulator of extracellular matrix (ECM) formation, such as fibronectin and collagen (Wang et al., 2005). PEDF could prevent the overexpression of fibro-genic factors, TGF-β1 and the connective tissue growth factor (CTGF) and reduce the production of ECM protein production in a streptozotocin (STZ)-induced diabetic rat kidney (Wang et al., 2006). Inhibition of TGF-β1 may be one pathway of the anti-fibrosis effect of PEDF. Inflammatory response can lead to increased collagen deposition and fibrosis. Wnt signaling promotes inflammation and oxidative stress. One study reported that PEDF inhibited the Wnt pathway-mediated fibrosis in renal proximal tubule epithelial cells (He et al., 2017). This result indicates that the anti-fibrosis effect of PEDF is mediated in part by inhibiting Wnt signaling. PEDF has an anti-inflammatory action, and it suppresses the expression of inflammatory cytokines including IL-1β, IL-6, TNF-α and IL-17A on the ocular surface in dry eye disease (Ma et al., 2021). PEDF can also suppress inflammation occurring in the retina, and then reduce macrophage infiltration and fibrosis (Ho et al., 2010).

2.6.7 PEDF for the treatment of CNV

PEDF displays anti-angiogenic activity. Many studies have attempted to use PEDF to treat ocular neovascular diseases, especially CNV. Intravitreal injection of an adenoviral vector encoding PEDF (Ad PEDF) could inhibit laser-induced mice CNV (Mori et al., 2001). Compared to an adenoviral

vector, the gene expression was prolonged through administration of Ad35, an alternate adenovector serotype, which inhibits CNV lesion to a much greater extent (Hamilton et al., 2008). Subretinal transplantation of iris pigment epithelial (IPE) cells expressing PEDF inhibited laser-induced CNV in a rat model (Semkova et al., 2002). Peptide can reach the choroid/RPE complex as functional active molecules. Subconjunctival administration of PEDF-derived peptide 34-mer inhibited vessel sprouting in laser induced rat CNV (Amaral et al., 2010). Subretinal transplanting of RPE cells transfected with the PEDF gene that express constant levels of biologically active recombinant PEDF (rPEDF) could inhibit laser-induced rat CNV (Johnen et al., 2015). As VEGF is involved in the pathogenesis of CNV, the dual-acting therapy based on the simultaneous expression of anti-VEGFA microRNAs (miRNAs) and secretion of antiangiogenic protein PEDF delivered by adeno-associated virus (AAV) vector was investigated. The multigenic AAV vectors displayed combined efficacy in the treatment of laser-induced mice CNV (Askou et al., 2019).

2.7 Aim of the study

2.7.1 Exploring the efficacy of PEDF alone and PEDF combined with anti-VEGF in the treatment of rat quiescent CNV *in vivo*

Currently, anti-VEGF therapy has become the standard treatment for CNV and has revolutionized the therapy for this disease. However, many side effects have been reported in both the clinic and animal experiments after anti-VEGF treatment. In blood vessels of surgically excised choroidal membranes from wet AMD, anti-VEGF treatment induced thrombosis and protein complex formation. VEGF drugs induced thrombotic microangiopathy in the choriocapillaris of monkeys after intravitreal application. The purpose of anti-VEGF therapy is to block vessel growth or remove the neovessels. However, the survival of photoreceptors requires the nutrient supply from the vessels. Long-term anti-VEGF treatment causes loss of the choriocapillaris and retinal photoreceptors degeneration, which induce visual impairment. Furthermore, PEDF has a neurotrophic, neuroprotective effect as well as antiangiogenic action. Many studies also reported an antifibrotic and anti-inflammatory effect. PEDF is reduced in patients with CNV. There may be a balance between PEDF and VEGF levels. Reduced PEDF or increased VEGF promote the formation of neovascularization.

Instead of inhibiting neo-choriocapillaris from the choroid, the aim of this study was to check

whether the PEDF can shift the neo-choriocapillaris growth into a newly-formed healthy and functional neo-choriocapillaris. The maximal thickness of CNV, the mature and immature collagen in the CNV, the VEGF level in the CNV and the apoptosis of photoreceptors above the CNV were examined. I hypothesise that the combination of a PEDF protein and an anti-VEGF drug may act synergistically to stabilize CNV and protect the retinal photoreceptors.

2.7.2 Establishing an *ex vivo* ischemic/hypoxic eye model and exploring the efficacy of PEDF in the treatment of ischemic/hypoxic eye disease.

Ischemia/hypoxia is a severe condition in ophthalmology. Many eye diseases can lead to ischemia in the ocular. However, little is known about the changes occurring to the retina and the choroidal blood vessels under ischemia/hypoxia. In the *ex vivo* experiment, we established an ischemic/hypoxic eye model. The effect of PEDF protein was examined and compared with the effects of an anti-VEGF drug (Avastin) and vehicle (PBS, pH7.3, 4µl). For immunohistochemistry, the immunohistochemical staining of VEGF and PEDF were performed. For EM, the morphology of the choroidal vessel, including the lumen, the fenestration and the endothelial cells of the vessel were examined. In addition, the oxygen concentration within the vitreous was measured by a calibrated fiber optic oxygen sensor which was inserted into the vitreous body of rat eyes in this *ex vivo* experiment and for comparison in the eyes of living rats under anesthesia. The apoptosis of retinal ganglion cells and inner nuclear layer (INL) cells was evaluated by terminal deoxynucleotidyl transferase dUTP nick end labeling (TUNEL) staining.

3 Materials and methods for the *in vivo* experiment

3.1 Animals

Six-week-old female Long Evans (LE) rats were purchased from Janvier Labs, Le Genest-Saint-Isle, France. There was no significant difference in gender for the morbidity of human CNV and the onset of CNV is not affected by gender (Colijn et al., 2017). Therefore, female rats were used in this experiment because of their docile behaviour. In total, 30 female rats were used in this study. All of the animals were handled in conformity with the German laws governing the use of experimental animals and were previously approved by the local agency for animal welfare (Einrichtung für Tierschutz, Tierärztlichen Dienst und Labortierkunde der Eberhard Karls

Universität Tübingen, Tuebingen, Germany) and the local authorities (Regierungspräsidium Tübingen, Tuebingen, Germany).

3.2 Experimental design

The experiment was divided into 5 groups with 6 rats in each group. The quiescent CNV rat model was induced by subretinal injection of AAV.VEGF-A^{165} vector (Sigma-Aldrich Chemie GmbH, Munich, Germany). The CNV was induced for each eye of all the rats. Intravitreal injection treatment was performed 3 weeks after the subretinal AAV.VEGF-A^{165} vector injection. Group 1 was the control group (AAV.VEGF-A^{165} vector alone), without intravitreal treatment; Group 2 was the vehicle treatment group (AAV.VEGF-A^{165} + Vehicle, PBS, pH7.3, 4μl); Group 3 was the PEDF treatment group (AAV.VEGF-A^{165} + PEDF protein, 10μg, 4μl); Group 4 was the Avastin treatment group (AAV.VEGF-A^{165} + Avastin, 50μg, 4μl); Group 5 was the PEDF/Avastin treatment group (AAV.VEGF-A^{165} + PEDF/Avastin, 10μg PEDF + 50μg Avastin, 4μl). The proposal is shown in Figure 2.

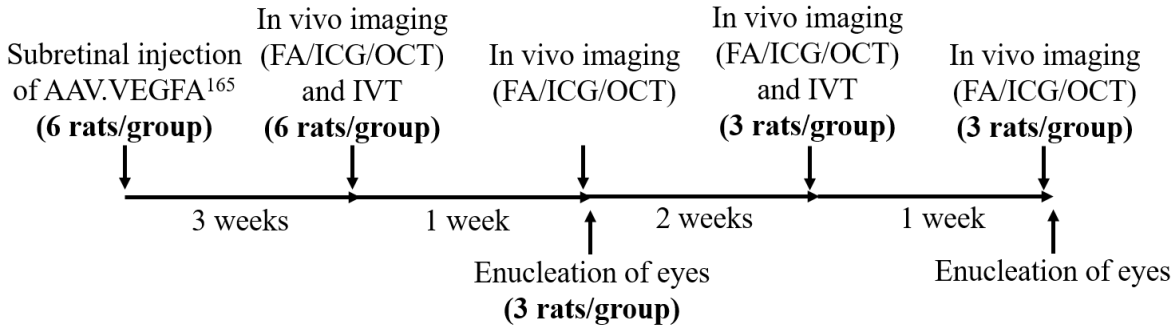

Figure 2. The proposal of the experiment. The rat quiescent CNV model was established by subretinal injection of AAV.VEGF-A^{165} for each eye. The FA, ICG and OCT examinations were performed at the third, fourth, sixth and seventh week after subretinal injection. The intravitreal injection was performed at the third and sixth week. At the fourth week, half of the rats for each group (3 rats/group) were sacrificed, and one eye of each rat was fixed with formalin and the other eye was fixed with 5% glutaraldehyde. At the seventh week, the remaining half number of rats (3 rats/group) were sacrificed and the eyes were fixed as before. AAV: Adeno-associated viral; FA: fluorescein angiography; ICG: indocyanine green angiography; OCT: optical coherence tomography; IVT: intravitreal injection.

3.3 Subretinal injection of AAV.VEGF-A^{165} vector to induce CNV

The LE rats were intraperitoneally anesthetized with three-component narcosis comprising 0.05 mg/kg of fentanyl, 5 mg/kg of midazolam, and 0.5 mg/kg of medetomidine. The rat cornea was

moistened by applying METHOCEL (Omni Vision, Puchheim, Germany). The subretinal injection was performed under a surgical microscope. The conjunctiva was cut and opened with ophthalmic surgical microscissor, and the sclera was opened with a 25G needle. Then 2×10^9 virus particles of the AAV.VEGF-A^{165} vector (Sigma-Aldrich Chemie GmbH, Munich, Germany) in 2µl PBS were injected into the subretinal space of the rat eye by using 10µl NanoFil syringe (World precision instruments) with a NanoFil 34-gauge blunt needle (Hamilton Co., Reno, NV, USA) (Figure 3). As shown in Figure 3, the vector was delivered into the subretinal space of the eye (between the RPE and the neuroretina). After injection, the rats were subcutaneously injected with the antidote, a mixture of 1.2 mg/kg of naloxone, 0.5 mg/kg of flumazenil and 2.5 mg/kg of atipamezole to neutralize the anaesthesia. Lastly, topical antibiotic eye drops Gentamicin-POS® (Ursapharm, Saarbrüken, Germany) were applied on both eyes.

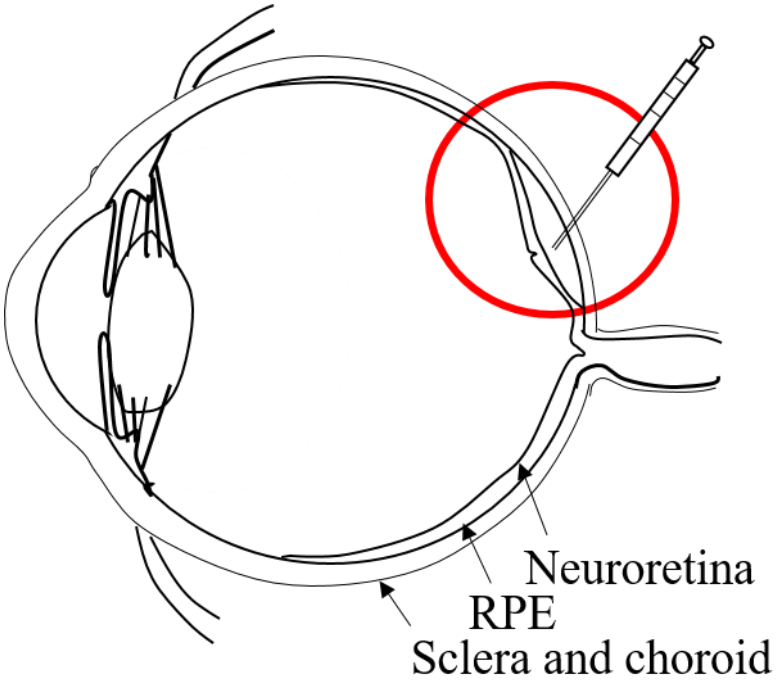

Figure 3. Subretinal injection of AAV.VEGF-A^{165} vector. The vector solution is delivered by the NanoFil 34-gauge bevelled needle (Hamilton Co., Reno, NV, USA) into the subretinal space between the RPE and the neuroretina.

3.4 *In vivo* imaging (SLO, FA, ICG and OCT)

Scanning laser ophthalmoscopy (SLO), fluorescein angiography (FA), indocyanine green angiography (ICG) and optical coherence tomography (OCT) were performed (at 3, 4, 6 and 7 weeks) after AAV.VEGF-A^{165} VEGF vector subretinal injection by using a Spectralis™ HRA+OCT

(Heidelberg Engineering, Heidelberg, Germany) device (Figure 4A). A +78 diopter (D) double aspheric lens (Volk Optical, Inc., Mentor, OH 44060, U.S.A.) (Figure 4B) was placed on the scan lens of the machine to modify for using with rats. The rats were anesthetized and the pupils were fully dilated. Both eyes were treated with methocel to get better adherent to the +3.5 diopter (D) contact lens and prevent dryness of cornea, as the dryness of corneal surface can degrade the resolution of images, especially for OCT images of CNV thickness. FA [42µl fluorescein (Alcon 10%), 208µl 0.9% NaCl] and ICG [250µl indocyanine green (5 mg/ml, diagnostic green)] dyes were injected in the tail vein. An additional custom-made +3.5 diopter contact lens was put on the rat cornea to obtain a proper image. The *in vivo* imaging was performed immediately for each eye to obtain the early phase FA and ICG angiograms. The late phase angiograms were performed 20 minutes after tail vein injection. For each eye, the early and the late phase angiograms and the thickness of CNV were acquired. The maximal thickness of CNV was measured 3 times manually and the mean value was used for analysis.

The SLO/OCT machine is designed for human patients, and the dimension in the x and y axes are not calibrated for the animal experiments. In contrast, the dimension in the z axis of the OCT image is displayed properly. Therefore, the data of CNV lesion thickness in the OCT image is correct.

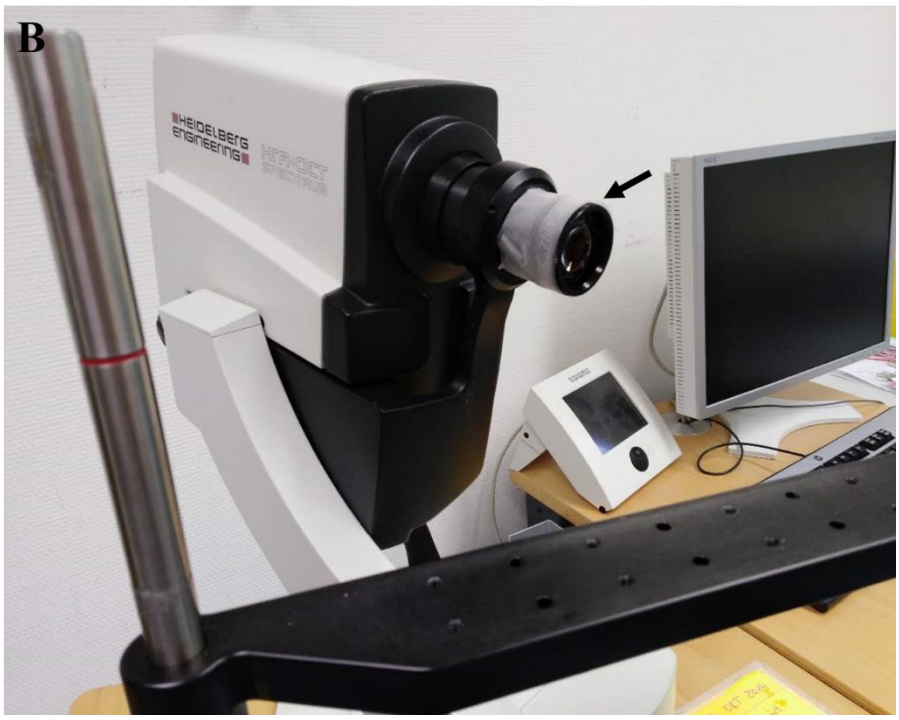

Figure 4 Spectralis^{TM} HRA+OCT device (Heidelberg Engineering, Heidelberg, Germany) (A). The device is modified for the use with the rat. (B). A +78 diopter (D) lens (shown by black arrow) was placed directly the scanning lens of the device.

3.5 Intravitreal injection (PBS, bevacizumab, PEDF, both bevacizumab and PEDF)

Four microliter of solution [PBS, 50µg bevacizumab (20mg/ml, Germany), 10µg PEDF protein (5.5mg/ml), both 50µg bevacizumab and 10µg PEDF protein] were delivered to the corresponding group through the pars plana into the vitreous cavity by using a 10µl NanoFil syringe (World precision instruments) with a NanoFil 34-gauge bevelled needle (Hamilton Co., Reno, NV, USA). As shown in Figure 5, the whole process was performed under a surgical microscope. In order to avoid leakage of the injection port, we paused for 3-5 seconds after the injection, then changed the direction of the needle, and pulled out the needle.

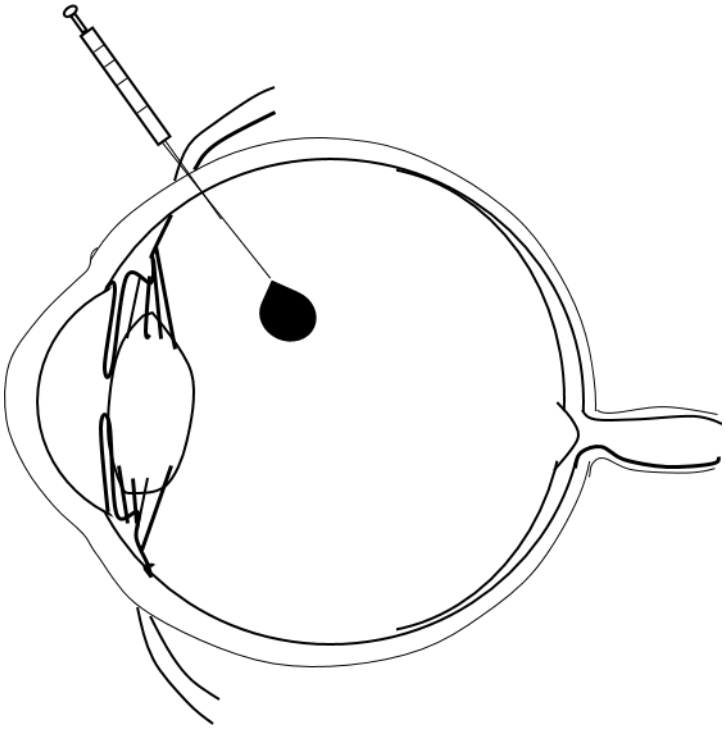

Figure 5. Intravitreal injection. The needle enters into the vitreous through the pars plana behind the corneal limbus. The solution (in black) was delivered into the vitreous cavity.

3.6 Preparation for paraffin embedding and sectioning

The rat eyes were enucleated and fixed immediately by 4.5% formalin (Roti Histofix, Carl Roth, Karlsruhe, Germany). After fixation for at least 3 days, the rat eyes were dehydrated according to an automated tissue processor (Leica TP1021, Leica Biosystems, Germany). The whole process is listed in Table 3.

Table 3. The process of dehydration of rat eyes before paraffin embedding

1. 70% Ethanol: 1 hour	2. 96% Ethanol: 1 hour
3. 96 Ethanol: 1 hour	4. 96% Ethanol: 1 hour
5. 99% Ethanol: 1 hour	6. 99% Ethanol: 1 hour
7. 99% Ethanol: 1 hour	8. Xylene: 1 hour
9. Xylene: 2 hours	10. Xylene: 2 hours
11. Paraffin: 2 hours	12. Paraffin: 2 hours

After dehydration, the rat eyes were embedded with paraffin wax by using a paraffin embedding machine (Leica EG 1140H, Leica Biosystems, Germany). A thickness of 4μm of the paraffin embedded sections was cut by manual microtome (Leica RM2235, Leica Biosystems, Germany). Next, the sections were put on the surface of the preheated water (50℃) in order to make the sections

sufficiently flat. Then we collected the sections by using glass slides (SuperFrost Ultra Plus™) which were coated with 0.01% Poly-L-lysine solution. Finally, the glass slides with sections were dried at 30℃ overnight. To obtain sections with CNV, the sections were observed first under light microscopy. RPE cells in the CNV area usually become evacuated. Sections which were recognized as CNV were selected. HE-staining was performed to determine whether they were CNV.

3.7 Preparation for electron microscopy (EM) specimen embedding

After the enucleation of the rat eye, the whole eye was fixed in 5 % glutaraldehyde in 0.1 M cacodylate buffer and kept at 4 °C in the fridge for at least one day. The cornea and lens were removed under the light microscope. The vitreous was gently removed and the eyecup was washed by 0.1M cacodylate buffer. The CNV part of the eye was selected according to the photos of angiographs and cut under the light microscope. Finally, the CNV and the remaining part of the eyeball were embedded in EPON (SPI-Pon™812 Epoxy Embedding Kit, SPI supplies, West Chester, PA). The epon was made by glycid ether 100 (53.6%), 2-Dodecenylsuccinic acid anhydride (6.7%), methylnacid anhydride (38.28%) and 2,4,6-Tris (dimethylaminomethyl) phenol (1.5%). The chemical reagents of Epon are listed in Table 4. The embedding protocol is listed in Table 5.

Table 4. The chemical reagents of EPON

	Reagents	Company
EPON	Glycid ether 100 for electron microscopy	Serva, Heidelberg, Germany
	2-Dodecenylsuccinic acid anhydride	
	Methylnacid anhydride	
	2,4,6-Tris (dimethylaminomethyl) phenol	

Table 5. The protocol of fixation and embedding for the electron microscope

Operating procedures	Chemical solution	Time
Fixation	5 % glutaraldehyde in 0.1 M cacodylate buffer (pH 7.4)	More than one day at 4°C
Washing	0.1 M cacodylate buffer (wash three times)	10 minutes each

Postfixation	0.1% osmium tetroxide and 0.1 M cacodylate buffer (1:1)	2 hours
Washing	0.1 M cacodylate buffer (wash three times)	10 minutes each
Dehydration	Ethanol (30%, 50%, 70%)	15 minutes each
Block staining	Saturated uranyl acetate in 70% Ethanol	Overnight at 4°C or 3 hours in room temperature
Dehydration	Ethanol (70%, 80%, 95%)	15 minutes each
	Absolute ethanol (two times)	20 minutes each
Intermedium	Propylenoxid (two times)	20 minutes each
Resin	Propylenoxid and Epon (1:1)	2 hours
	Epon	2 hours
	Epon	1 hour
Polymerisation	60°C	48 hours

3.8 Preparation for electron microscopy (EM) specimen sectioning

The epon block was trimmed to get a flat trapezoid-shape surface by using a razorblade. Then the epon block was fixed to the cantilever, and the distance from the epon block to the knife was ajusted. In order to detect CNV, the semithin sections (0.7μm) were first cut and stained with toluidine blue (0.5% toluidine blue in 2.5% $NaHCO_3$). The epon block was cut by using Reichert-Jung Ultracut E Ultramicrotome (Leica, Nussloch, Germany). Before transferring the already cut semithin section from the boat of the knife to the glass slide, a drop of distilled water was first placed on the surface of the glass slide. The floating semithin section was transferred from the boat to the drop of distilled water on the glass slide by using a glass stick with a metal loop in one end. The glass slide was put on a warm plate to evaporate the water and make the semithin section adhere tightly to the glass slide lastly, the semithin section was stained with toluidine blue. The CNV structure could be identified under light microscopy.

When the CNV was found in the semithin sections, the ultrathin section (0.05μm thickness) was then cut by using Reichert-Jung Ultracut E Ultramicrotome (Leica, Nussloch, Germany) and an

ultra-diamond knife. The ultrathin section was collected by formvar-coated grids and kept at room temperature until dryness. Then the ultrathin section was stained with lead citrate (0.1g/25ml) to improve the contrast of the cell membrane system, lipids and glycogen particles. It is important that the side of the grid with the ultrathin section should face the staining droplet. After staining, the grid with ultrathin section was kept at room temperature until dryness again.

Finally, the ultrathin specimen was examined by transmission electron microscopy (TEM) with a Zeiss 900 TEM (Zeiss Axioplan2 imaging, Zeiss, Jena, Germany). The TEM consists of five parts: illumination system (the electron gun and condenser lenses), imaging system (the specimen room and object lenses), vacuum system, recording system, and power supply system.

3.9 Hematoxylin and eosin (HE) staining

The paraffin sections were deparaffinized in xylene and rehydrated in gradient alcohol, then stained by hematoxylin and eosin (HE). The procedures of HE-staining are listed below:

1. Deparaffinize and rehydrate paraffin sections

   Xylene: 4 times, 5 minutes each time.

   99% Ethanol: 2 times, 1 minute each time.

   96% Ethanol: 2 times, 1 minute each time.

   70% Ethanol: 2 times, 1 minute each time.

   Distilled water: 2 times, 1 minute each.
2. Immerse the glass slides with sections in Harris hematoxylin solution for 10 minutes.
3. Wash the slides with running tap water until the water is clear.
4. Immerse the slides in HCL-alcohol for 3 seconds.
5. Wash the slides with distilled water until the water is clean.
6. Immerse the slides in distilled water for 10 minutes.
7. Immerse the slides in Eosin for 2 minutes.
8. Dehydrate the sections with gradient ethanol and xylene.

   70% Ethanol: 1 time, 1 minute each time.

   96% Ethanol: 2 times, 1 minute each time.

   99% Ethanol: 2 times, 1 minute each time.

   Xylene: 4 times, 1 minute each time.

9. Dry the slides, mount by cover slip.

The HE-staining was used to determine the existence and the location of CNV in the paraffin section. Then the subsequent immunohistochemical staining was performed.

3.10 Immunohistochemistry

Immunohistochemistry was performed on 4μm-thick sections of formalin-fixed, paraffin-embedded samples. The samples were dewaxed in xylene (4 × 5minutes) and rehydrated in three grades of ethanol (99%, 96%, and 70%) for 1 min each. The specimens were boiled at high pressure in citrate buffer (pH 6.0) solution for 2 minutes for antigen retrieval and then taken out and cooled down. Endogenous peroxidase and AP activity was blocked by 10 min incubation with Vector Bloxall (Vector, SP-6000 VECTOR LABORATORIES, Burlingame, USA). Next, the slides were incubated with ready-to-use 2.5% normal horse serum from Vector secondary antibody kits for 20 minutes to reduce nonspecific adsorption of antibodies to tissue. The test sections were stained with anti-vascular endothelial growth factor receptor (VEGF) prediluted antibody (ab27620, Abcam, Cambridge, UK) or other primary antibodies (shown in Table 6) for 30 minutes at 37℃. Following a thorough wash with 1× Tris-buffered saline (TBS; Merck, Darmstadt, Germany) (3 × 5min), ImmPRESS Poly-AP Anti-Rabbit (MP5401; Vector laboratories, Peterborough, UK) antibody or ImmPRESS Poly-AP Anti-mouse (MP5402; Vector laboratories, Peterborough, UK) antibody was applied for 30 minutes at room temperature. After another washing step in 1× TBS (3 × 5min), precipitation was performed using the VECTOR Red Alkaline Phosphatase substrate kit (SK-5100; Vector laboratories, Peterborough, UK). Counterstaining was performed with hematoxylin (Carl Roth, Karlsruhe, Germany) for 25 seconds and washed completely by tap water. The slides were rehydrated in ethanol (96%, 99%) for 2 minutes each and dehydrated in xylene (4 × 1minute), then dried and coverslipped.

Table 6. List of primary antibodies and staining solution

Target protein/cell type	Host/Company	Dilution
Collagen I and III		
Picrosirius Red Stain Kit	Polysciences	Prediluted

Collagen IV		
Collagen IV polyclonal antibody	From rabbit, Thermo Fisher Scientific	1:200
VEGF		
Anti-VEGF antibody	From rabbit, Abcam	Prediluted
PEDF		
Anti-PEDF antibody	From rabbit, Abcam	1:500

3.11 Picrosirius red staining and analysis

Picrosirius red stain (Polysciences, Warrington, PA, USA) was used to quantify collagen content and maturity. Paraffin-embedded sections were deparaffinized in xylene (4 times × 5 minutes) and rehydrated with distilled water (2 times × 1 minute). Slides were stained in Weigerts Hematoxylin for 8 minutes, rinsed in distilled water and immersed in 0.2% phosphomolybdic acid hydrate for 2 minutes. After another distilled water washing, slides were incubated in direct Picrosirius red for 60 minutes and 0.01 N HCl solution for an additional 2 minutes. Samples were rinsed in 75% ethanol for 45 seconds, dehydrated in xylene (4 times × 1minute), dried and mounted with coverslips.

Photomicrographs were taken by light microscopy at ×20 magnification to obtain clear CNV optical photos first (Figure 6A). The specimen must be kept from moving. Then photomicrographs were taken at ×20 magnification by light microscopy (Zeiss Axioplan2 imaging system; Zeiss, Jena, Germany) with a polarized lens (Figure 6B). The red-orange area (mature collagen) and the green-yellow area (immature collagen) in the CNV were taken separately. The total collagen content in the CNV was calculated as follows: [(red-orange area) + (green-yellow area)]/(total area of CNV) ×100. The mature and immature collagen in the CNV was calculated as follows: (red-orange area)/ (total area of CNV) ×100; (green-yellow area) / (total area of CNV) ×100. The CNV figures were processed by ImageJ software as follows: I put the CNV light microscope figure into the ImageJ software, manually selected the CNV area (the boundary between CNV and the neural retina was clearly distinguishable, and the boundary between CNV and the sclera usually distinguished by RPE

cells), selected the CNV area from the light microscope figure (Figure 6C). We then put the polarized figure (Figure 6B) into the ImageJ software and the CNV area in the polarized figure automatically corresponds to the selected CNV area in the light microscope figure (Figure 6C). Then the CNV area in the polarized figure was selected (Figure 6D). The area of CNV and the area of mature and immature collagen was calculated by a set color program. Three photomicrographs per CNV were selected to analyze, and the percentages of the total collagen, mature and immature collagen to the total area of CNV was calculated.

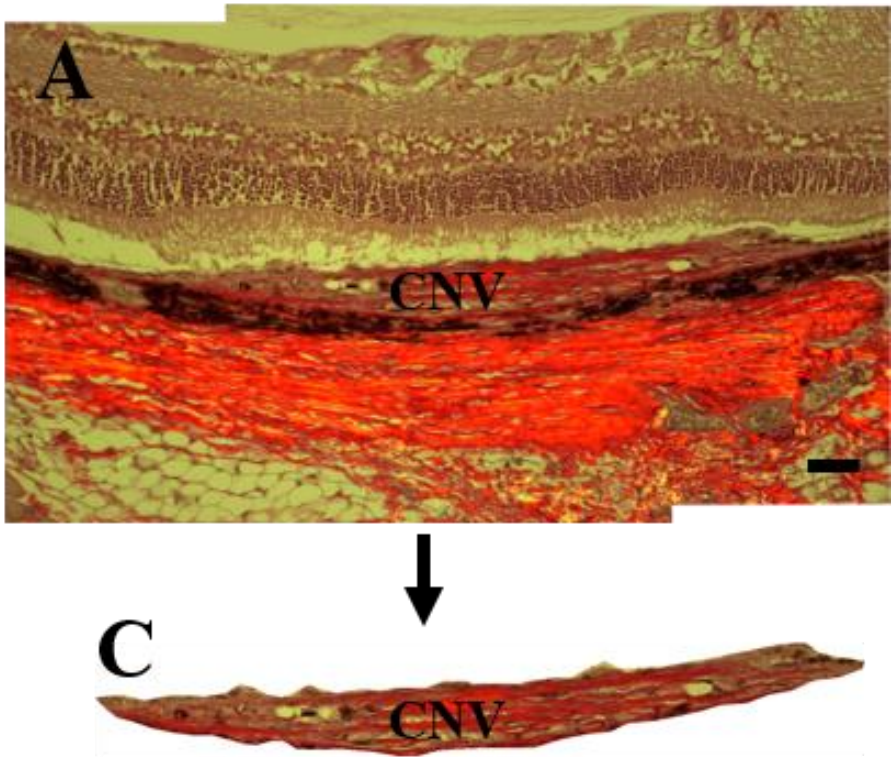

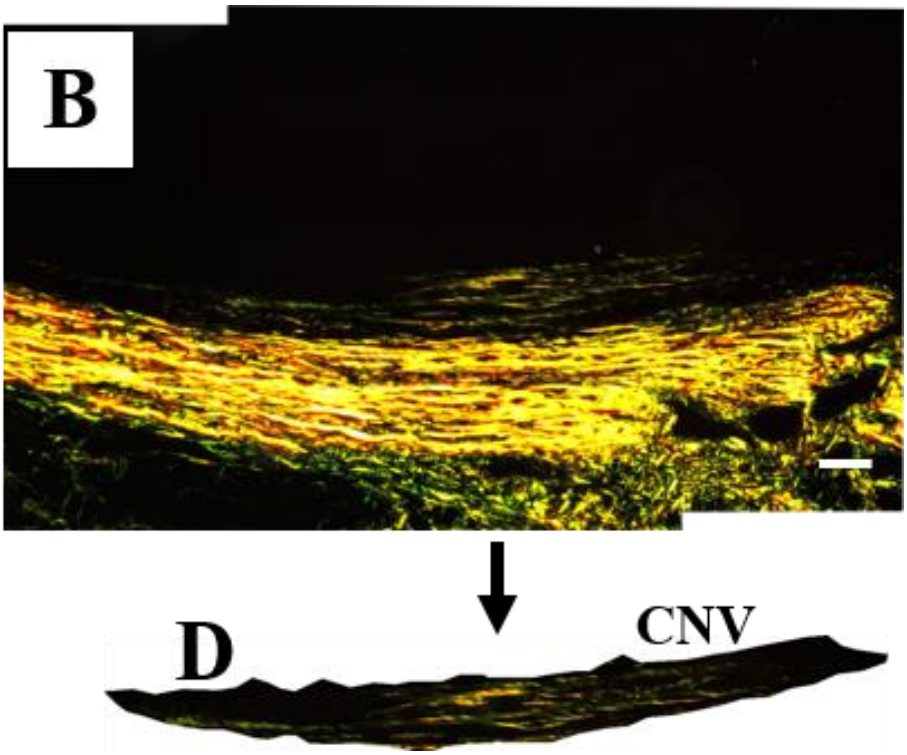

Figure 6. Representative Picrosirius red photomicrographs at ×20 magnification. (A): The photomicrograph was taken by light microscopy. (B): The photomicrograph was taken by polarized microscopy. (C): The manually selected CNV area from the light microscope figure. (D): The corresponding CNV area in the polarized microscope figure. Scale bar: 50μm.

3.12 Terminal deoxynucleotidyl transferase (TdT)-mediated dUTP nick end labeling (TUNEL) assay

Cell death was assessed using the TUNEL assay by means of an in situ cell death detection TMR red TUNEL kit (Roche Diagnostics, Mannheim, Germany). The paraffin sections were deparaffinized in xylene (4 times × 5 minutes) and rehydrated with distilled water (2 times × 1 minute). After washing in 0.1 M phosphate buffer saline (PBS) (3 times × 5 minutes), the samples were incubated in proteinase K (1.5μg/μl) for 5 min for cell permeabilization. Then the sections were incubated with alcohol acetic acid mixture (62% EtOH, 11% Acetic Acid, 27% H_2O) for 5 min. After three 5 min washes in TBS, the sections were incubated in blocking solution (1% BSA, 10% normal goat serum, 1% fish gelatine) for 1 hour. Finally, samples were incubated in terminal deoxynucleotidyl transferase enzyme at 37°C for 60 min in the dark and washed twice by PBS. Nuclei were counterstained with 4',6-diamidino-2-phenylindole (DAPI). The slides were photographed with an Imager Z2 ApoTome microscope (Carl Zeiss Microscopy GmbH, Oberkochen, Germany). For each eye with CNV, the number of apoptotic outer nuclear layer (ONL)

cells above the CNV area was counted, and the number of apoptotic cells related to the length of CNV (1000μm) was analyzed. Waveforms (White arrows are shown in Figure 7) often appear in the outer nuclear layer of the retina in the CNV area. The waveforms of ONL can be used as a sign to identify the CNV area.

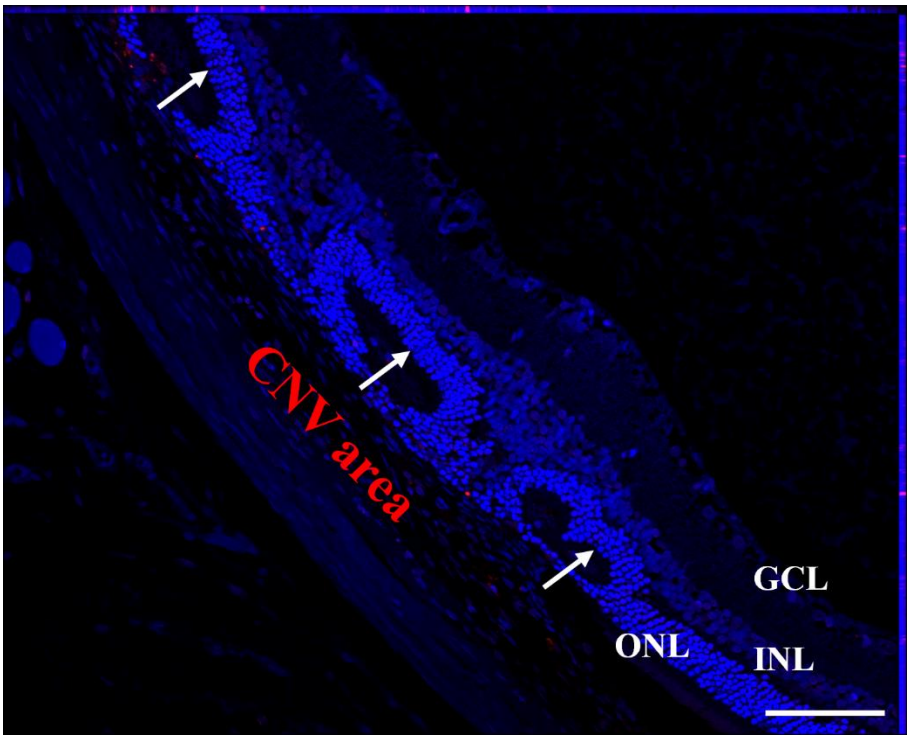

Figure 7. Representative image of TUNEL-staining in the retina above CNV. The outer nuclear layer cells showed waveform change (shown with white arrows) above the CNV area. The CNV rat eye was fixed by formalin immediately after enucleation and the apoptotic cells were undetectable in the ganglion cell layer and the inner nuclear layer cells. A very few apoptotic cells are occasionally observed in the outer nuclear layer. GCL: ganglion cell layer; INL: inner nuclear layer; ONL: outer nuclear layer. Scale bar = 50μm.

3.13 Microscopy and image processing

For the collection of fluorescent pictures of TUNEL staining, Z-stack images were captured on an Imager Z2 ApoTome microscope using a 20× (Carl Zeiss Microscopy GmbH, Oberkochen, Germany). The Zen Lite (v.3.1) software was used to reconstruct images. For the collection of optical micrographs, the figures were taken by light microscopy (Zeiss Axioplan2 imaging system; Zeiss, Jena, Germany).

3.14 Quantitative analyses of the maximal thickness of the CNV

lesion

The SLO/OCT machine (Heidelberg Engineering, Heidelberg, Germany) has a function to scan and obtain a series of OCT images in a specified region. The hyper-fluorescent region in the angiograph was CNV. The whole area of the CNV lesion was scanned and the images were collected for each eye (Figure 8). In order to get the thickest part of the CNV, the scanning area can be moved manually, and the image of the thickest area of CNV is collected. The maximal thickness of the CNV was measured three times and the mean value was used for statistical analysis.

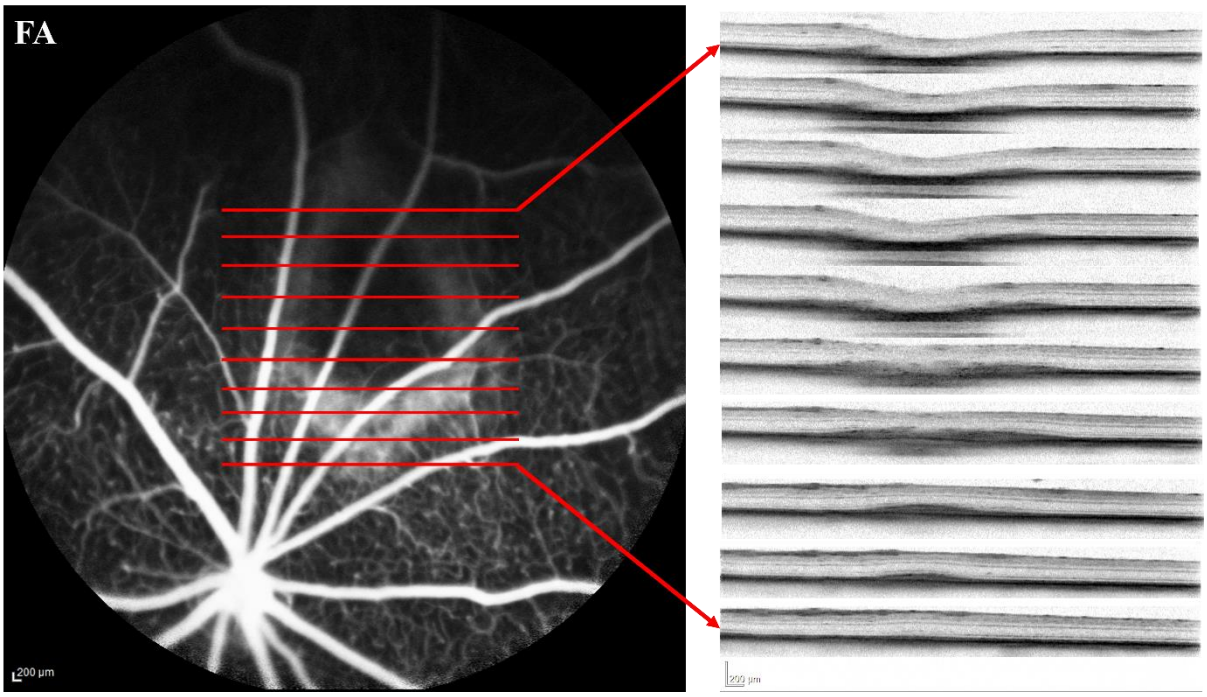

Figure 8. A series of the OCT images for a CNV lesion. The hyper-fluorescent area in the angiographic image is the CNV lesion. The scanned area was marked by red lines (Figure 8 FA and ICG). A series of OCT images of the CNV lesion (Shown with blue arrows) were collected. The hyper-fluorescent region in the FA and ICG was corresponded to the OCT images. FA: Fluorescein angiography, ICG: Indocyanine green angiography

The maximal thickness of CNV was measured manually in each OCT image by the computer's measurement program at the third, fourth, sixth and seventh week after subretinal injection of AAV.VEGF.A^{165} vector. The CNV thickness of each OCT image was measured three times, and the mean value was used to do analysis. The measurement methods were shown in Figure 9.

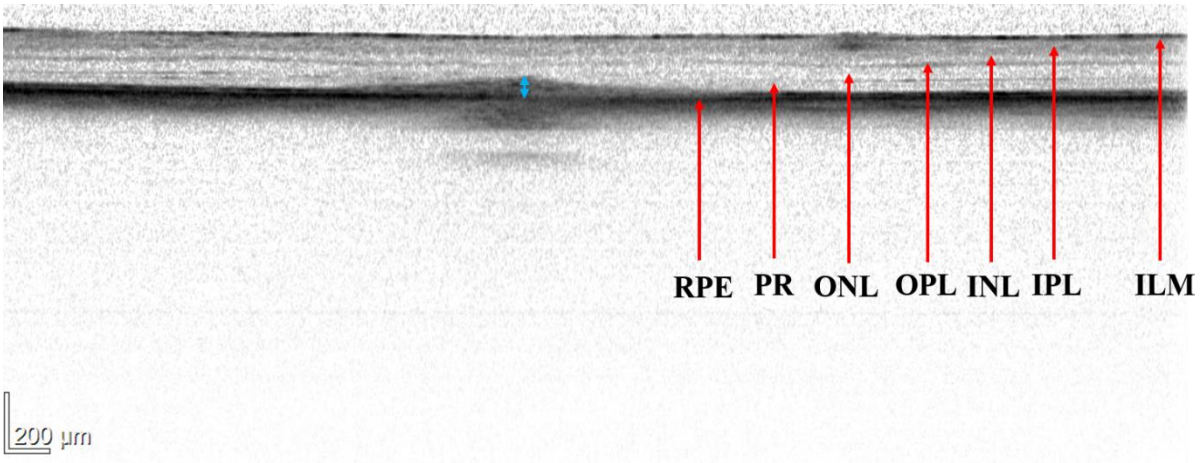

Figure 9. The method of measuring CNV thickness in the OCT image. The thickness of CNV was marked with a blue double-headed arrow. Different layers of the rat retina were marked with red arrows in the OCT image. ILM: inner limiting membrane; IPL: inner plexiform layer; INL: inner nuclear layer; OPL: outer plexiform layer; ONL: outer nuclear layer; PR: photoreceptor; RPE: retinal pigmented epithelium.

3.15 Quantification of the collagen by histology

The mature and immature collagen areas in the CNV were detected by picrosirius red staining, and the images were taken under polarized microscopy. The area of mature (orange-red color) and immature (green-yellow color) collagen in the CNV was calculated and automatically analyzed by a pre-set program in ImageJ software 9.0. The ImageJ software was set to identify the color of mature collagen and immature collagen in the CNV first. When the figure was put into the software, the software calculated the area according to different colors. The percentage of mature and immature collagen area in the CNV to the total CNV area was compared between each group. The type Ⅳ collagen was examined by immunohistochemistry (IHC), and the percentage of immunopositive staining area of collagen Ⅳ in the CNV to the total area of CNV was analyzed and compared between each group. For each eye with CNV, three specimens were included for analysis.

3.16 Quantification of VEGF and PEDF expression by IHC

The expression of VEGF and PEDF in the CNV was detected by IHC. PEDF-positive immunohistochemical staining was examined by anti-human PEDF antibody (because the intravitreal-injected protein was human PEDF protein) in the PEDF treatment group and the PEDF/Avastin treatment group. The number of eyeballs with CNV used for analysis is shown in

table 7. All of the analyzed images were taken under light microscopy and the CNV lesion area was selected manually by ImageJ software 9.0. The percentage of immunopositive staining area to the total CNV area was calculated. For each eye with CNV, three specimens were included for analysis.

Table 7. The number of eyeballs with CNV used for quantification of collagen, VEGF and PEDF for each group

Groups	Rat number	Collagen analysis	VEGF analysis	PEDF analysis	Other information
Group 1 (Control group)	1	√	√		
	2	√	√		
	3	√	√		
	4	×	×		Not found in PS
	5	√	√		
	6	√	√		
Group 2 (Vehicle treatment)	7	√	√		
	8	√	√		
	9	×	×		Not found in PS
	10	√	√		
	11	√	√		
	12	√	√		
Group 3 (PEDF treatment)	13	√	√	√	
	14	√	√	√	
	15	√	√	√	
	16	√	√	√	
	17	×	×	×	Dead after EP
	18	√	√	√	
Group 4 (Avastin treatment)	19	√	√		
	20	√	√		
	21	√	√		
	22	√	√		
	23	√	√		
	24	√	√		
Group 5 (PEDF + Avastin treatment)	25	√	√	√	
	26	√	√	√	
	27	√	√	√	
	28	√	√	√	
	29	√	√	√	
	30	√	√	√	

PS: paraffin sectioning, EP: experiment, √ : used for analysis, ×: not used for analysis

3.17 Quantification of the outer nuclear layer (ONL) area as a percentage of the corresponding CNV area

To test the effect of intraocular injection on retinal photoreceptor cells, the analysis of the outer nuclear layer (ONL) area (marked yellow in Figure 10) as a percentage of the corresponding CNV area (mark red in Figure 10) was performed for each group. All of the figures were taken under light microscopy. The area of ONL and the area of CNV were manually selected and cut by using ImageJ software 9.0. In some histological figures, the CNV or ONL area was severely distorted or structurally incomplete and was excluded from the analysis. The specific number of eyeballs with CNV included in each group is shown in Table 8.

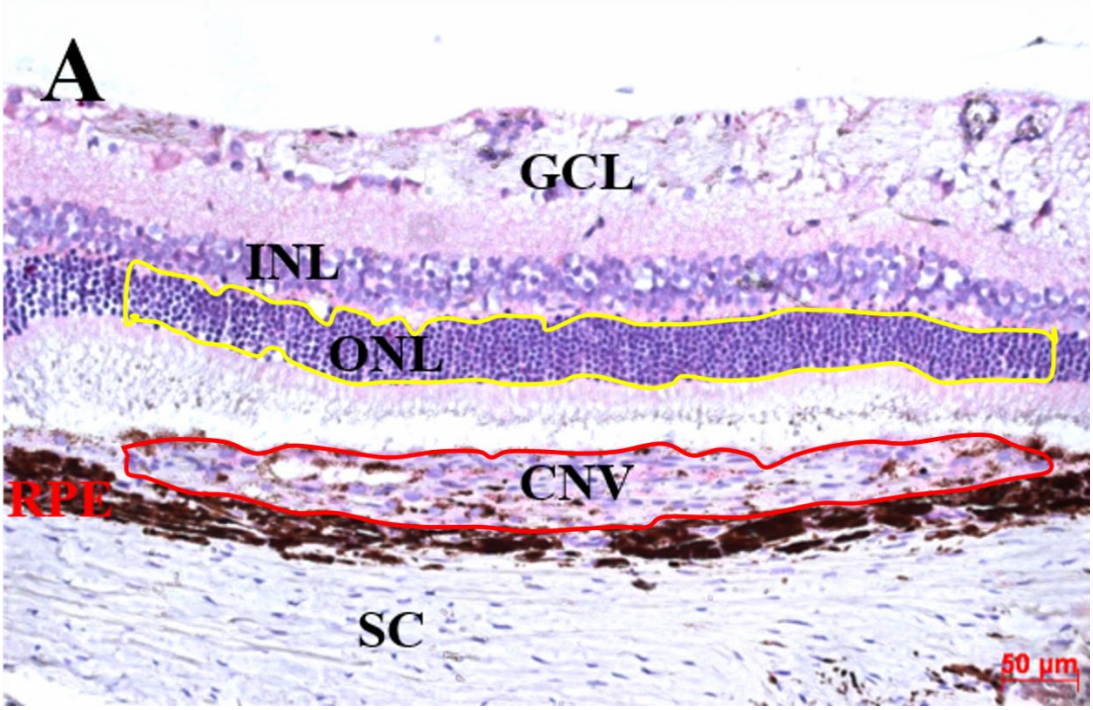

Figure 10. Representative figure of the area of CNV and the corresponding outer nuclear layer (ONL) area. The CNV area is marked by a-red line and the ONL area is marked by a yellow line. GCL: ganglion cell layer; INL: inner nuclear layer; ONL: outer nuclear layer; RPE, retinal pigment epithelium; SC: sclera. Scale bar = 50μm.

Table 8. The number of eyes included in each group for the analysis of the outer nuclear layer (ONL) area as a percentage of the corresponding CNV area

Groups	Number of eyes
Group 1 (Control group)	4
Group 2 (Vehicle treatment)	3
Group 3 (PEDF treatment)	5

Group 4 (Avastin treatment)	6
Group 5 (PEDF + Avastin treatment)	6

3.18 Statistics

The data were analyzed by using IBM SPSS Statistics 25.0 software. A one-way ANOVA test was used for the multiple comparisons of the different groups when the data followed a normal distribution. The value was described by mean ± SD. The number of TUNEL-positive nuclei per 1000μm above the CNV area was analyzed between each group by the ANOVA test. If the data was an abnormal distribution, the analysis was performed by the Wilcoxon test, and the value was described by percentile (M1, M3). The area of collagen and the area of VEGF-positive immunohistochemical staining in the CNV to the total CNV area, and the outer nuclear layer (ONL) area as a percentage of the corresponding CNV area were analyzed between each group by the Wilcoxon test with the Kruskal-Wallis test. The percentage of PEDF-positive immunohistochemical staining area in the CNV to the total CNV area was analyzed by the Wilcoxon test with the Kolmogorov-Smimov Z test (because this is a comparison of two sets of non-normally distributed data). The maximal thickness of CNV was compared between each group by the Tukey HSD test with the Steel-Dwass test. For the entire analysis, the statistical significance was set at $P < 0.05$.

4 Materials and methods for the *ex vivo* experiment

4.1 Animals and ethics statement

For the study, adult Long Evans rats (Charles River, Sulzfield, Germany) were used. The experiments were conducted in accordance with the ARVO statement for use of animals in ophthalmic and visual research and were in compliance with §4 section 3 of the German law on animal protection. They were reviewed and approved by the "Einrichtung für Tierschutz, Tierärztlichen Dienst und Labortierkunde, Tübingen". The rats were sacrificed by exposure to isoflurane in their cages until their breathing stopped, and then left for an additional minute, after that the animals were euthanized by cervical dislocation. Four pigmented rats were used to detect the oxygen concentration in the vitreous *in vivo*. The detailed information of the eyes is shown in Table 9.

Table 9. List of rats for the experiments

	4 pigmented rats (8	4 eyes	Oxygen concentration measurement *in vivo*

22 pigmented rats	eyes)	4 eyes	Oxygen concentration measurement *ex vitro*
	18 pigmented rats (36 eyes)	5 eyes	PEDF treatment and incubated for 14 hours and fixed for EM
		5 eyes	PEDF treatment and incubated for 14 hours and fixed for IHC
		6 eyes	Vehicle treatment and incubated for 14 hours and fixed for IHC
		5 eyes	Without treatment and incubated for 14 hours and fixed for EM
		5 eyes	Without treatment and incubated for 14 hours and fixed for IHC
		4 eyes	Fixed immediately for EM
		6 eyes	Fixed immediately for IHC
6 albino rats	3 albino rats (6 eyes)	3 eyes	PEDF treatment and incubated for 14 hours and fixed for EM
		3 eyes	Fixed immediately for EM
	3 albino rats (6 eyes)	6 eyes	Fixed immediately for IHC

PEDF: pigment epithelial derived factor; IHC: immunohistochemistry; EM: electron microscope

4.2 Investigation of the oxygen pressure in the vitreous of the living rats

Each analysed rat was anesthetized using an isoflurane-narcosis unit. The unit provided 3.5% isoflurane-air mixture into a mask fixed on the rat's head. The rat was kept on a cushion at 37°C. For the measurements we used the WPI oxygen micro unit (WPI, Sarasota USA) according to the manufacturer's instructions. After application of local anesthesia on the eye (Novesine, Puchheim, Germany) and puncturing of the sclera with a sharp needle, the syringe -like oxygen sensor (BioOxy Sensor, WPI) fixed on a micromanipulator system was inserted into the vitreous of the rat's eye. The system's own temperature sensor (°C) was applied rectally (Figure 11 A). After the experiment

the animals were euthanised and the unanalysed eye was used for the *ex vivo* analysis. Four rats were used for the analyses.

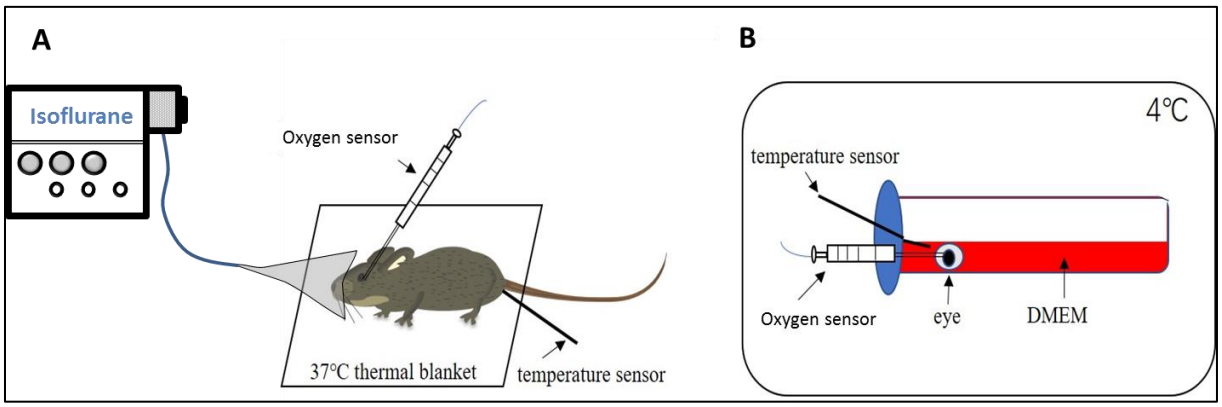

Figure 11. Schematic setup of the measurement of the oxygen concentration in the vitreous of the living rats and in the enucleated rat eyes. Measurement method *in vivo* (A). Measurement method *ex vivo* (B).

4.3 Investigation of the oxygen pressure in the vitreous of the enucleated eyes

The same WPI oxygen micro unit was used for the *ex vivo* studies. After the enucleation of the rat's eye, a hole was punctured immediately in the eye behind the corneal limbus using a sharp needle and the oxygen-microsensor was inserted into the vitreous. Then, the eye was put in a 50mL tube filled with 25mL of Dulbecco's modified Eagle's medium (DMEM) solution and kept at 4°C in the refrigerator for 14 hours. The temperature sensor was kept in the medium (Figure 11 B).

4.4 Intravitreal injection

Intravitreal injections in the enucleated eyes were performed using a 10µl NanoFil syringe (Hamilton Co., Reno, NV, USA). A volume of 5µl PBS alone or 5µl PBS with 15µg of PEDF protein was injected into the vitreous through a puncture on the sclera 1 mm from the limbus.

4.5 *Ex vivo* whole eye model

Immediately after the rats were sacrificed, the rats' eyes were enucleated and put in DMEM and kept in a refrigerator at 4°C for 14 hours. Additional eyes were enucleated and fixed immediately in glutaraldehyde or in formalin for EM- and light microscopical analyses respectively and used as controls. The methods of immunohistochemistry, TUNEL-staining and electron microscopy have

been explained in the *in vivo* experimental methods, so these methods will not be repeated here.

4.6 Analysis of the ratios of the area of the vessels' lumina and endothelial cells divided by the length of the Bruch's membrane for the PEDF and PBS injected eyes

Electron micrographs (20000 X magnification) from the choriocapillaris in ten randomly selected areas in proximity to the optic nerve from each three of the PEDF and PBS treated eyes were analysed. The total area of the lumen and the total area of the endothelial cells were calculated. The results of the area were divided by the corresponding length of the Bruch's membrane associated with the vessels, to gain the area/μm of Bruch's membrane value and to make these values comparable.

4.7 Analysis of immunohistochemistry

The immunohistochemical staining intensity was quantified. The staining intensity is graded from 0 to 4. Grade 0 is completely negative and grade 4 is the most strongly stained. The schematic diagram of the staining intensity is shown in Figure 12 (for neural retina, the RPE and the choroidal vessel). For each eye, the staining intensity was evaluated for the whole neural retina, RPE and choroid under light microscopy at a magnification of 40× (The width of each image is about 350μm). From one end of the retina to the other end of retina, each field of view is given a grade according to the staining intensity.

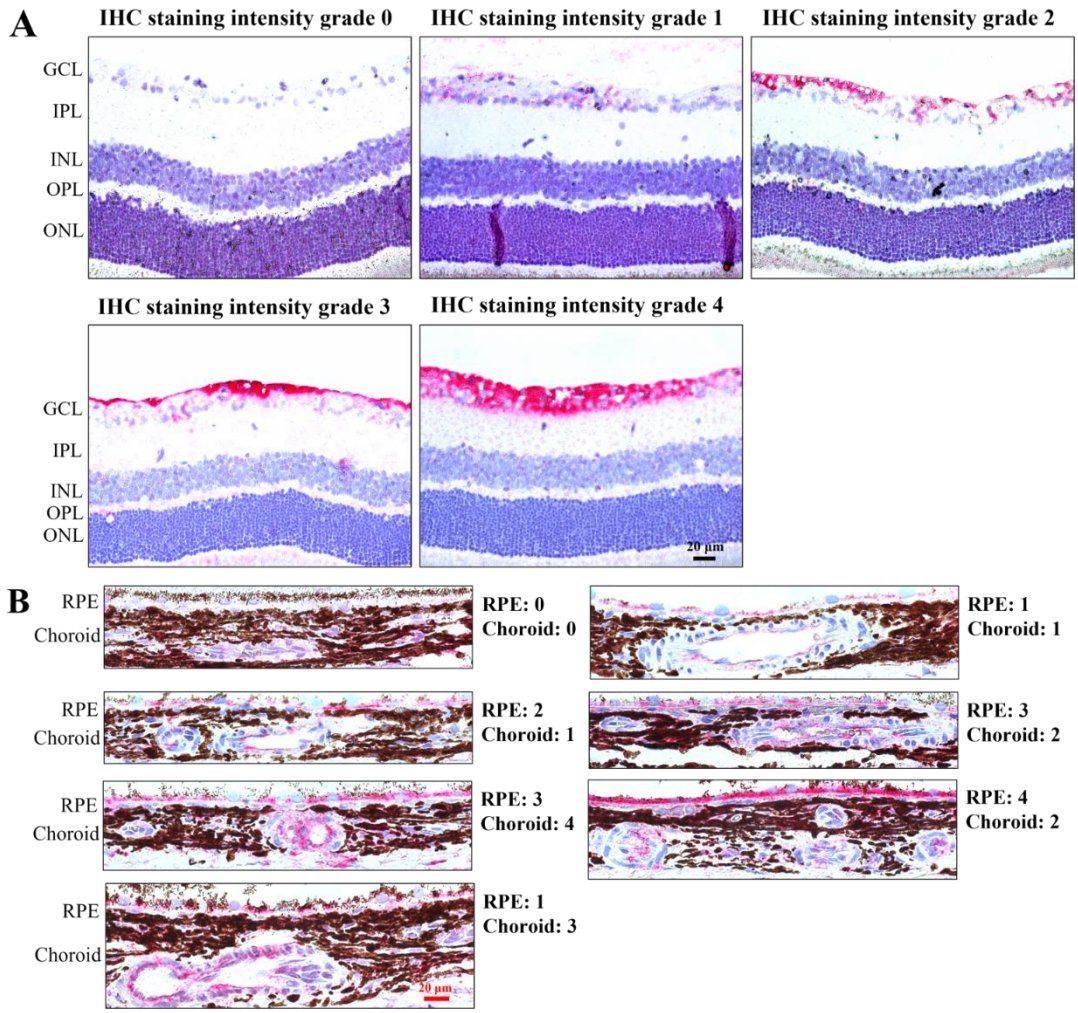

Figure 12. Grading of the immunohistochemical staining intensity in the neural retina, the RPE and the choroidal vessel. The staining intensity gradually increases from grade 0 to grade 4. Grade 0 is negative, without any staining. Grade 4 is positive, with the strongest degree of staining. GCL: ganglion cell layer; IPL: inner plexiform layer; INL: inner nuclear layer; OPL: outer plexiform layer; ONL: outer nuclear layer; RPE: retinal pigmented epithelium. Scale bar = 20μm.

4.8 Statistical Analysis

The statistical analyses were performed using the SPSS 25.0 version. The results of the area of vessel lumen and the area of endothelial cells measurements were analysed using the Student's t test. The results of TUNEL experiments were analyzed by the Wilcoxon test with the Kruskal-Wallis test (abnormal distribution) or the ANOVA test (normal distribution).

5 Results of the *in vivo* experiment

5.1 Angiography (fluorescein and indocyanine green) of the CNV

The retinal blood vessels and the CNV lesion could be clearly detected by fluorescein angiography

(FA) and indocyanine green (ICG) angiography. Three weeks after subretinal injection of AAV-VEGF-A^{165} vector, the formation of CNV was detected in 100% of the rat eyes by using FA and ICG, indicating a very high successful induction rate. As shown in the FA/ICG images, the ring-shaped hyper-fluorescent area was CNV (marked with red arrows) (Figure 13). No obvious leakages were observed in the CNV lesion. As our previous research described, it was a rat model of treatment-naïve quiescent CNV (Liu et al., 2020).

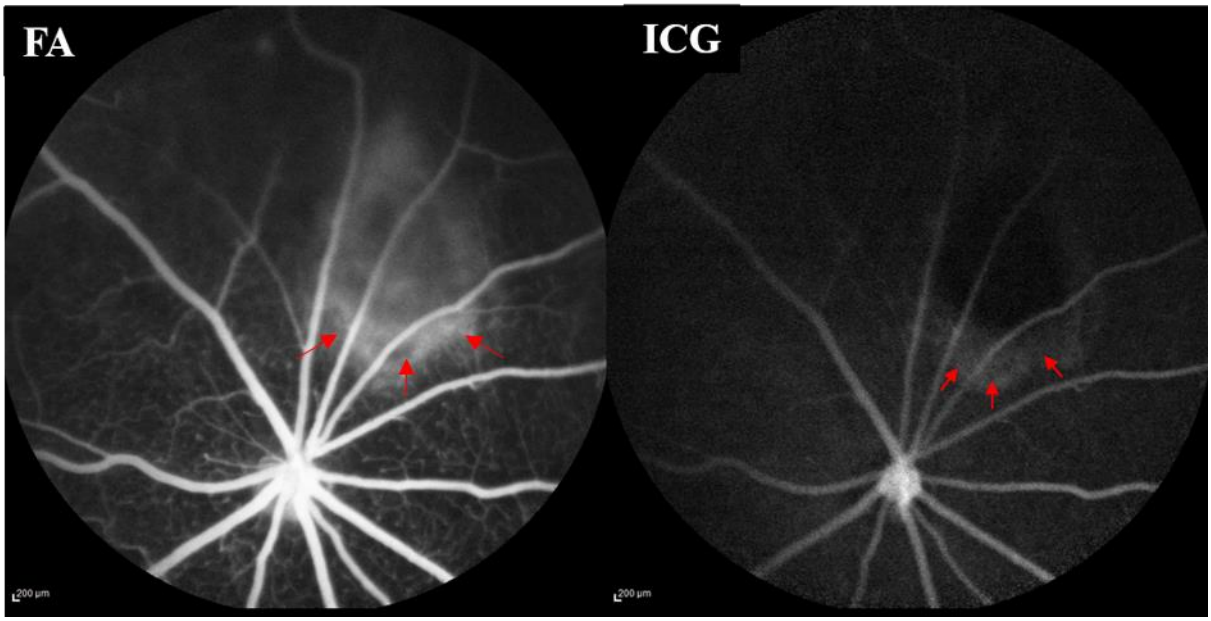

Figure 13. The fluorescein angiography (FA) and indocyanine green (ICG) angiography image from the AAV-VEGF-A^{165} vector induced quiescent CNV. The FA and ICG images are taken at the third week after subretinal injection of AAV-VEGF-A^{165} vector. The CNV lesion (shown with red arrows) is detected in the FA/ICG angiography. FA: Fluorescein angiography, ICG: Indocyanine green.

5.2 Investigation of the formation of CNV and other complications after subretinal injection and intravitreal injection

The formation of CNV was found in all the rat eyes after subretinal injection of AAV.VEGFA^{165}. Before the end of the experiment, cataract caused by intravitreal injection was found in 6/60 rat eyes, and 3 rats died during or after anesthesia. It is not possible to obtain the CNV thickness data in the eyes of rats with cataract through OCT examination. The eyes of the rat that died after the experiment cannot be used for histological examination. The detailed information is shown in Table 10.

Table 10. The information of each group of rats during the experiment

Groups	Rat number	Third week	Fourth week	Sixth week	Seventh week

Group 1 (Control group)	1	CNV (√)			
	2	CNV (√)			
	3	CNV (√)			
	4	CNV (√)			
	5	CNV (√)			
	6	CNV (√)			
Group 2 (Vehicle treatment)	7	CNV (√)			
	8	CNV (√)			
	9	CNV (√)	cataract (right)		
	10	CNV (√)	cataract (right)		
	11	CNV (√)		Dead during EP	
	12	CNV (√)			
Group 3 (PEDF treatment)	13	CNV (√)			
	14	CNV (√)			
	15	CNV (√)	cataract (right)		
	16	CNV (√)		cataract (left)	
	17	CNV (√)	Dead after EP		
	18	CNV (√)	cataract (both)		
Group 4 (Avastin treatment)	19	CNV (√)			
	20	CNV (√)			
	21	CNV (√)	Dead during EP		
	22	CNV (√)			
	23	CNV (√)			
	24	CNV (√)	cataract (both)		
Group 5 (PEDF + Avastin treatment)	25	CNV (√)			cataract (right)
	26	CNV (√)			
	27	CNV (√)			
	28	CNV (√)			
	29	CNV (√)			
	30	CNV (√)	cataract (both)		

EP: Experiment

5.3 Investigation of the maximal thickness of CNV

The thickness of the CNV lesion (the hyper-fluorescence area in Figure 14) could be clearly detected by SLO/OCT (shown with a red arrow in Figure 14), and no exudation was found in the subretinal or intraretinal space from the OCT image, which further proved that it was quiescent CNV (Liu et al., 2020). The maximal thickness of CNV (marked with a yellow double-headed arrow in Figure 14) at the third week, fourth week, sixth week and seventh week was compared within each group and the results are shown in Figure 15 (A-E). The Avastin treatment group showed the most significant reduction of the maximal CNV thickness.

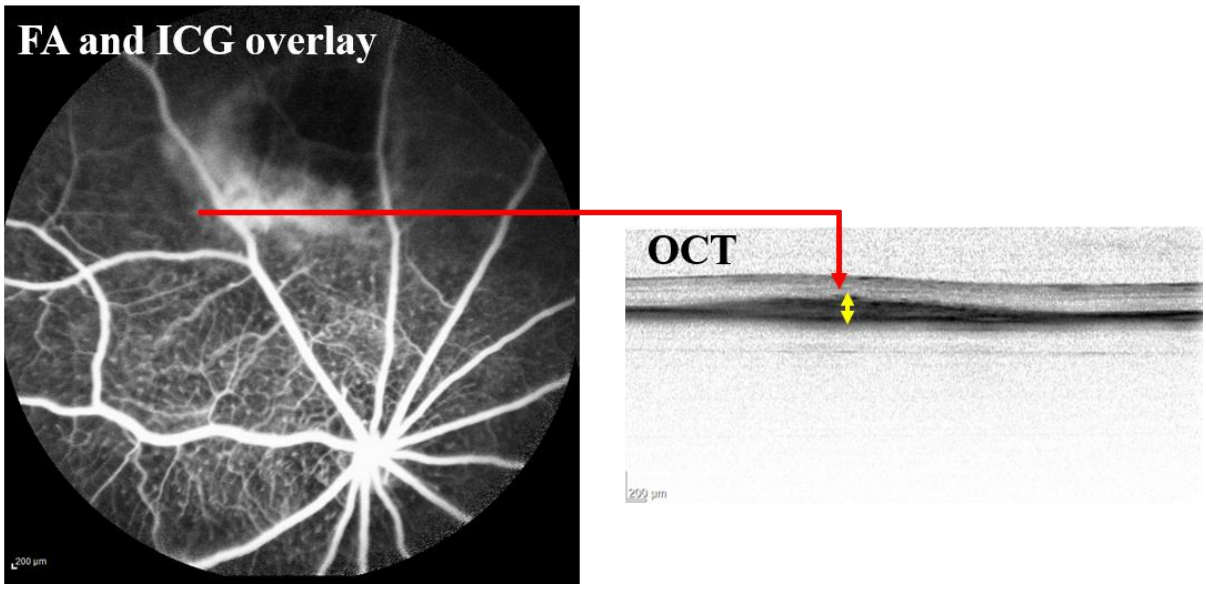

Figure 14. Fluorescein and indocyanine green angiography (FA and ICG) and the corresponding optical coherence tomography (OCT). The thickness of CNV was measured by scanning laser ophthalmology optical coherence tomography (SLO/OCT). The whole area of the CNV lesion was measured in each eye and the maximal thickness part (yellow double-headed arrow) of the CNV was used for statistical analysis. Scale bar: 200µm.

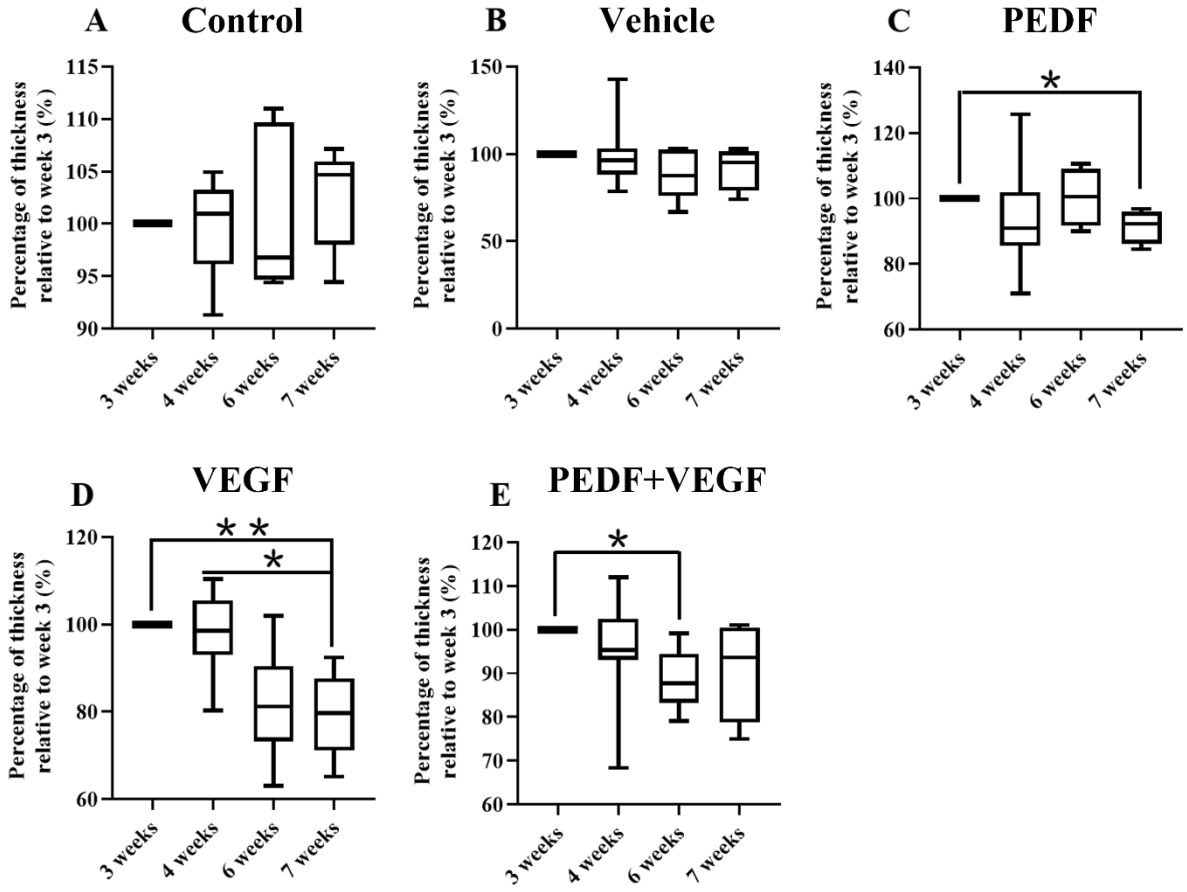

Figure 15. OCT measurement of the maximal thickness of CNV. For each group, the maximal thickness of CNV at 3 weeks was set as 100 percent, and the maximal CNV thickness at 4 weeks,

6 weeks and 7 weeks was normalized to the maximal thickness at 3 weeks. The maximal thickness of CNV was not significantly different between each week in group 1 (AAV-VEGF-A^{165} alone) (**A**) and group 2 (AAV-VEGF-A^{165} + Vehicle) (**B**). The maximal thickness of CNV at 7 weeks (91.455±5.175, n=4) is significantly reduced compared to the maximal thickness at 3 weeks (100±0.0, n=12) in group 3 (AAV-VEGF-A^{165} + PEDF) (**C**). The maximal thickness of CNV at 7 weeks (79.391±9.573, n=6) is significantly reduced compared to the maximal thickness at 4 weeks (97.707±9.538, n=11) and 3 weeks (100±0.0, n=11) in group 4 (AAV-VEGF-A^{165} + Avastin) (**D**). The maximal thickness of CNV at 6 weeks (88.537±7.164, n=6) is significantly reduced compared to the maximal thickness at 3 weeks (100±0.0, n=12) in group 5 [AAV-VEGF-A^{165} + (PEDF + Avastin)] (**E**). Data were analyzed by the Tukey HSD test with the Steel-Dwass test ($^{*}P < 0.05$, $^{**}P < 0.01$). (n: number of eyes).

5.4 The information of CNV found in the paraffin-embedded sections

Many eyes didn't show evidence of the existence of CNV. The reasons may be that the CNV was too small to be found, or the CNV was lost during the slicing process. The information of CNV found in the paraffin sections was shown in Table 11.

Table 11. The information of CNV found in the paraffin-embedded sections

Groups	Rat number	Paraffin-embedded eye	CNV found in the section	Other information
Group 1 (Control group)	1	right	CNV (√)	
	2	right	CNV (√)	
	3	left	CNV (√)	
	4	left	CNV (×)	
	5	right	CNV (√)	
	6	left	CNV (√)	
Group 2 (Vehicle treatment)	7	left	CNV (√)	
	8	left	CNV (√)	
	9	left	CNV (×)	
	10	right	CNV (√)	
	11	left	CNV (√)	
	12	right	CNV (√)	
Group 3 (PEDF treatment)	13	right	CNV (√)	
	14	right	CNV (√)	
	15	right	CNV (√)	
	16	right	CNV (√)	
	17		CNV (×)	Dead after EP
	18	right	CNV (√)	
Group 4 (Avastin	19	right	CNV (√)	
	20	right	CNV (√)	
	21	right	CNV (√)	

treatment)	22	left	CNV (√)	
	23	right	CNV (√)	
	24	right	CNV (√)	
Group 5 (PEDF + Avastin treatment)	25	left	CNV (√)	
	26	right	CNV (√)	
	27	right	CNV (√)	
	28	right	CNV (√)	
	29	right	CNV (√)	
	30	left	CNV (√)	

EP: Experiment. √ :with CNV; ×: without CNV

5.5 Investigation of the mature and immature collagen in the CNV

Picrosirius red staining worked well at staining mature collagen and immature collagen in this quiescent CNV model (Figure 16A). The mature (orange-red color) and immature (green-yellow color) collagen can be easily distinguished under the polarized microscopy (Figure 16B). There was no significant difference between each group in the percentage of mature collagen (P = 0.095), immature collagen (P = 0.279) and the total collagen (P = 0.091) (Figure 16C, D and E). However, from the analysis of collagen in this quiescent CNV model, it could be found that the percentage of immature collagen was higher than that of mature collagen. The collagen content in this quiescent CNV model was mainly immature collagen, which meant that the CNV was still in progress.

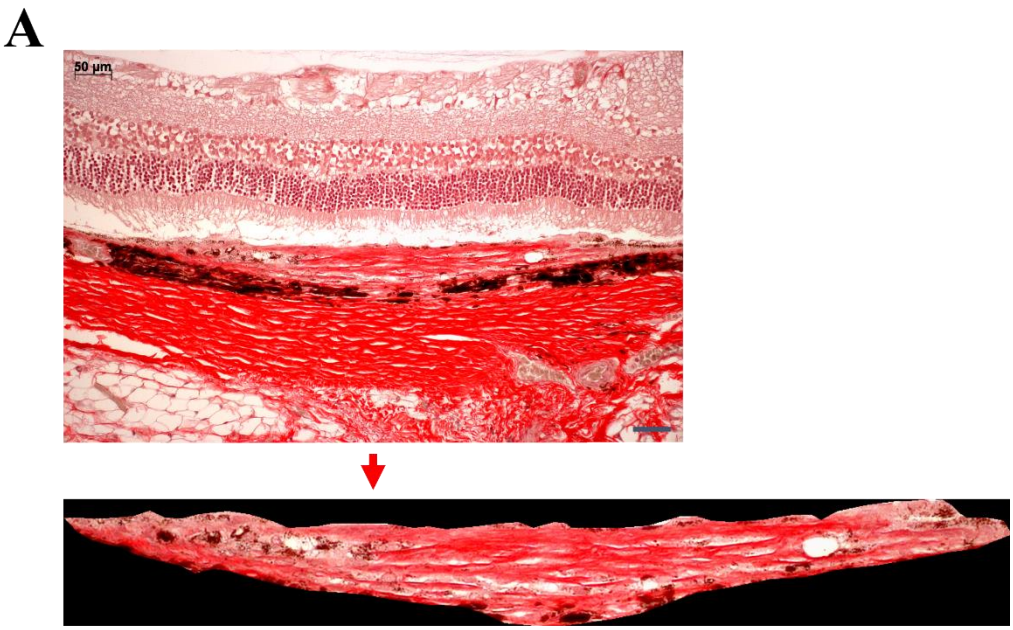
A
50 μm
choroidal neovascularization (CNV)
B
green-yellow = immature collagen
orange-red = mature collagen

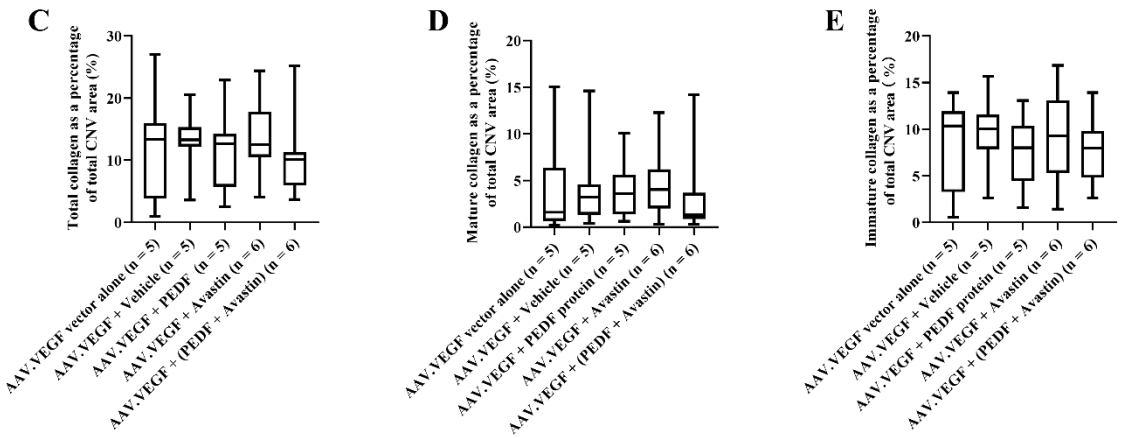
C
Total collagen as a percentage of total CNV area (%)
0
10
20
30
AAV.VEGF vector alone (n = 5)
AAV.VEGF + Vehicle (n = 5)
AAV.VEGF + PEDF (n = 5)
AAV.VEGF + Avastin (n = 6)
AAV.VEGF + (PEDF + Avastin) (n = 6)
D
Mature collagen as a percentage of total CNV area (%)
0
5
10
15
20
AAV.VEGF vector alone (n = 5)
AAV.VEGF + Vehicle (n = 5)
AAV.VEGF + PEDF protein (n = 5)
AAV.VEGF + Avastin (n = 6)
AAV.VEGF + (PEDF + Avastin) (n = 6)
E
Immature collagen as a percentage of total CNV area (%)
0
5
10
15
20
AAV.VEGF vector alone (n = 5)
AAV.VEGF + Vehicle (n = 5)
AAV.VEGF + PEDF protein (n = 5)
AAV.VEGF + Avastin (n = 6)
AAV.VEGF + (PEDF + Avastin) (n = 6)

Figure 16. Picrosirius red stain of choroidal neovascularization (CNV) and the statistics of mature and immature collagen in the CNV. (A): Representative picrosirius red stain image under the light microscope at ×20 magnification shows the area of CNV. (B): Representative picrosirius red stain image under the polarized microscope at ×20 magnification shows the content of collagen in the CNV. Green-yellow color indicates immature collagen, and orange-red color indicates mature collagen. Scale bar = 50μm. There is no significant difference between each group in the percentage of total collagen (P = 0.091) (C), mature collagen (P = 0.095) (D), and immature collagen (P = 0.279). Data were analyzed by the Wilcoxon test with the Kruskal-Wallis test. (n: number of eyes).

5.6 Investigation of the collagen Ⅳ in the CNV

Type IV collagen is localized to the established vessels and is a prominent structural component of blood vessel basement membranes (Figure 17A). Collagen IV is significantly reduced in the intravitreal injection eyes (Vehicle treatment, PEDF treatment, Avastin treatment and PEDF/Avastin treatment eyes) compared to the non-injection control eyes (Figure 17B).

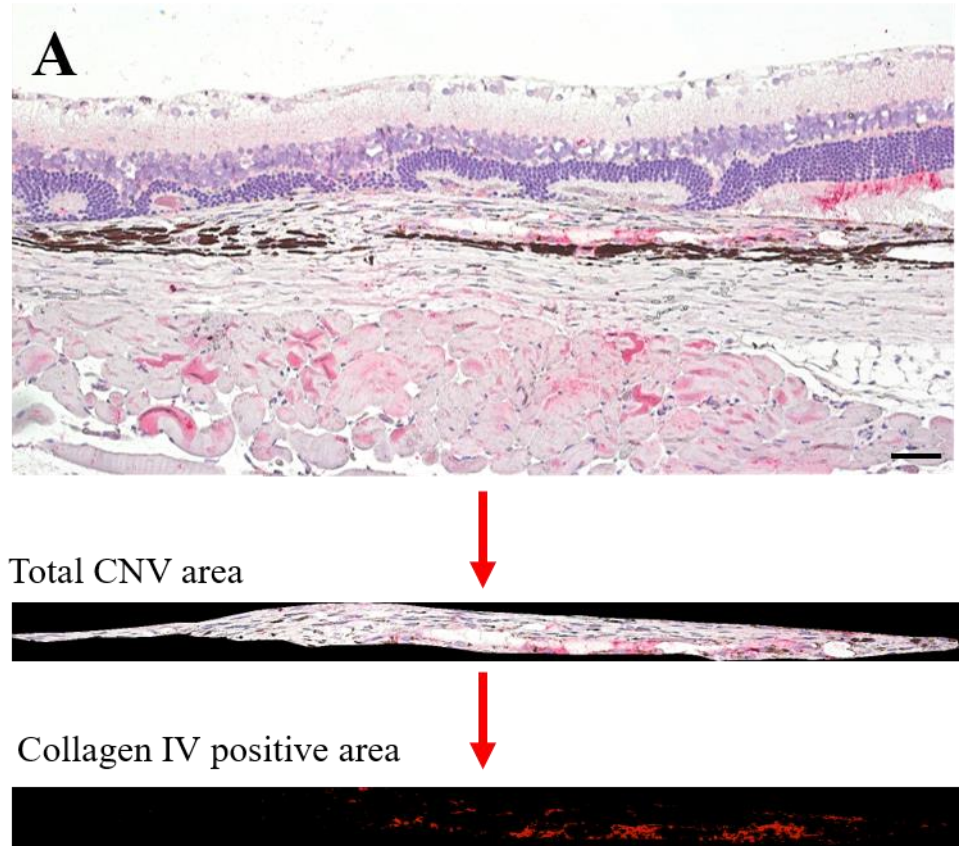

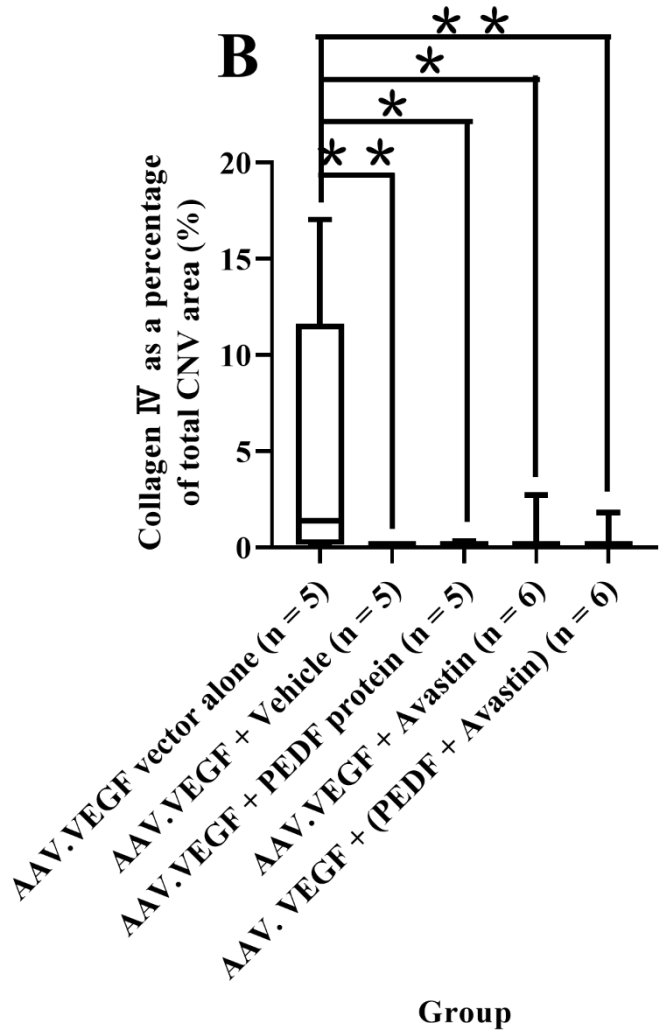

Figure 17. The positive area of collagen IV in the CNV to the total area of CNV. (A): Representative image of immunohistochemical staining of collagen IV. Scale bar = 50μm. (B): The positive collagen IV area as a percentage of the total CNV area. Compared to the AAV.VEGF vector alone group (0.1262, 11.6234), the positive collagen Ⅳ area as a percentage of the total CNV area is significantly reduced in the PEDF/Avastin treatment group (0.0028, 0.0322) ($P < 0.001$), the Avastin treatment group (0.0083, 0.0817) ($P = 0.011$), the PEDF treatment group (0.0047, 0.1402) ($P = 0.002$), and the vehicle treatment group (0.0028, 0.0322) ($P < 0.001$). The value is described by percentile (M1, M3). Data were analyzed by the Wilcoxon test with the Kruskal-Wallis test. ($^{*}P < 0.05$; $^{**}P < 0.001$). (n: number of eyes).

5.7 Immunohistochemical staining of VEGF in the CNV

The VEGF was strongly detected in the CNV area for each group (Figure 18A), as the CNV was induced by subretinal injection of AAV.VEGF-A^{165} vector, which continuously expresses VEGF. Compared to the control group (12.52, 21.16) and the PEDF treatment group (12.11, 32.80), the percentage of VEGF-immunopositive staining area was significantly reduced in the PEDF/Avastin treatment group (5.10, 13.91) ($P < 0.05$) (Figure 18B). Figure 18A shows that VEGF staining is

stronger in the left part of the retina than the right part of the retina. I checked the immunostaining of the nearby specimen which showed the same staining result. This may be related to the uneven distribution of the injected AAV.VEGF-A^{165} vector in the retina.

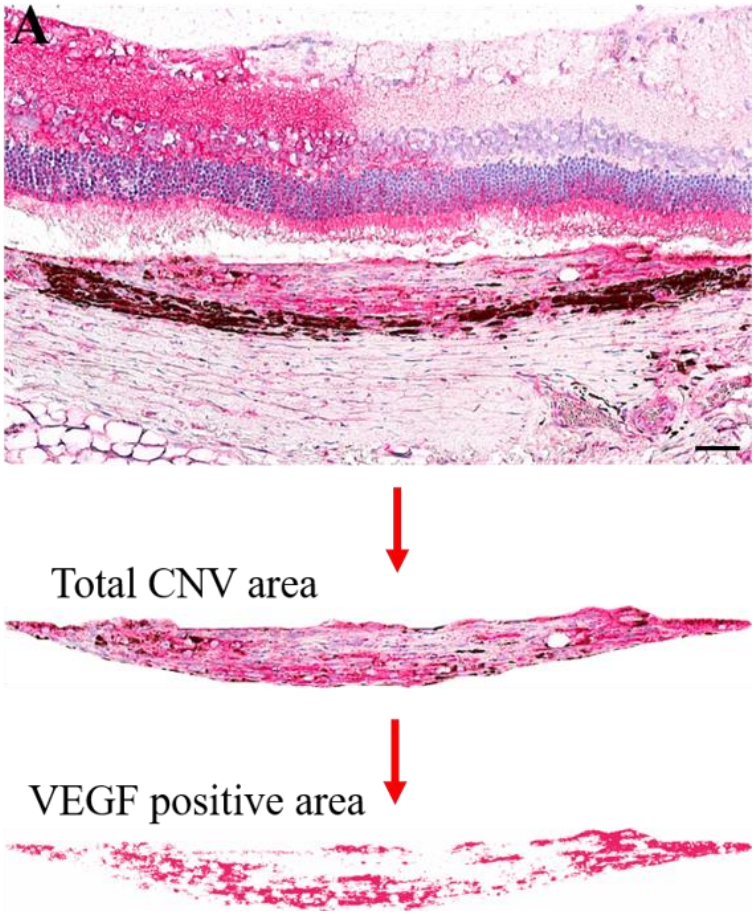

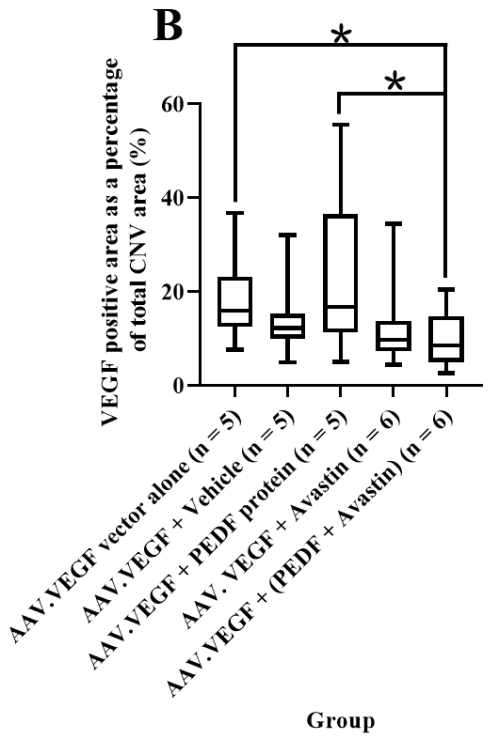

Figure 18. The positive area of VEGF in the CNV to the total area of CNV. (A): Representative image of immunohistochemical staining of VEGF. The total area of CNV and the positive area of VEGF in the CNV were selected by ImageJ software. Scale bar = 50μm. (B): VEGF positive area as a percentage of the total CNV area in each group. The percentage of VEGF positive area to the total CNV area is significantly reduced in the PEDF/Avastin treatment group (5.10, 13.91) compared to the AAV.VEGF alone group (12.52, 21.16) ($P = 0.031$) and the PEDF treatment group (12.11, 32.80) ($P = 0.046$). The value is described by percentile (M1, M3). Data were analyzed by the Wilcoxon test with the Kruskal-Wallis test. ($^{*}P < 0.05$). (n: number of eyes).

5.8 Immunohistochemical staining of PEDF in the CNV

The CNV was stained with anti-PEDF antibody (anti-human PEDF antibody) to confirm the content of the injected PEDF protein in the PEDF-treatment group and the PEDF/Avastin treatment group. PEDF was weakly detected in the quiescent CNV area (Figure 19A). The reason for the low level of human PEDF protein in the CNV might be attributed to the high level of VEGF which inhibits PEDF. PEDF positive area as a percentage of total CNV area showed no significant difference between the PEDF treatment group and the PEDF/Avastin treatment group (Figure 19B).

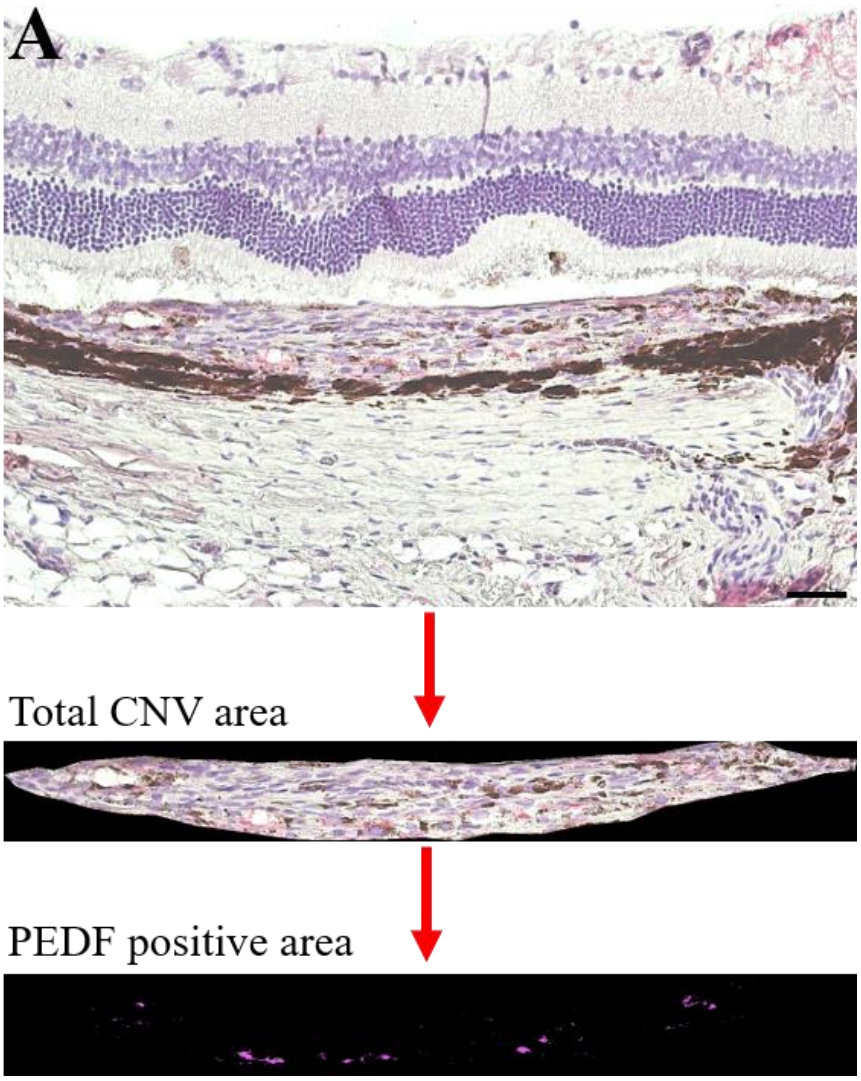
A
Total CNV area
PEDF positive area

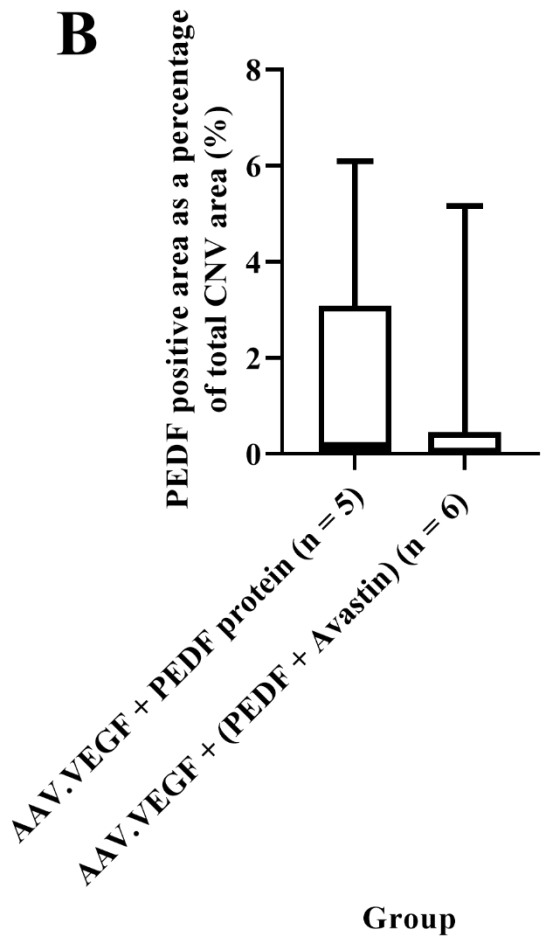

Figure 19. The positive area of PEDF in the CNV to the total area of CNV. (A): Representative image of PEDF staining. The total area of CNV and the area of PEDF-positive immunohistochemical staining were measured by ImageJ software. Scale bar = 50μm. (B): PEDF positive area as a percentage of total CNV area. There is no significant difference between the PEDF treatment group (0.00, 3.09) and the PEDF/Avastin treatment group (0.005, 0.45) (P = 0.585). The value is described by percentile (M1, M3). Data were analyzed by the Wilcoxon test with the Kolmogorov-Smimov Z test. (n: number of eyes).

5.9 The outer nuclear layer area as a percentage of the corresponding CNV area

The effect of CNV on the outer nuclear layer was detected, and the percentage of the area of outer nuclear layer (ONL) to the corresponding CNV area was analyzed for each group. Figure 20A shows an example of the PEDF treatment group. The ONL above the CNV area keeps a normal structure and does not become thin or shrunk. Figure 20B shows an example of the Avastin treatment group. Part of the ONL above the CNV area becomes thin and many ONL cells disappear. The percentage was significantly increased in the PEDF treatment group compared to the control group (P <

0.05), the vehicle treatment group ($P < 0.05$) and the Avastin treatment group ($P < 0.001$) (Figure 20C). Regarding the number of intraocular injections, I separately analyzed the data of an intraocular injection given once and an intraocular injection given twice. The results are shown in Figure 21. The intraocular injection given twice showed a much more obvious significant difference than the intraocular injection given once.

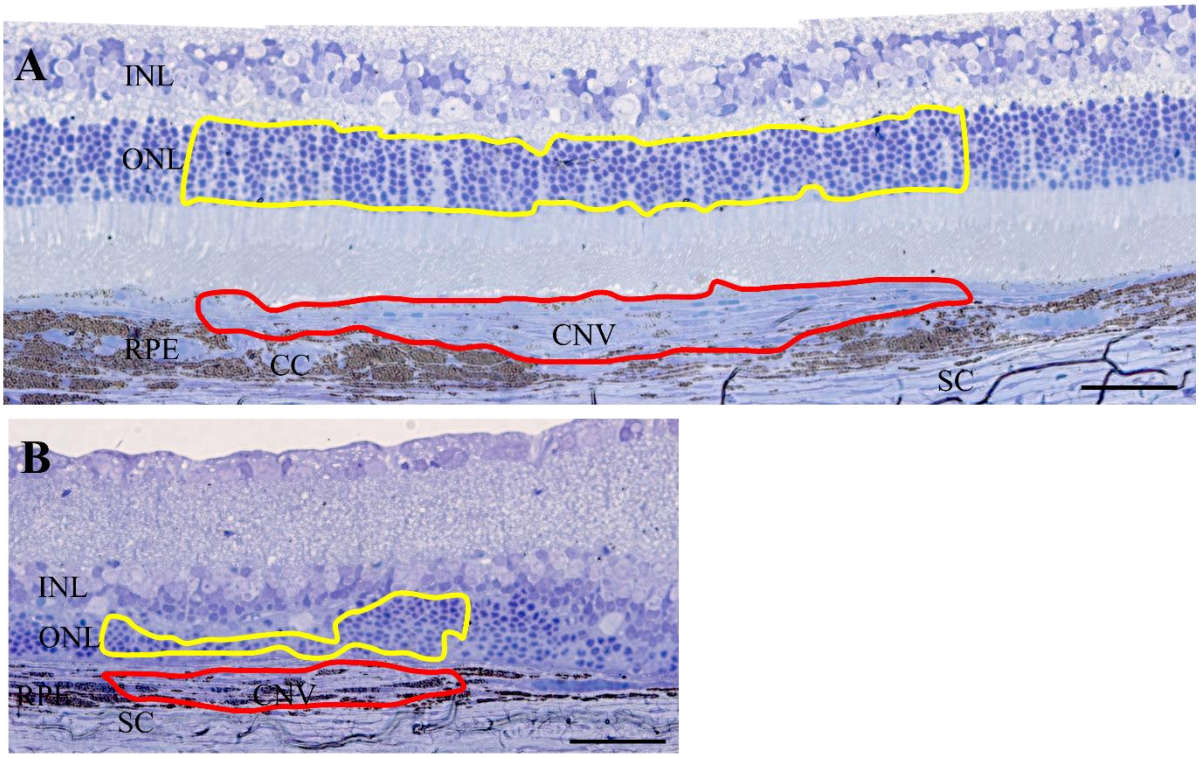

Figure 20. The analysis of the ONL area as a percentage of the corresponding CNV area. (A) Light microscopical image of a CNV section from the PEDF treatment group. The structure of the ONL layer (marked with a yellow line) above the corresponding CNV area (marked with red line) is nearly normal. (B) Light microscopical image of a CNV section from the Avastin treatment group. The ONL layer (marked with a yellow line) above the corresponding CNV area (marked by a red line) becomes thin and many ONL cells disappear. (C) The percentage of the ONL area to the corresponding CNV area. The percentage is significantly increased in the PEDF treatment group (92.29, 120.27) compared to the control group (63.50, 99.74) ($P = 0.004$), the vehicle treatment group (71.45, 89.62) ($P = 0.001$) and the Avastin treatment group (55.11, 75.59) ($P < 0.001$). The percentage is significantly increased in the PEDF/Avastin treatment group (78.61, 113.18) compared to the Avastin treatment group (55.11, 75.59) ($P < 0.001$). The value is described by percentile (M1, M3). Data were analyzed by the Wilcoxon test with the Kruskal-Wallis test. (n: number of eyes). ($^{*}P < 0.05$, $^{**}P < 0.001$). INL: inner nuclear layer; ONL: outer nuclear layer; RPE, retinal pigment epithelium; CNV: choroidal neovascularization; SC: sclera. Scale bar = 50μm.

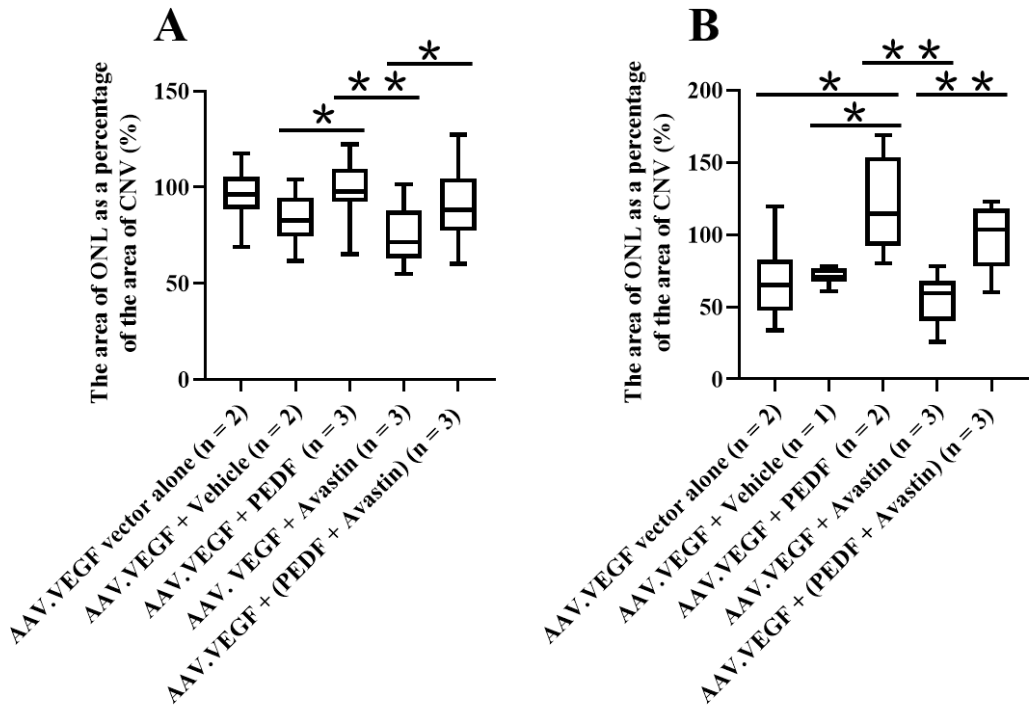

Figure 21. The analysis of the ONL area as a percentage of the corresponding CNV area. (A) Intravitreal injection treatment given once. The percentage is significantly increased in the PEDF treatment group (92.28, 109.68) compared to the vehicle treatment group (74.26, 94.73) ($P = 0.006$) and the Avastin treatment group (63.14, 87.97) ($P < 0.001$). The percentage is significantly increased in the PEDF/Avastin treatment group (77.33, 104.51) compared to the Avastin treatment group ($P = 0.003$). The value is described by mean ± SD. Data were analyzed by the one-way ANOVA test. (B) Intravitreal injection treatment given twice. The percentage is significantly increased in the PEDF treatment group (92.26, 153.65) compared to the control group (47.26, 82.61) ($P = 0.001$), the vehicle treatment group (67.26, 76.54) ($P = 0.046$) and the Avastin treatment group (40.42, 67.96) ($P < 0.001$). The percentage is significantly increased in the PEDF/Avastin treatment group (77.97, 117.97) compared to the Avastin treatment group ($P < 0.001$). The value is described by percentile (M1, M3). Data were analyzed by the Wilcoxon test with the Kruskal-Wallis test. (n: number of eyes). ($^{*}P < 0.05$, $^{**}P < 0.001$).

5.10 Analysis of TUNEL staining of the retina above the CNV

The apoptosis of the neural retina above the CNV area was analyzed. The TUNEL-positive cell was undetectable in the ganglion cell layer and the inner nuclear layer (as the eyes were fixed by formalin immediately). Very few TUNEL-positive cells were detected in the outer nuclear layer (ONL), and the positive staining cells were mainly located at the junction of ONL and CNV (Figure 22K-P). Compared to the vehicle treatment group (2.26 ± 0.95), the number of TUNEL-positive cells in the ONL per 1000μm was significantly reduced in the PEDF treatment group (0.95 ± 0.60) ($P < 0.001$), the Avastin treatment group (1.21 ± 0.63) ($P < 0.001$) and the PEDF/Avastin treatment group (1.30 ± 0.69) ($P < 0.001$) (Figure 22Q).

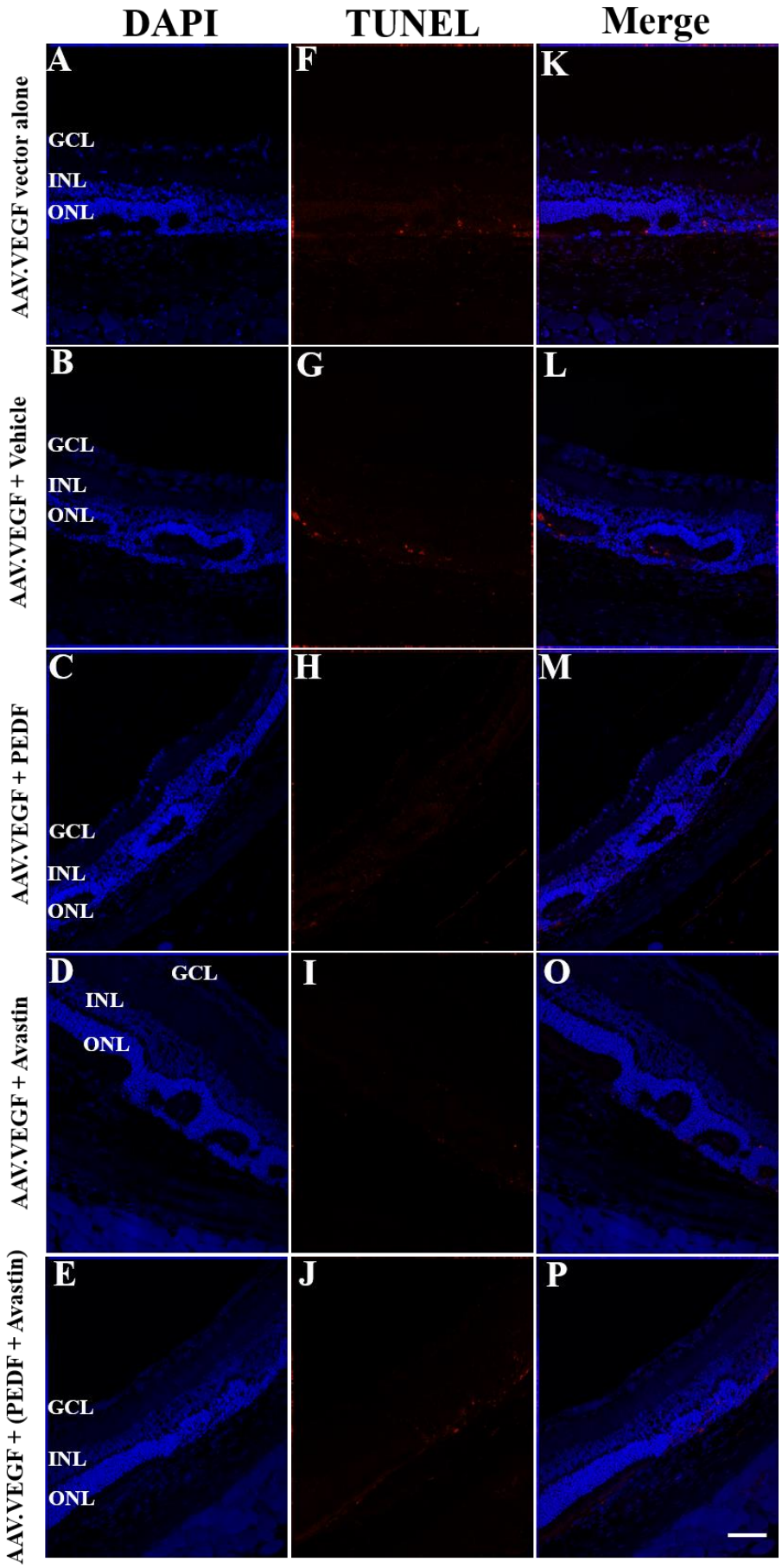
DAPI
TUNEL
Merge
AAV.VEGF vector alone
AAV.VEGF + Vehicle
AAV.VEGF + PEDF
AAV.VEGF + Avastin
AAV.VEGF + (PEDF + Avastin)
A
B
C
D
E
F
G
H
I
J
K
L
M
O
P
GCL
INL
ONL

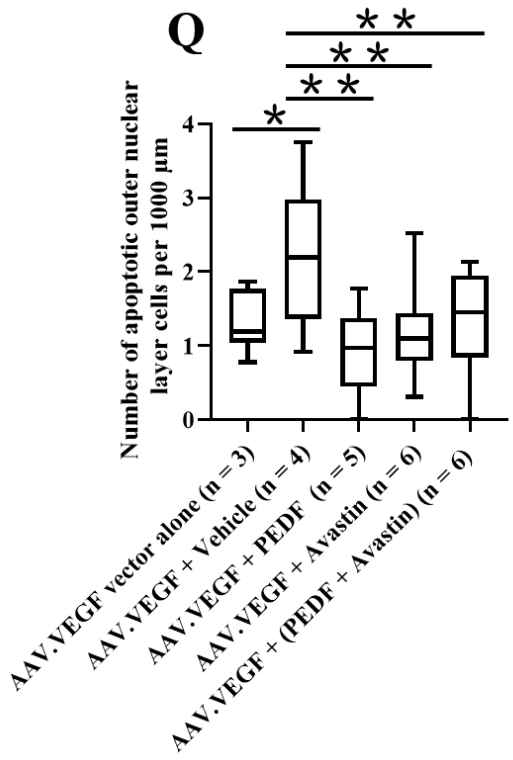

Figure 22. **Representative immunofluorescence staining of TUNEL in the retina above CNV.** Figures **A-E** show the DAPI counterstain, figures **F-J** show TUNEL-positive staining (red) and figures **K-P** show the merged TUNEL/DAPI overlay. Figure **Q** shows the number of TUNEL-positive cells in the outer nuclear layer cells per 1000µm. Compared to the vehicle treatment group (2.26 ± 0.95), the number of TUNEL-positive cells was significantly reduced in the control group (1.32 ± 0.13) *(*$P = 0.002$), the PEDF treatment group (0.95 ± 0.60) ($P < 0.001$), the Avastin treatment group (1.21 ± 0.63) ($P < 0.001$) and the PEDF/Avastin treatment group (1.30 ± 0.69) ($P < 0.001$). ($^{*}P < 0.05$, $^{**}P < 0.001$). (n: number of eyes). The value is described by Mean ± SD. Data were analyzed by a one-way ANOVA test. The TUNEL-analysis was performed using the in-situ cell death detection TMR red TUNEL kit as recommended by the manufacturer. GCL: ganglion cell layer; INL: inner nuclear layer; ONL: outer nuclear layer. Scale bar = 50µm.

6 Results of the *ex vivo* experiment

6.1 Intravitreal oxygen saturation eyes from living rats and the *ex vivo* eyes

The value of oxygen concentration in the vitreous of living rats is around 16.4% of the oxygen concentration in the air (Figure 23A). The value of oxygen concentration in the vitreous of the incubated eyes was gradually reduced and fell to half of the initial value (50%) within approximately 400 minutes (Figure 23B). These results showed that there was hypoxia in the vitreous of the incubated eyes.

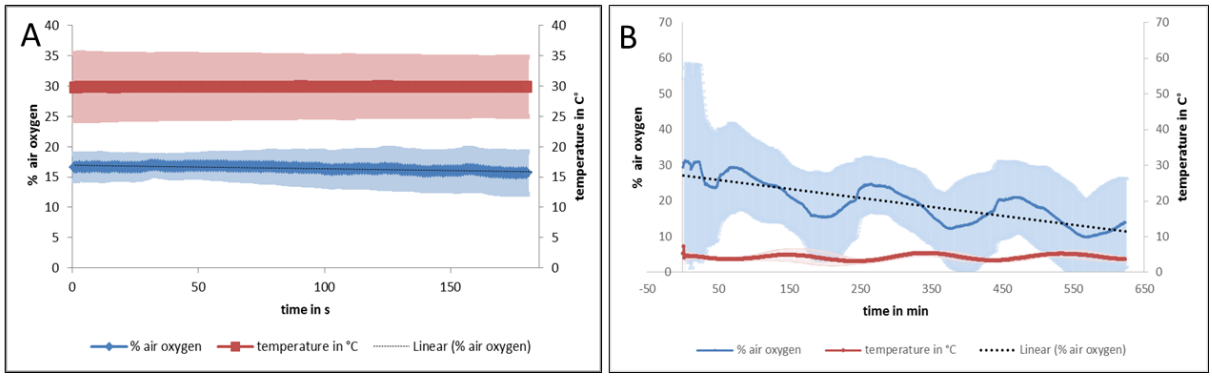

Figure 23. The results of oxygen saturation combined with temperature in the living rats and the enucleated eyes. (A) The value of oxygen saturation in the vitreous of the living rats (n = 4). (B) The value of oxygen saturation in the vitreous of the enucleated eyes (n = 4). n: number of eyes.

6.2 Light microscopic imaging of the retina and choroid

Compared to the control group (Figure 24A), the gross structure of the retinal and the choroidal tissue looks relatively abnormal in the ischemic eyes (Figure 24B). The photoreceptors and RPE cells of the ischemic eyes were slightly swollen and disorganized. The RPE cell layer was sometimes separated from the retina. Detailed information of changes in the retinal and choroidal vasculature were not observed at this level of magnification.

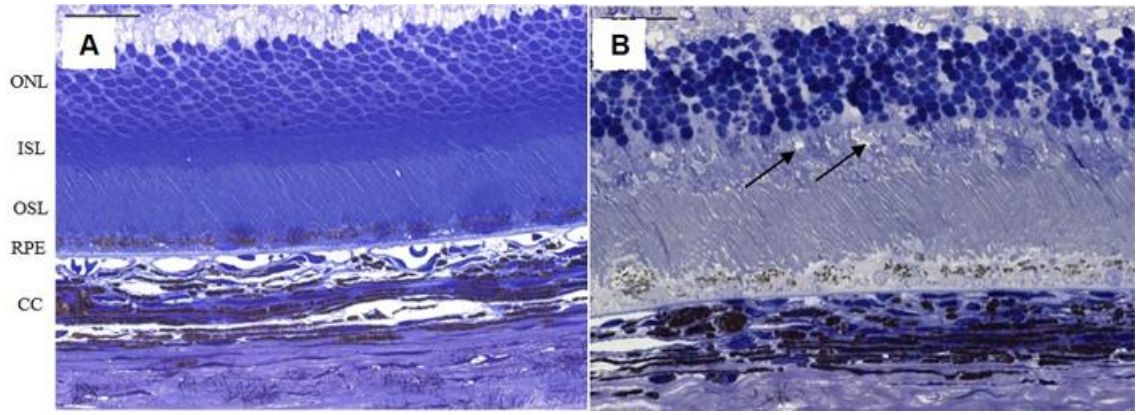

Figure 24. Representative light micrographs of a typical rat retina and choroidal tissue section and hypoxia related changes in the ischemic group. The control retina (A) contains typically structured layers. The retinas of rats after 14 hours of ischemia (B) show a slightly disorganized structure of the RPE and photoreceptors, especially within the inner segments and the nuclear layer. The photoreceptor inner segment layer (ISL) of the ischemic group is indicated by black arrows, they are slightly swollen and disorganized, as is the retinal pigment epithelium (RPE). ONL, outer nuclear layer; ISL, inner photoreceptor segments layer; OSL, outer photoreceptor segments layer; RPE, retinal pigmented epithelium; CC, choriocapillaris layer. Bar = 50µm.

6.3 The number of visual fields evaluated for IHC staining intensity

For each eye, the IHC staining intensity was evaluated for the whole retina and choroid from one end to the other under light microscopy at a magnification of 40×. The number of visual fields evaluated for each group is shown in Table 12.

Table 12. The number of visual fields evaluated for different primary antibody-staining in each group

Antibody	0-hour control group	ischemia alone group	vehicle treatment group	PEDF treatment group
VEGF-neural retina	77	71	91	79
VEGF-RPE	69	80	94	86
VEGF-choroid	69	79	94	85
PEDF-RPE	44	49	49	47
PEDF-choroid	40	50	49	49

VEGF: vascular endothelial growth factor, RPE: retinal pigmented epithelium

6.4 Expression of VEGF in the neural retina

The immunohistochemical staining for VEGF is shown in Figure 25. The immunohistochemical

staining was nearly negative in the neural retina in both the control and the ischemic retina (Figure 25A and B). The strong immunohistochemical staining was found in the vehicle treatment group (Figure 25C) and the PEDF treatment group (Figure 25D). Immunohistochemical staining intensity of VEGF in the neural retina (Figure 25E). There was a significant difference between the PEDF treatment group (1, 3) and the 0-hour control group (0, 2) ($P < 0.001$), the 14-hour ischemia alone group (0, 1) ($P < 0.001$). The value is described by percentile (M1, M3).

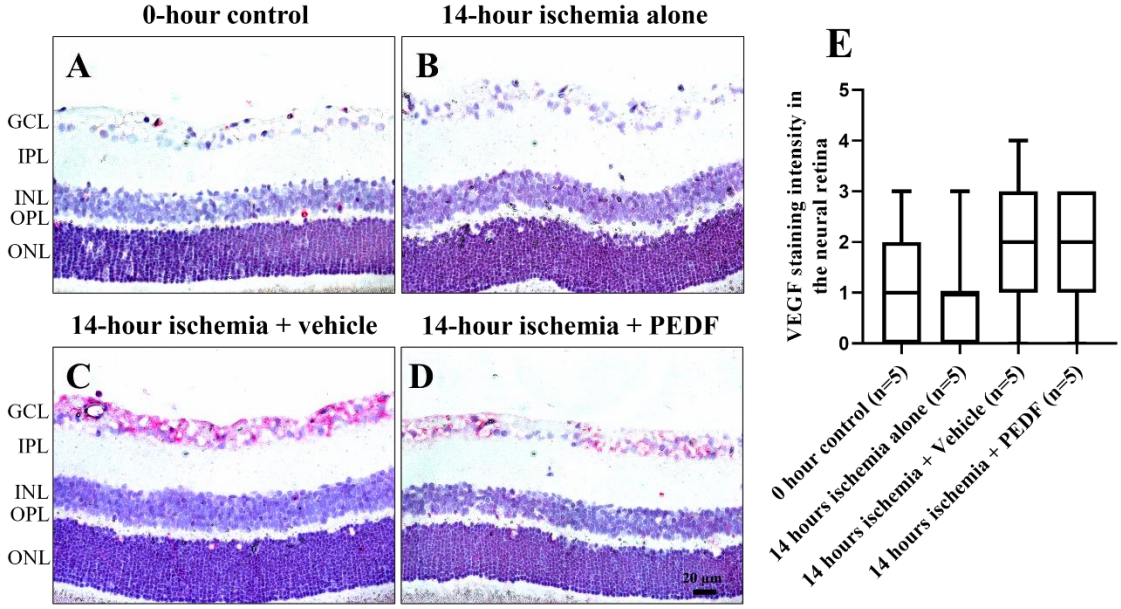

Figure 25. Immunohistochemical staining of VEGF in the neural retina (A-D). The VEGF was nearly undetectedable in the 0-hour control group (A). After 14 hours of ischemia, the immunohistochemical staining of VEGF was nearly negative in the 14 hours hypoxia alone group (B). The strong immunohistochemical staining was found in the vehicle treatment group (C) and the PEDF treatment group (D). Immunohistochemical staining intensity of VEGF in the neural retina (E). (n: number of eyes). GCL: ganglion cell layer; IPL: inner plexiform layer; INL: inner nuclear layer; OPL: outer plexiform layer; ONL: outer nuclear layer. Scale bar = 20μm.

6.5 Expression of VEGF in the RPE cells and the choroidal vessels

Immunohistochemical staining of VEGF in the RPE layer and the choroid (Figure 26A-D). The VEGF staining was weakly expressed in the RPE layer and the choroid of the 0-hour control group (Figure 26A) and the 14-hour ischemia alone group (Figure 26B). The VEGF was increased to some extent in the RPE layer and the choroid of both the vehicle group (Figure 26C) and the PEDF treatment group (Figure 26D), but there was no significant difference. Immunohistochemical staining intensity of VEGF in the RPE layer (Figure 26E). There was no significant difference between the four groups ($P = 0.087$). Immunohistochemical staining intensity of VEGF in the

choroid (Figure 26F). There was a significant difference between the PEDF treatment group (0, 1) and the vehicle treatment group (0, 1) ($P = 0.006$). The value is described by percentile (M1, M3).

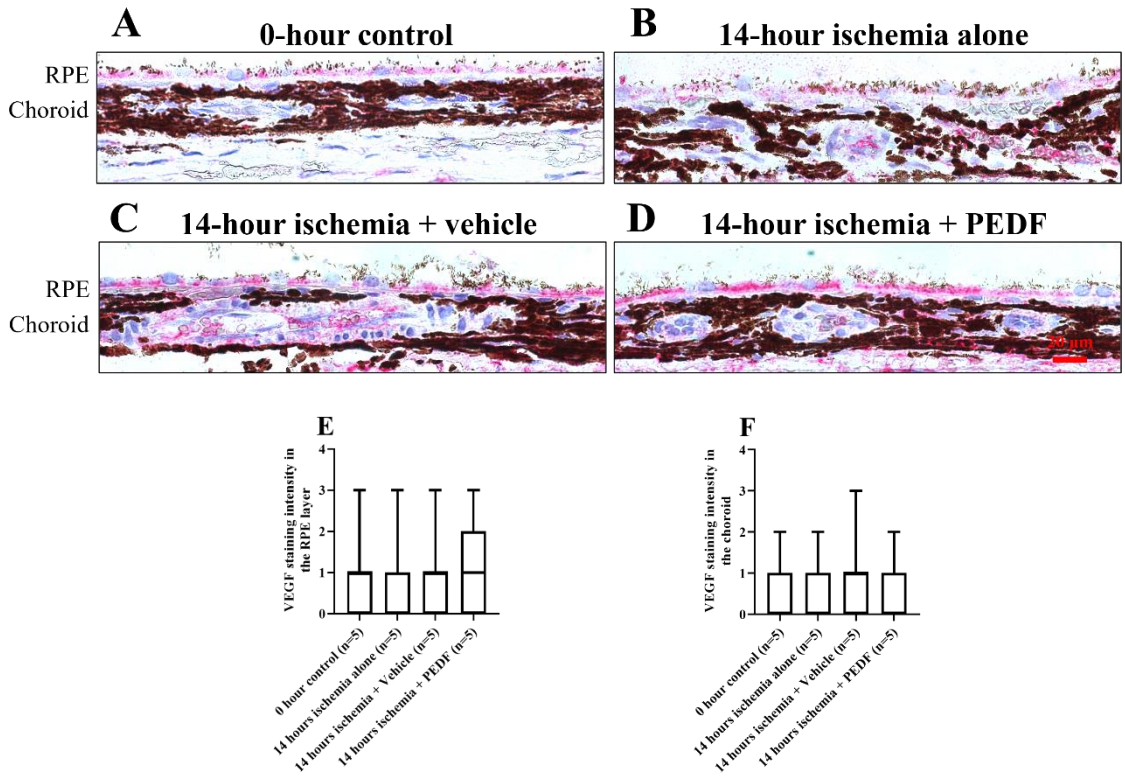

Figure 26. Immunohistochemical staining of VEGF in the RPE layer and the choroid (**A-D**). The VEGF staining was weakly expressed in the RPE layer and the choroid of the 0-hour control group (**A**). After 14 hours of ischemia, the staining intensity of VEGF was not significantly increased in either the RPE layer or the choroid (**B**). The VEGF was increased to some extent in the RPE layer and the choroid in both the vehicle treatment group (**C**) and the PEDF treatment group (**D**). (n: number of eyes). RPE, retinal pigmented epithelium; CC, choriocapillaris layer. Scale bar = 20μm.

6.6 Electron microscopic imaging of the choroidal vessels

The retinal and choroidal vessels looked morphologically viable, their mitochondria were unsuspicious with no sign of apoptosis, and there was no necrotizing tissue damage after 14 hours of incubation at 4 °C, no vacuolization or blebbing of nuclear or cytoplasmic material, no nuclear envelope fragmentation, and no permeabilization of cell membranes.

The morphology of the choroidal vessels, especially the choriocapillaris, was changed considerably in the ischemic group compared to the control group (Figure 27A). We found the following changes:

1. Vessels consisting of endothelial cells with varying thickness (Figure 27B).

2. Choriocapillaris (CC) vessels contained fenestrations not only on the wall facing the RPE, but also very prominently on the opposite side (Figure 27C and G).

3. Endothelial cells made filopodia-like projections into the choriocapillaris (CC) lumen (Figure 27B-E, G, H).

4. Filopodia-like projections formed a labyrinth or maze-like structure which nearly closed the vessel lumen (Figure 27B-D). This kind of labyrinth capillary may be responsible for the leakage of the choroidal vessels.

5. Filopodia-like projections often had fenestrations (Figure 27G and H).

6. Filopodia-like projections usually touched the erythrocytes or completely surrounded them (Figure 27D and G).

7. Choriocapillaris lumens showed open connections towards the interstitium (Figure 27C and E).

8. Pericytes also became elongated and produced filopodia-like projections which pointed to the surrounding tissue (Figure 27B and D).

9. There were vessels with endothelial cells or filopodias which attempted to build up a new lumen inside the existing one (Figure 27F-H).

10. Bruch's membrane contained cells (Figure 27D and F).

In a healthy choriocapillaris, only some small filopodia-like projections can be observed (Figure 27A). After 14 hours of ischemia, the number of filopodia-like projections had grown and the area of their surface had increased (Figure 27B-H).

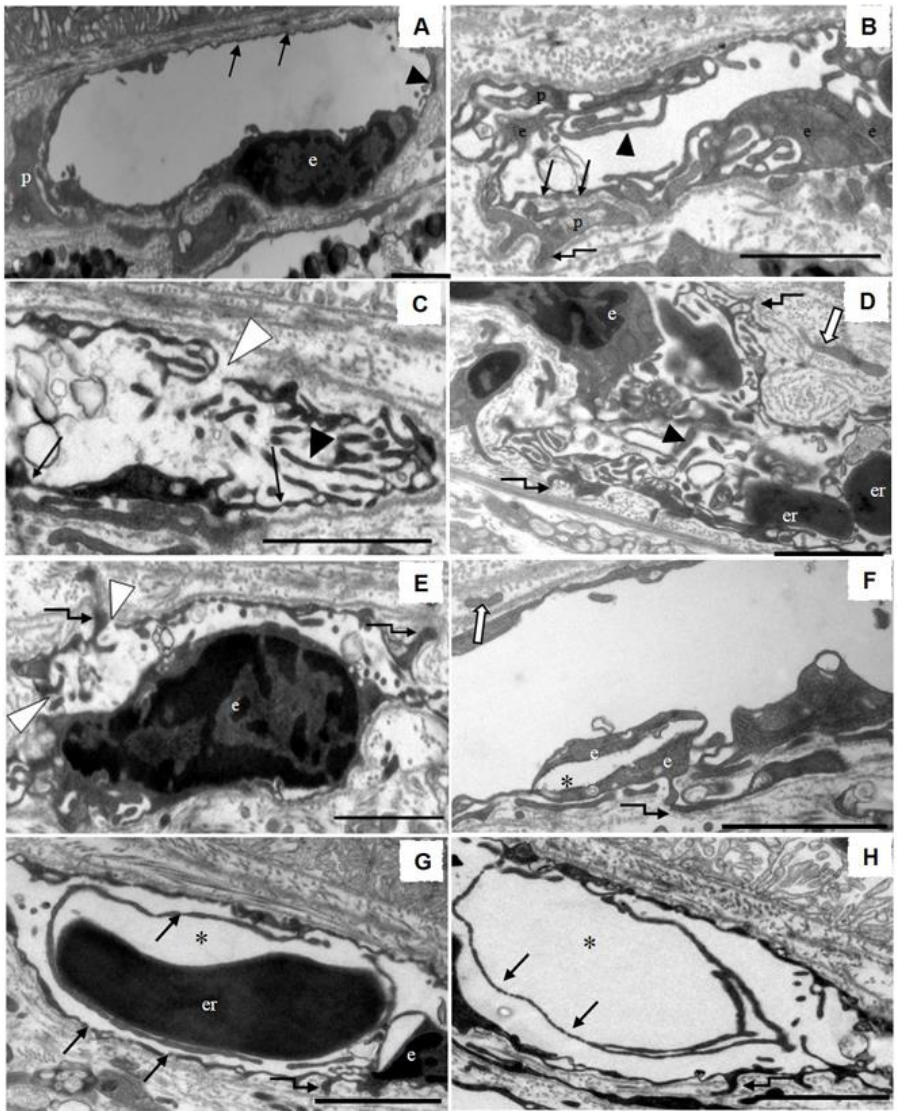

Figure 27. The morphology of the choriocapillaris under the electron microscope. Ultrastructure of a typical rat choriocapillaris vessel (A), hypoxia related changes in the ischemic group (B-H), and PEDF-treated eyes (I and J). The control choriocapillaris (CC) vessel (A) contains a regular, thin endothelium; fenestrations are predominantly facing the retina side and are marked by black arrows. There are a few unsuspicious small projections to the vessel lumen which are indicated by a black arrowhead (same labels used also in the following images). CC of rats after 14 hours of ischemia (B-D). B: There are a lot of filopodia-like projections into the vessel lumen (black arrowhead). Pericytes and endothelium cells also have projections to the surrounding tissue, marked by zigzagged black arrows. C: In addition, there are losses of cell connections, so a white arrowhead marks an endothelial gap (see also E). D: Filopodia-like projections to the lumen (black arrowhead) often create a labyrinth in the vessel lumen. A cell in Bruch's membrane is indicated by a white arrow (see also F). E: Endothelium cells made projections to Bruch's membrane (zigzagged black arrows). F: Endothelium cells organized a new lumen in the previous existing vessel (black asterisk). G: Filopodia-like projections often have fenestrations which are marked by black arrows. These projections could form a new lumen around the erythrocytes by partitioning the luminal space (asterisk, see also in H). Fenestrations can also be found at the basal side of the CC, facing the deeper choroid. e–endothelial cell; p–pericyte; er–erythrocyte. Scale bar = 2µm.

6.7 Inhibition of choriocapillaris collapse and labyrinth capillary formation by PEDF protein

Rat eyes were injected with PEDF protein and then exposed to DMEM solution at 4℃ for 14 hours. Control rat eyes were also exposed to DMEM solution at 4℃ for 14 hours without injection. Ultrathin sections of the eyes were investigated in EM. In the PEDF-treated eyes, the lumen of the choriocapillaris were well preserved (Figure 28A). In the control eyes, the choriocapillaris was often collapsed and lead to complete loss of the capillary lumen (Figure 28B).

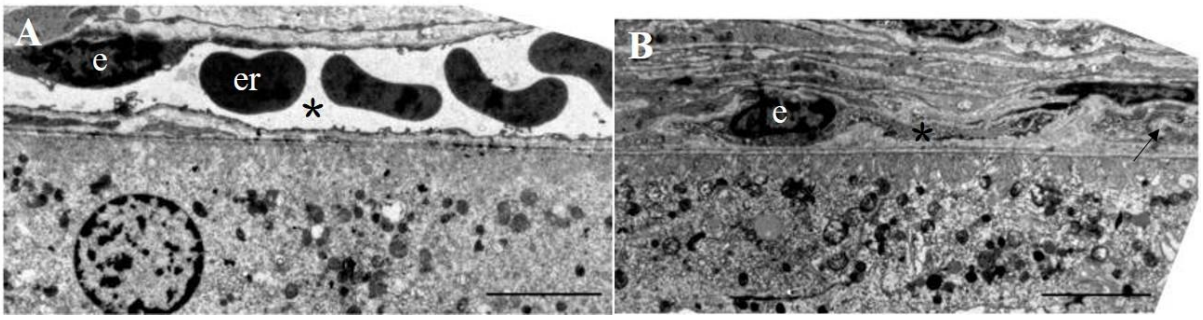

Figure 28. PEDF protein inhibits the formation of labyrinth capillaries and stabilizes the blood vessels as judged by EM. (**A**) With intravitreal PEDF injection and with hypoxia, labyrinth capillaries did not develop and the lumen of the capillaries is maintained as *in vivo* (asterisk). (**B**) With hypoxia and without PEDF injection, the lumen of the capillaries is collapsed (asterisk) or nearly closed (arrow). e –endothelial cell, er–erythrocyte. Scale bar = 5μm.

6.8 The lumen and the vessel areas between the PEDF treated group and the non-treated ischemic control group

The area of lumen ($\mu m^2/\mu m$ of Bruch's membrane) and the area of the whole vessel ($\mu m^2/\mu m$ of Bruch's membrane) were analyzed. There was a significant difference between the PEDF-treated group ($1.034\pm0.077 \mu m^2/\mu m$) and the non-treated ischemic group ($0.308\pm0.087 \mu m^2/\mu m$) ($P < 0.001$) in the area of the lumen (Figure 29A). There was a significant difference between the PEDF-treated group ($1.583\pm0.094 \mu m^2/\mu m$) and the non-treated ischemic group ($0.675\pm0.048 \mu m^2/\mu m$) ($P < 0.001$) in the area of the whole vessel (Figure 29B).

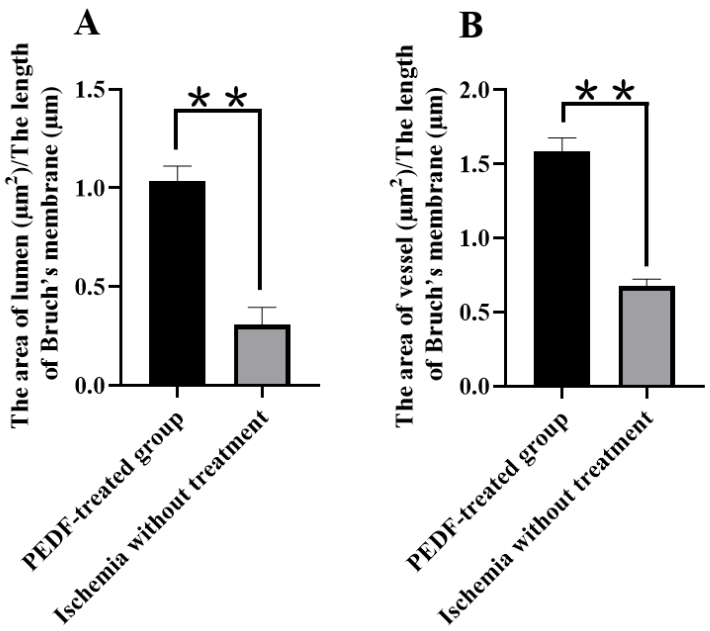

Figure 29. The area of lumen and the area of vessel for each micron of Bruch's membrane. (A) There was a significant difference between the PEDF-treatment group (1.034±0.077μm^2/μm) (n = 3) and the control group (0.308±0.087μm^2/μm) (n = 3) ($^{**}P < 0.001$) in the area of the lumen; (B) There was a significant difference between the PEDF treatment group (1.583±0.094μm^2/μm) (n = 3) and the control group (0.675±0.048μm^2/μm) (n = 3) ($^{**}P < 0.001$) in the area of the vessel. n: number of eyes.

6.9 The binding position of PEDF protein in the retina

Immunohistochemical staining of human PEDF was done in the PEDF treatment group to detect the binding position in the retina. PEDF mainly combined to the nerve fiber layer (NFL), ganglion cell layer (GCL), the inner nuclei layer (INL) and the rod and cones layer (RCL) of the retina (Figure 30A). These binding positions may help PEDF exert its neuroprotective effects in the neural retina.

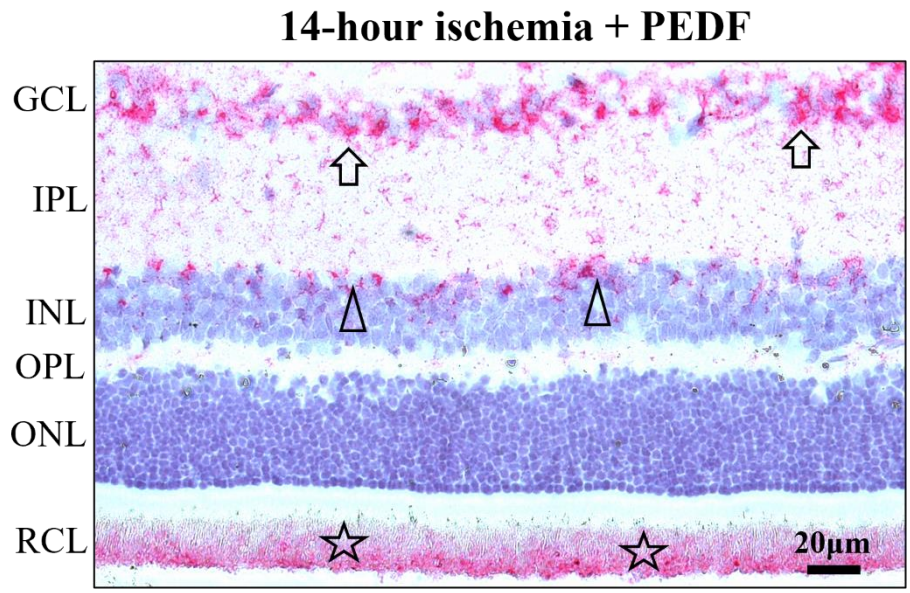

Figure 30. Immunohistochemical staining of PEDF in the retina. The PEDF was detected in the GCL (black arrow), the INL (black arrowhead) and the RCL (Star) of the PEDF treatment group (**A**). GCL, ganglion cell layer; IPL, inner plexiform layer; INL, inner nuclear layer; OPL, outer plexiform layer; ONL, outer nuclear layer; RCL, rod and cones layer. Scale bar (retina) = 20μm.

6.10 Expression of PEDF in the RPE cells and the choroidal vessels

Immunohistochemical staining of PEDF in the RPE layer and the choroid (Figure 31A-D). The PEDF staining was detected in the RPE layer and it was nearly negative in the choroid of the 0-hour control (Figure 31A) and the 14-hour ischemia alone group (Figure 31B). The immunohistochemical staining of PEDF was nearly negative in the RPE and the choroid of the vehicle treatment group (Figure 31C). The positive immunohistochemical staining in the RPE layer and the choroidal vessels, especially the RPE layer, was found in the PEDF treatment group (Figure 31D). Immunohistochemical staining intensity of PEDF in the RPE (Figure 31E). There was a significant difference between the PEDF treatment group (2, 3) and the 0-hour control group (1, 2) ($P < 0.001$), the 14-hour ischemia alone group (0, 2) ($P < 0.001$), the vehicle treatment group (0, 1) ($P < 0.001$). Immunohistochemical staining intensity of PEDF in the choroid (Figure 31F). There was a significant difference between the PEDF treatment group (0, 1) and the 0-hour control group (0, 0) ($P < 0.001$), the 14-hour ischemia alone group (0, 0) ($P < 0.001$), the vehicle treatment group (0, 0) ($P < 0.001$). The value is described by percentile (M1, M3).

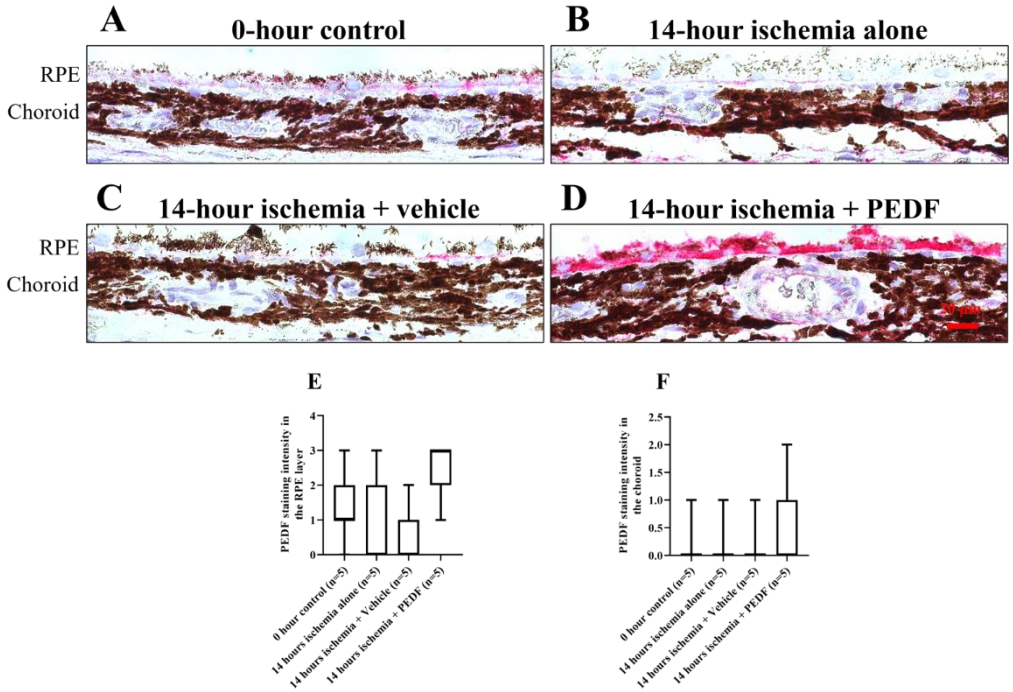

Figure 31. Immunohistochemical staining of PEDF in the RPE layer and the choroid (**A-D**). The PEDF staining was detected in the RPE layer and was nearly negative in the choroid of the 0-hour control (**A**), the 14-hour ischemia alone group (**B**) and the 14-hour vehicle treatment group (**C**). The immunohistochemical staining in the RPE layer and the choroidal vessel was found in the 14 hours ischemia + PEDF treatment group (**D**). Immunohistochemical staining intensity of PEDF in the RPE (**E**) and the choroid (**F**). (n: number of eyes). RPE: retinal pigmented epithelium, CC: choriocapillaris layer. Scale bar = 20 μm.

6.11 TUNEL-positive cells were reduced in the PEDF treatment group

The apoptosis of ganglion cells, the inner nuclear cells and the outer nuclear cells was analyzed by terminal deoxynucleotidyl transferase dUTP nick end labeling (TUNEL) assay. TUNEL-positive cells were mainly located in the inner retina, especially the GCL (Figure 32I-L). However, TUNEL-positive nuclei were rarely observed in the outer nuclear layer. In the GCL, the percentage of TUNEL-positive cells per 100μm was significantly reduced in the PEDF treatment group (2.36, 2.89) compared to the 14-hour ischemia alone group (3.14, 3.75) (P = 0.015) and the vehicle treatment group (3.14, 3.70) (P = 0.015) (Figure 32M). The number of TUNEL-positive cells in the inner nuclear layer cells per 1000μm (Figure 32N). The number of TUNEL-positive cells was significantly reduced in the PEDF treatment group (15.81, 22.89) compared to the 14-hour ischemia group (33.69, 45.22) (P = 0.001) and the vehicle treatment group (26.63, 43.97) (P = 0.023). The

number of TUNEL-positive cells per 1000μm in the outer nuclear layer (ONL) was analyzed (Figure 32O). Compared to the 0-hour control group (1.03 ± 1.26), the number of TUNEL-positive cells was significantly increased in the 14-hour ischemia group (2.81 ± 1.37) (P = 0.007) and the vehicle treatment group (2.77, 1.26) (P = 0.004). The value is described by percentile (M1, M3) (abnormal distribution) or mean ± SD (normal distribution).

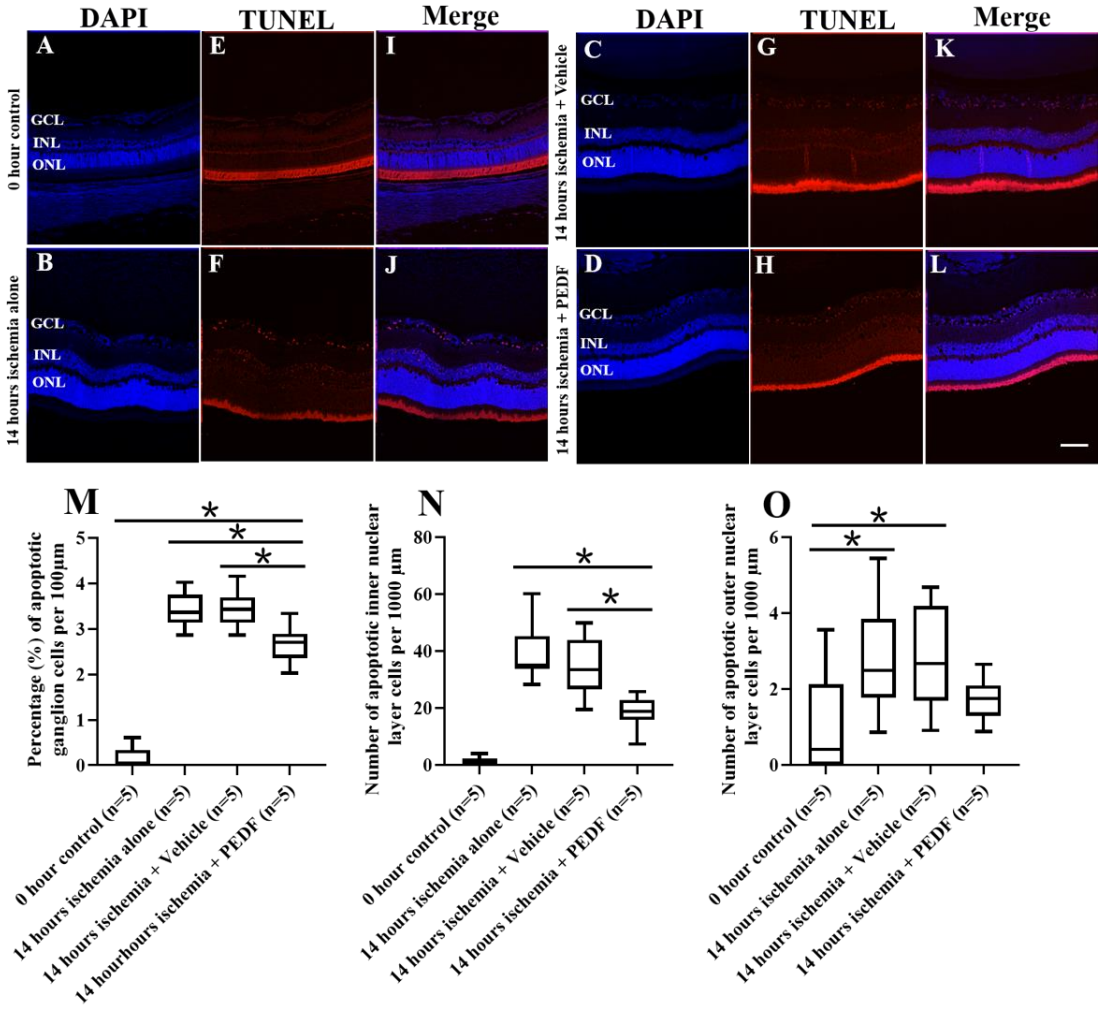

Figure 32. Representative immunofluorescence staining of TUNEL in the central part of the retina. Figures **A-D** show the DAPI counterstain, figures **E-H** show TUNEL-positive staining (red) and figures **I-L** show the merged TUNEL/DAPI overlay. Positive staining cells were mainly in the inner layers, especially in the GCL. There were nearly no positive staining cells in the control group (**I**). Following 14 hours of ischemia, TUNEL-positive cells (red) were predominantly in the GCL. Some inner nuclear layer cells, especially the inner part of the INL were positively stained (**J**). In the vehicle-treated group, TUNEL-positive cells (red) were predominantly in the GCL and some inner nuclear layer cells (**K**). In the PEDF-treated group, some ganglion cells were positively stained and some ganglion cells were negatively stained (**L**). The TUNEL-analysis was performed using the in situ cell death detection TMR red TUNEL kit as recommended by the manufacturer. The analysis of TUNEL-positive cells in the ganglion cells, the inner nuclear layer cells and the

outer nuclear layer cells (**M-O**): The percentage of TUNEL-positive cells to the total number of ganglion cells per 100μm length of the retina (**M**). The number of TUNEL-positive cells in the inner nuclear layer cells per 1000μm (**N**) and the number of TUNEL-positive cells in the outer nuclear layer cells per 1000μm (**O**). Data were analyzed by the Wilcoxon test with the Kruskal-Wallis test (abnormal distribution) or the ANOVA test (normal distribution) ($^{*}P < 0.05$). GCL: ganglion cell layer; INL: inner nuclear layer; ONL: outer nuclear layer. Scale bar = 50μm.

7 Discussion of the *in vivo* experiment

7.1 PEDF alone or in combination with an anti-VEGF drug in the inhibition of CNV

In view of the anti-angiogenic effect of PEDF, many reports exist which have used PEDF to treat animal CNV models. For example, the intraocular injection of adeno-associated viral (AAV) vector containing expression constructs coding for PEDF (Mori et al., 2002), subconjunctival administration of PEDF-derived peptide 34-mer (Amaral et al., 2010), eye drop administration of PEDF peptide 335 (Sheibani et al., 2019), intravitreal injection of lentivirus-mediated PEDF gene transfer (Yu et al., 2016), and intravitreal injection or eye drop administration of PEDF peptide/collagen mixture (Kim et al., 2019), which all had therapeutic effects in animal models of laser-induced CNV. Although the safety of AAV has been determined and reported in some animal experiments, no clinical studies have been conducted for AAV vector and AAV-PEDF. The duration of gene expression is too short, and it is not easy to maintain the gene in its activated state and expressing stably. Due to the short half-life of the PEDF–derived peptide, it has limitations in clinical application. In this study, I endeavored to use PEDF protein as an intravitreal injection. The maximal thickness of CNV was compared before and after treatment. The anti-VEGF treatment group showed the most significant reduction of CNV thickness. Anti-VEGF treatment suppresses CNV thickness by inhibiting neovascularization. However, the stable neovascularization provides nutrients for photoreceptor cells and help them survive. Excessive inhibition of neovascularization leads to loss of photoreceptor cells. In the PEDF treatment group, the maximal thickness of CNV decreased significantly after two intravitreal injections. Intravitreal injection of PEDF protein alone showed inhibition of CNV, while in the PEDF/anti-VEGF treatment group, the maximal thickness of CNV decreased significantly after the first intravitreal injection. PEDF protein and anti-VEGF drugs have a synergistic effect in inhibiting CNV in the early stage. PEDF protein can also be metabolically cleaved and rapidly cleared, which limits the time that PEDF can perform its function.

Moreover, PEDF protein exerts a therapeutic effect in a short period of time, which further proves the biological function of PEDF. The rat CNV model was induced by subretinal injection of an AAV.VEGF-A^{165} vector, which continuously expresses VEGF. This VEGF-driven angiogenesis of CNV was inhibited after two intravitreal injections of PEDF protein. Thus, PEDF is a potential candidate drug for the treatment of CNV.

7.2 The effect of PEDF on the collagen in the *in vivo* rat CNV model

CNV is associated with damage to the RPE-Bruch's membrane-choriocapillaris complex and abnormalities of extracellular matrix formation. The deposition of extracellular matrix in the retina affects visual function. Thus, a better understanding of the pathological features of extracellular matrix in the CNV may lead to a new treatment method. PEDF is a glycoprotein that belongs to the superfamily of serine, and it has multiple functions including anti-oxidative, anti-inflammatory and antifibrotic activities. Many studies have reported the antifibrotic property of PEDF. For example, suppressing cardiac fibrosis by reducing transforming growth factor-β (TGF-β) and type III collagen expression (Ueda et al., 2011), preventing liver fibrosis and hepatic stellate cell activation through down-regulation of the platelet-derived growth factor (PDGF) receptor (Tsai et al., 2014), and inhibiting the Wnt pathway-mediated fibrosis in primary renal proximal tubule epithelial cells (He et al., 2017). The deposition of collagen in CNV will gradually form fibrosis and eventually lead to scar formation, which seriously affects vision. If PEDF reduces the formation of extracellular matrix in CNV, the scar will be minimized and the distance for the supply of oxygen and nutrition from the choroidal vessels towards the photoreceptors will be shortened. Collagen is the predominant extracellular matrix protein which plays an important role in cell adhesion and migration (Sekiya et al., 2011). PEDF can bind to collagen, the combination is spatially heterogeneous and occurs at the interfaces between collagen fibrils (Cauble et al., 2017). Therefore, we studied the effect of PEDF on the collagen in the *in vivo* rat CNV model. Unexpectedly, PEDF did not reduce mature (collagen type I) and immature (collagen type III) collagen levels in the CNV. The possible reasons are that the CNVs are not in their late stage but still in their early stages and there are still new collagens that continue to be synthesized. In this *in vivo* experiment, PEDF was intravitreally injected only once or twice for each rat eye. Fewer injections affect the inhibitory effect of PEDF on collagen. In addition, only one kind of concentration of PEDF protein was used

in the *in vivo* experiment, and it may not be the optimal concentration for PEDF to function. Different concentrations of PEDF protein should be tried in future research. PEDF tends to bind more to other extracellular matrix components rather than to collagen, which influences the effect of PEDF on collagen, or PEDF has no effect on collagen. Collagen type IV is a prominent structural component of blood vessel basement membranes and a prominent structural component of the upper part of Bruch's membrane (Viheriälä et al., 2021). Interestingly, collagen type IV is significantly reduced in the CNV of all intravitreal injected eyes, even the vehicle-treatment control eyes. The mechanism underlying this observation is unclear.

7.3 Quantification of VEGF after treatment with an anti-VEGF drug alone or in combination with PEDF in CNVs

Many studies have attempted to investigate the mechanism by which PEDF inhibits VEGF. PEDF downregulated VEGF expression might partially perform this via inhibition of mitogen-activated protein kinase (MAPK)-mediated HIF-1 activation, as VEGF is one of the expression factors of HIF-1 (Zhang et al., 2006). PEDF binds directly to both VEGF receptor-1 (VEGFR-1) and VEGFR-2 and promotes the receptor internalization and/or degradation to limit VEGF responses (Johnston et al., 2015). The balance between PEDF and VEGF may play a key role in maintaining the homeostasis of the ocular blood vessels. PEDF is expressed mainly in the apical side of RPE cells rather than in the basal side, while VEGF is expressed in the basal side of RPE cells rather than the apical side (Fields et al., 2017). The imbalance between PEDF and VEGF may promote a pathological condition in RPE cells and contribute to CNV formation. Intravitreal injection of an anti-VEGF drug is the main method of clinical treatment of CNV. In this *in vivo* experiment, the VEGF positive area as a percentage of the total CNV area was significantly reduced in the PEDF/anti-VEGF treatment group, compared to the control group and the PEDF treatment group. Intravitreal PEDF/Anti-VEGF treatment is more effective in inhibiting VEGF than anti-VEGF treatment alone and has a synergistic effect on inhibiting VEGF in the CNV. In the clinical treatment of CNV, multiple intravitreal injections increase the risk of complications, such as cataract, retinal detachment and endophthalmitis. More importantly, while inhibiting neovascularization, it also reduces the nutrient supply of photoreceptor cells, which can cause geographic atrophy (GA) in AMD patients. The combination of PEDF and anti-VEGF therapy may reduce the number of intravitreal injections and may help to maintain healthy blood vessels. Thereby, the induction of GA

may be avoided.

7.4 The effect of PEDF on the photoreceptors in the *in vivo* rat CNV model

CNV breaks through Bruch's membrane into the subretinal space or into the neuroretina, causing fluid leakage and ultimately resulting in retinal scar, which damages photoreceptor cells and severely impairs visual acuity. CNV is associated with dysfunction and atrophy of the RPE cells, which phagocytose damaged photoreceptor outer segments and provide critical support for photoreceptor survival and function (Al-Ani et al., 2020). PEDF is a neural trophic and neural protective factor and is mainly expressed by RPE cells in a directional fashion toward the neuroretina. PEDF protects photoreceptors against apoptosis in the murine model of focal retinal degeneration (Wang et al., 2013), the mouse model of retinitis pigmentosa (Hernández-Pinto et al., 2019), and the focal phototoxicity induced cone photoreceptor cell loss in mouse (Valiente-Soriano et al., 2020). The mechanism by which PEDF-mediated photoreceptors survived is unclear. Cell surface labeling showed that a PEDF-receptor is required because the biological activities of PEDF depend on binding to cell surfaces (Subramanian et al., 2013). The protective effect, at least in part, may be via inhibition of photoreceptor degeneration (Miyazaki et al., 2003), down regulating the inflammatory state, and suppression of anti-angiogenic pathways (Wang et al., 2013). Expression of PEDF is significantly reduced in the RPE cells of patients with AMD or CNV (Bhutto et al., 2006). The damage to RPE cells in CNV patients further reduces the secretion of PEDF and aggravates the damage to the retinal photoreceptor cells, and finally results in rapid vision loss. Thus it should be noted that earlier intervention before the RPE and photoreceptors are severely damaged (for example, during intermediate AMD, to prevent GA development) may be more successful (Fleckenstein et al., 2021). In the *in vivo* experiment, the ratio of the ONL-area /CNV-area was significantly increased after intravitreal injection of PEDF, indicating that PEDF is effective in protecting photoreceptors from apoptosis. PEDF protein injected intravitreally can diffuse through the retina and remain biologically active and supports photoreceptor survival. To our knowledge, this is the first report documenting the neuroprotective effects of PEDF protein in the AAV.VEGF-A^{165} vector induced rat quiescent CNV model *in vivo*. Thus, it could be useful for developing a novel approach for the potential treatment of CNV.

7.5 The effect of PEDF on the endothelial cells in both healthy and pathological vessels

Although PEDF is an endogenous inhibitor of angiogenesis, it also plays an important role in maintaining endothelial function. PEDF has a significant effect on endothelial cell adhesion, migration, proliferation and capillary morphogenesis (Falero-Perez et al., 2017). On the other hand, isolated choroidal endothelial cells from PEDF-deficient ($PEDF^{-/-}$) mice exhibited increased proliferation, decreased adhesion, delayed capillary morphogenesis, and produced increased levels of pro-inflammatory cytokines (Farnoodian et al., 2018). PEDF suppresses the proliferation and migration of VEGF-induced choroidal capillary endothelial cells, without affecting normal choroidal endothelial cell proliferation and migration (Wang et al., 2007). VEGF promotes vascular permeability and blood vessel leakiness, which leads to retina edema and impaired visual acuity. However, one previous study reported that PEDF blocked VEGF-induced vascular permeability via a novel γ-secretase dependent pathway. PEDF prevents dissociation of endothelial adherens junctions (AJs) and tight junctions (TJs) (Cai et al., 2011). In the clinic, the subretinal CNV known as quiescent CNV exists without reducing the visual acuity of the patients. So, if we can stabilize CNV, it will help to reduce retinal edema and photoreceptor cell damage. Anti-VEGF treatment blocks the newly-formed blood vessels. But the neovascularization may help photoreceptors to survive. In this experiment, neither PEDF treatment nor PEDF/Avastin treatment significantly inhibited neovascularization in the rat quiescent CNV model. If the quiescent CNV is continuously stabilized without leakage, it may be helpful for photoreceptor survival, reducing retinal scar and maintaining vision.

7.6 The safety evaluation and clinical trial of PEDF

The toxicity of PEDF peptide was evaluated after intravitreal injection of 2µl of 2 mM peptide solution in laser-induced mice CNV eyes. No cytotoxicity was detected on the viability of three retinal cell lines (retinal astrocytes, endothelial cells and pericytes) and two choroidal cell lines (choroidal endothelial cells and pericytes) (Sheibani et al., 2019). Two weeks after intravitreal injection, the impact of PEDF peptide on retinal function was assessed by electroretinography (ERG). The amplitude of a-wave and b-wave for 10 cd s/m^2 flash intensity showed no significant

difference between PEDF-peptide-treatment and control groups. Thus no potential toxicity of PEDF to the retina and choroid has been found until now. There are not many clinical trials of PEDF at present. One clinical trial investigated the tolerability and potential activity of intravitreal injection of Ad(GV)PEDF.11D in patients aged 50 or over with severe wet AMD. Ad(GV)PEDF.11D showed potential activity to inhibit wet AMD (Rasmussen et al., 2001).

8 Discussion of the *ex vivo* experiment

8.1 The advantages and disadvantages of the currently established ischemic eye model

Ocular ischemic diseases can lead to blindness if not adequately treated. To address the clinical needs, various animal models of ocular ischemia have been developed *in vivo*, including laser occlusion of the retinal veins (Neo et al., 2020), permanent unilateral common carotid artery occlusion (UCCAO) (Lee et al., 2020), transient bilateral common carotid artery occlusion (tBCCAO) (Lee et al., 2020) and elevation of intraocular pressure to cut off the blood supply from the retinal artery (Lin et al., 2018). The ophthalmic artery is the main supplying vessel of the retina and choroid and it originates from the branches of the common carotid artery. However, the common carotid artery occlusion also interrupts blood supply to the brain and leads to severe brain damage, Moreover, the individual variation for the treatment cannot be excluded. Unfortunately, elevated intraocular pressure (IOP) cannot be performed for a long period of time in the living rat, and it also damages the retinal tissue. On the other hand, *in vivo* experiments are very costly and current social ethics advocate reducing the use of laboratory animals (Schnichels et al., 2019). However, these *in vivo* models have their advantages, as the retina has a physiological micro-environment during the process of ischemia/hypoxia. But *ex vivo* organ culture does effectively contribute to the reduction of the number of animals used and the donated animal eyeballs are easy to obtain. Thus to establish a retinal ischemic/hypoxic model, some animal experiments are replaced by organotypic cultures of retina. Many studies attempted to use chemical solutions such as N_2-saturated PBS containing iodoacetic acid (Catalani et al., 2007), PBS containing iodoacetic acid and sodium cyanide (Mastrodimou et al., 2005), and cobalt chloride ($CoCl_2$) (Tsai et al., 2020) to induce an ischemic/hypoxic environment for retina explants. Among these solutions, $CoCl_2$ has long been accepted as a suitable *in vitro* ischemic/hypoxic agent. However, $CoCl_2$ causes toxic effects,

including mitochondrial damage, generation of oxygen radicals and excessive formation of reactive oxygen species (ROS) (Karovic et al., 2007). All these toxic effects contribute to $CoCl_2$-induced cell death. Furthermore, $CoCl_2$ has a strong damaging effect on microglia, and the microglia number is reduced during the process of cultivation (Hurst et al., 2020). The chemical solution induction of hypoxia cannot completely simulate the real ischemic/hypoxic conditions during the process of retinal diseases (Tang et al., 2017), and cannot mimic the physiological micro-environment for the retina. A new retinal ischemic/hypoxic model similar to the physiological microenvironment needs to be established. Therefore, I demonstrated an *ex vivo* eye model by incubating the fresh whole rat eye at 4℃ in DMEM solution for 14 hours. This *ex vivo* eye model is easy to operate and the experimental conditions are more controllable. Furthermore, the usage of the whole eyeball avoids retina trauma during the process of making retina explants and keeps a stable micro-environment around the retina. This *ex vivo* eye model is suitable to evaluate the pathophysiology of ischemic retinopathy and the effects of ischemia on the choroidal vessels.

8.2 Filopodia-like projections were found in the lumen of the choroidal vessels of the ischemic eye model

In this *ex vivo* eye model, filopodia-like endothelial projections were found in the lumen of the choroidal vessels, which were similar to the labyrinth capillaries already described in the human CNV membranes. The sub-macular CNV membranes in humans had previously been investigated by high-resolution electron microscopy and a new type of pathological capillary designated a labyrinth capillary was found (Schraermeyer et al., 2015). This pathological capillary is probably responsible for the permanent leakage in human CNV, as the leaky sites in this kind of labyrinth capillary cannot be closed by thrombocytes because of the reduced lumen, and thus the thrombocytes cannot enter (Schraermeyer et al., 2015). It is likely that this vessel type can cause chronic plasma exudation and is the origin of edema. In this *ex vivo* eye model, the choriocapillaris changed into practically the same vessel type that was found in human CNV. This can be taken as evidence that labyrinth capillaris in human CNV are caused by hypoxia.

8.3 The oxygen concentration in the vitreous of both the living rat

eye and the ischemic eye

The oxygen concentration in the vitreous was measured both *in vivo* and *ex vivo* by an oxygen sensor. Compared to the living rats, the oxygen saturation in the vitreous of the incubated eyes is decreased and the result curve shows a waveform downtrend. The formation of the wavy line is due to the influence of temperature fluctuations. The value of oxygen concentration in the vitreous of the incubated eyes was gradually reduced and fell to half the value (50%) directly after enucleation within approximately 400 minutes. There is no specific value of oxygen concentration to indicate tissue hypoxia. However, this can be deduced from the definition of tissue hypoxia, a pathological process that causes abnormal changes in the metabolism, function, and morphology of the tissue due to insufficient oxygen supply. This *ex vivo* eye model shows typical signs of hypoxia as apoptosis of ganglion cells and therefore can be used to study drugs that should protect against damage induced by hypoxia.

8.4 The expression of VEGF in the retina of the *ex vivo* eye model

In this experiment, hardly any immunopositive staining of VEGF was found in the neural retina in either the control or the ischemic eyes. This means that VEGF is not elevated after a 14-hour period of ischemia. Furthermore, hypothermia also affects the expression of VEGF. Many studies reported that hypothermia decreased VEGF secretion in cultured RPE cells (Takeyama et al., 2015; Coassin et al., 2010). The effect of hypoxia on increasing VEGF secretion by these cells is mitigated by hypothermia. However, there was a strong immunopositive staining of VEGF in the GCL in the intravitreal treatment groups. The expression of VEGF in the GCL may be caused by the increased expression of HIF-1α, as the VEGF gene is a target of HIF-1α. On the other hand, the over-expression of VEGF in the ganglion cell layer indicates that the ganglion cells are still active during this ischemic process. Under the same experimental conditions, rat RPE cells and choroidal endothelial cells could be used for cell culture, indicating that these cells are still alive (Langenfeld et al., 2015). VEGF is known to induce increased permeability and development of endothelial fenestrations in endothelial cells (Roberts et al., 1995). Also, ultrastructural analysis revealed that VEGF–induced newly formed blood vessels contained high numbers of endothelial fenestrations (Cao et al., 2004), which mediated high permeability of the vascular wall. Over expression of VEGF by the RPE cells is a very important potential factor in inducing the formation of CNV (Udono et

al., 2001).

8.5 The location of intravitreal injected PEDF protein in the retina and the choroid

Immunohistochemical staining of PEDF in the PEDF treatment group showed that the location of PEDF protein was mainly in the INL, GCL, RPE layer and the choroidal vessel walls. This indicates that PEDF protein can penetrate the retina and is transported into the choroid after intravitreal injection. Thus, the distribution feature of PEDF in the whole retina and the choroid makes neuroprotective effects in the neural retina and anti-angiogenetic effects in the choroid possible. The neuroprotective effect of PEDF on the retinal neurons has been confirmed by previous studies (Bürger et al., 2020; Valiente-Soriano et al., 2020). In this study, I investigated the effect of PEDF on the ganglion cells, and the inner and outer nuclear cells under ischemia by TUNEL staining. As has been proved by a previous experiment, one hour of ischemia results in retinal ganglion cell apoptosis in the rat retina (Sellés-Navarro et al., 1996). Retinal ganglion cells are more sensitive to hypoxia than other retinal neural cells, and it is the first cell type which develops apoptosis under ischemia. However, in this ischemic rat eye experiment, PEDF protected the retinal ganglion cells and the inner nuclear cells from apoptosis. More retinal ganglion cells survived in the PEDF treatment group than in other groups. Thus, PEDF may be a promising agent in the treatment of ischemic eye diseases.

8.6 The treatment of ischemic eye diseases

The main methods for clinical treatment of retinal ischemia are laser photocoagulation and intravitreal administration of anti-angiogenic agents targeting VEGF. However, both laser photocoagulation and anti-VEGF drugs are unable to solve the underlying retinal neurodegeneration and ischemia caused by the occluded blood vessel (Jalilian et al., 2020). Laser photocoagulation of the ischemic retina reduces the expression of VEGF caused by ischemia, but the thermal effect of the laser can damage the adjacent normal retina (Shimada et al., 2021). Although long-term anti-VEGF therapy has been widely used in clinical treatment and is effective in inhibiting neovascularization, it also affects a physiological amount of VEGF essential for retinal homeostasis

(Ibuki et al., 2020). VEGF is necessary for the survival of choroidal endothelial cells and protects choroidal blood vessel integrity (Semeraro et al., 2015). After repeated anti-VEGF treatment, geographic macular atrophy, which seriously affects visual acuity is usually formed in the clinic (Spooner et al., 2020). Anti-VEGF agents can enter the bloodstream in a significant amount and the systemic safety risks of anti-VEGF agents should be considered (Avery et al., 2017). Animal experiments reported that after injection of anti-VEGF drugs, there was a risk of thrombotic microangiopathy in retinal blood vessels (Schraermeyer and Julien, 2012; Julien et al., 2013). PEDF could prevent ischemia-induced retinopathy and inhibited neovascularization without overt harm to established retinal vessels. (Ogata et al., 2001; Stellmach et al., 2001). In this experiment, the EM results showed that the endothelial cells of the choroidal vessels were relatively regular. PEDF inhibits the formation of filopodia-like projections which have practically the same morphology as in the labyrinth capillaris found in human CNV. Due to the reduced lumen, thrombocytes are hindered by the filopodia-like projections and cannot reach the open gaps between the endothelial cells which are probably responsible for the permanent leakage of fluid. The area of the choroidal lumen and vessel were significantly larger in the PEDF-treated eyes compared to the ischemic non-treated eyes, indicating that PEDF prevents ischemia-induced damage and keeps the choroidal vessels open and maintains blood supply to the choroidal and retinal tissue. The protective mechanism is not clear. Based on a previous study, P78-PEDF peptide treatment resulted in preservation of podocyte structural integrity and prevention of the marked disruption and organization of the actin cytoskeleton produced by treatment with puromycin aminonucleoside (PAN) and preservation of podocyte actin mRNA expression (Awad et al., 2013). PEDF may play a role in protecting the integrity of choroidal blood vessels by protecting actin from disruption and stabilizing the cytoskeleton of endothelial cells. The effect of PEDF on pathological vessels is twofold. On the one hand it stabilizes the vessel lumen and maintains the blood supply. On the other hand it inhibits filopodia formation which allows thrombocytes to reach and close open gaps between endothelial cells.

9 Outlook

Nowadays, CNV is treated by routine intraocular injection of anti-VEGF agents, which has improved or maintained the visual prognosis, but in many instances, vision deteriorates because of the persistent fluid exudation, subretinal fibrosis, geographic atrophy in the macular area in dry AMD, and photoreceptor loss near the fovea. The major reason is the leakiness of CNV induced by VEGF. PEDF has a dual function, neurotrophic/neuroprotective and antiangiogenic activity. The neuroprotective effect of PEDF on the neural retina has been demonstrated in our study. So far, we do not yet know whether PEDF prevents the VEGF-induced vascular leakiness and stabilizes the vessel. If PEDF can stabilize the CNV, it may reduce subretinal fibrosis, geographic atrophy in dry AMD and then photoreceptor apoptosis. PEDF is among the most important factors of angiogenesis and neuroprotection in the eye.

The treatment methods for ischemic retinopathy are anti-VEGF therapy and laser photocoagulation. The aim of these treatments is to reduce VEGF and avoid the formation of neovascularization. However, under ischemic/hypoxic conditions, HIF-1α is increased. The pathological activation of the HIF pathway leads to expression of pro-angiogenic genes and causes ocular neovascularization. VEGF is one of the downstream transcription factors of HIF-1α. Compared to anti-VEGF drugs, anti-HIF therapies can delimitate the production and secretion of many angiogenic factors. Anti-HIF treatment may be more effective in the treatment of ischemic retinopathy.

The half-life of PEDF protein is unclear. Extending the half-life of PEDF is beneficial to prolong the action time of the PEDF. Anti-VEGF drugs combined with PEDF to treat CNV still need to be verified by animal experiments, and then conducted in clinical trials. The optimal ratio of anti-VEGF drugs to PEDF requires large sample clinical trials for testing. Due to PEDF's dual function and the results of the combined therapy, an anti-VEGF drug combined with PEDF is recommended for the treatment of CNV.

In addition, the drugs are administered intravitreally and delivered directly to the lesion. However, intravitreal injections are associated with various complications, such as endophthalmitis, a sight-threatening ocular disease. Patients with CNV or other retinal diseases usually have to undergo

multiple injections. So, developing a sustained delivery platform to the retinal or choroidal lesions is of great interest. A longer half-life of a drug can also reduce the frequency of intravitreal injections. However, the multiple barriers against drug penetration such as the cornea and the choroid are challenges.

10 References

Ablonczy, Z., Prakasam, A., Fant, J., Fauq, A., Crosson, C., and Sambamurti, K. (2009). Pigment epithelium-derived factor maintains retinal pigment epithelium function by inhibiting vascular endothelial growth factor-R2 signaling through gamma-secretase. J Biol Chem *284*, 30177-30186.

Al-Ani, A., Sunba, S., Hafeez, B., Toms, D., and Ungrin, M. (2020). In Vitro Maturation of Retinal Pigment Epithelium Is Essential for Maintaining High Expression of Key Functional Genes. Int J Mol Sci *21*.

Alder, V.A., Ben-Nun, J., and Cringle, S.J. (1990). PO_2 profiles and oxygen consumption in cat retina with an occluded retinal circulation. Invest Ophthalmol Vis Sci *31*, 1029-1034.

Alves, C.H., Fernandes, R., Santiago, A.R., and Ambrósio, A.F. (2020). Microglia Contribution to the Regulation of the Retinal and Choroidal Vasculature in Age-Related Macular Degeneration. Cells *9*.

Amaral, J., and Becerra, S.P. (2010). Effects of human recombinant PEDF protein and PEDF-derived peptide 34-mer on choroidal neovascularization. Invest Ophthalmol Vis Sci *51*, 1318-1326.

An, S.H., and Jeong, W.J. (2020). Early-scatter laser photocoagulation promotes the formation of collateral vessels in branch retinal vein occlusion. Eur J Ophthalmol *30*, 370-375.

Askou, A.L., Alsing, S., Benckendorff, J.N.E., Holmgaard, A., Mikkelsen, J.G., Aagaard, L., Bek, T., Corydon, T.J. (2019). Suppression of Choroidal Neovascularization by AAV-Based Dual-Acting Antiangiogenic Gene Therapy. Mol Ther Nucleic Acids *16*, 38-50.

Avery, R.L., Castellarin, A.A., Steinle, N.C., Dhoot, D.S., Pieramici, D.J., See, R., Couvillion, S., Nasirm M.A., Rabena, M.D., Maia, M., Van, Everen, S., Le, K., and Hanley, W.D. (2017). SYSTEMIC PHARMACOKINETICS AND PHARMACODYNAMICS OF INTRAVITREAL AFLIBERCEPT, BEVACIZUMAB, AND RANIBIZUMAB. Retina *37*, 1847-1858.

Awad, A.S., Gao, T., Gvritishvili, A., You, H., Liu, Y., Cooper, T.K., Reeves, W.B., and Tombran-Tink, J. (2013). Protective role of small pigment epithelium-derived factor (PEDF) peptide in diabetic renal injury. Am J Physiol Renal Physiol *305*, 891-900.

Bakri, S.J., Thorne, J.E., Ho, A.C., Ehlers, J.P., Schoenberger, S.D., Yeh, S., and Kim, S.J. (2019). Safety and Efficacy of Anti-Vascular Endothelial Growth Factor Therapies for Neovascular Age-Related Macular Degeneration: A Report by the American Academy of Ophthalmology. Ophthalmology *126*, 55-63.

Bascuas, T., Kropp, M., Harmening, N., Asrih, M., Izsvák, Z., and Thumann, G. (2020). Induction and Analysis of Oxidative Stress in Sleeping Beauty Transposon-Transfected Human Retinal Pigment Epithelial Cells. J Vis Exp *11*.

Becerra, S.P., Fariss, R.N., Wu, Y.Q., Montuenga, L.M., Wong, P., and Pfeffer, B.A. (2004). Pigment epithelium-derived factor in the monkey retinal pigment epithelium and interphotoreceptor matrix: apical secretion and distribution. Exp Eye Res *78*, 223-234.

Bermudez, M.A., and Gonzalez, F. (2020). Differential sensitivity of the On and Off visual responses to retinal ischemia. Exp Eye Res *191*.

Bhutto, I.A., McLeod, D.S., Hasegawa, T., Kim, S.Y., Merges, C., Tong, P., and Lutty, G.A. (2006). Pigment epithelium-derived factor (PEDF) and vascular endothelial growth factor (VEGF) in aged human choroid and eyes with age-related macular degeneration. Exp Eye Res *82*, 99-110.

Bhuvaneswari, R., Gan, Y.Y., Yee, K.K., Soo, K.C., and Olivo, M. (2007). Effect of hypericin-mediated photodynamic therapy on the expression of vascular endothelial growth factor in human nasopharyngeal carcinoma. Int J Mol Med *20*, 421-428.

Blaauwgeers, H.G., Holtkamp, G.M., Rutten, H., Witmer, A.N., Koolwijk, P., Partanen, T.A., Alitalo, K., Kroon, M.E., Kijlstra, A., van, Hinsbergh.V.W., and Schlingemann, R.O. (1999). Polarized vascular endothelial growth factor secretion by human retinal pigment epithelium and localization of vascular endothelial growth factor receptors on the inner choriocapillaris. Evidence for a trophic paracrine relation. Am J Pathol *155*, 421-428.

Boyd, S.R., Zachary, I., Chakravarthy, U., Allen, G.J., Wisdom, G.B., Cree, I.A., Martin, J.F., and Hykin, P.G. (2002). Correlation of increased vascular endothelial growth factor with neovascularization and permeability in ischemic central vein occlusion. Arch Ophthalmol *120*, 1644-1650.

Bürger, S., Meng, J., Zwanzig, A., Beck, M., Pankonin, M., Wiedemann, P., Eichler, W., and Unterlauft, J.D. (2020). Pigment Epithelium-Derived Factor (PEDF) Receptors Are

Involved in Survival of Retinal Neurons. Int J Mol Sci *22*, 369.

Cai, J., Wu, L., Qi, X., Li, Calzi, S., Caballero, S., Shaw, L., Ruan, Q., Grant, M.B., and Boulton, M.E. (2011). PEDF regulates vascular permeability by a γ-secretase-mediated pathway. PLoS One *6*.

Campochiaro, P.A., Bhisitkul, R.B., Shapiro, H., and Rubio, R.G. (2013). Vascular endothelial growth factor promotes progressive retinal nonperfusion in patients with retinal vein occlusion. Ophthalmology *120*, 795-802.

Cao, R., Eriksson, A., Kubo, H., Alitalo, K., Cao, Y., and Thyberg, J. (2004). Comparative evaluation of FGF-2-, VEGF-A-, and VEGF-C-induced angiogenesis, lymphangiogenesis, vascular fenestrations, and permeability. Circ Res *94*, 664-670.

Cao, W., Tombran-Tink, J., Elias, R., Sezate, S., Mrazek, D., and McGinnis, J.F. (2001). In vivo protection of photoreceptors from light damage by pigment epithelium-derived factor. Invest Ophthalmol Vis Sci *42*, 1646-1652.

Carnevali, A., Sacconi, R., Querques, L., Marchese, A., Capuano, V., Rabiolo, A., Corbelli, E., Panozzo, G., Miere, A., Souied, E., Bandello, F., and Querques, G. (2018). Natural History of Treatment-Naïve Quiescent Choroidal Neovascularization in Age-Related Macular Degeneration Using OCT Angiography. Ophthalmol Retina *2*, 922-930.

Catalani, E., Cervia, D., Martini, D., Bagnoli, P., Simonetti, E., Timperio, A.M., and Casini, G. (2007). Changes in neuronal response to ischemia in retinas with genetic alterations of somatostatin receptor expression. Eur J Neurosci *25*, 1447-1459.

Cauble, M., Yang, P., Baumann, U., Gebauer, J.M., Orr, B.G., Duong, L.T., and Banaszak, Holl.M.M. (2017). Microstructure dependent binding of pigment epithelium derived factor (PEDF) to type I collagen fibrils. J Struct Biol *199*, 132-139.

Cayouette, M., Smith, S.B., Becerra, S.P., and Gravel, C. (1999). Pigment epithelium-derived factor delays the death of photoreceptors in mouse models of inherited retinal degenerations. Neurobiol Dis *6*, 523-532.

Chen, L., Zhang, S.S., Barnstable, C.J., and Tombran-Tink, J. (2006). PEDF induces apoptosis in human endothelial cells by activating p38 MAP kinase dependent cleavage of multiple caspases. Biochem Biophys Res Commun *348*, 1288-1295.

Chew, E.Y., Ferris, F.L.3rd., Csaky, K.G., Murphy, R.P., Agrón, E., Thompson, D.J., Reed, G.F., and

Schachat, A.P. (2003). The long-term effects of laser photocoagulation treatment in patients with diabetic retinopathy: the early treatment diabetic retinopathy follow-up study. Ophthalmology *110*, 1683-1689.

Cho, H.J., Kim, K., Lim, S.H., Kang, D.H., and Kim, J.W. (2020). Retinal pigment epithelial atrophy after anti-vascular endothelial growth factor therapy for polypoidal choroidal vasculopathy. Br J Ophthalmol *104*, 1443-1447.

Coassin, M., Duncan, K.G., Bailey, K.R., Singh, A., and Schwartz, D.M. (2010). Hypothermia reduces secretion of vascular endothelial growth factor by cultured retinal pigment epithelial cells. Br J Ophthalmol *94*, 1678-1683.

Coelho, J., Ferreira, A., Abreu, A.C., Monteiro, S., Furtado, M.J., Gomes, M., and Lume, M. (2021). Choroidal neovascularization secondary to pathological myopia-macular Bruch membrane defects as prognostic factor to anti-VEGF treatment. Graefes Arch Clin Exp Ophthalmol *21*.

Coleman, D.J., Silverman, R.H., Rondeau, M.J., Lloyd, H.O., Khanifar, A.A., and Chan, R.V. (2013). Age-related macular degeneration: choroidal ischaemia? Br J Ophthalmol *8*, 1020-1023.

Colijn, J.M., Buitendijk, G.H.S., Prokofyeva, E., Alves, D., Cachulo, M.L., Khawaja, A.P., Cougnard-Gregoire, A., Merle, B.M.J., Korb, C., Erke, M.G., *et al*. (2017). Prevalence of Age-Related Macular Degeneration in Europe: The Past and the Future. Ophthalmology. *124*, 1753-1763.

Comitato, A., Subramanian, P., Turchiano, G., Montanari, M., Becerra, S.P., and Marigo, V. (2018). Pigment epithelium-derived factor hinders photoreceptor cell death by reducing intracellular calcium in the degenerating retina. Cell Death Dis *9*.

Costa, J.V., Moura-Coelho, N., Abreu, A.C., Neves, P., Ornelas, M., and Furtado, M.J. (2021). Macular edema secondary to retinal vein occlusion in a real-life setting: a multicenter, nationwide, 3-year follow-up study. Graefes Arch Clin Exp Ophthalmol *259*, 343-350.

Costa, R.A., Navajas, E.V., Farah, M.E., Calucci, D., Cardillo, J.A., and Scott, I.U. (2005). Polypoidal choroidal vasculopathy: angiographic characterization of the network vascular elements and a new treatment paradigm. Prog Retin Eye Res *5*, 560-586.

Daniel, E., Pan, W., Ying, G.S., Kim, B.J., Grunwald, J.E., Ferris, F.L.3rd., Jaffe, G.J., Toth, C.A., Martin, D.F., Fine, S.L., and Maguire, M.G. (2018). Comparison of Age-related Macular

Degeneration Treatments Trials. Development and Course of Scars in the Comparison of Age-Related Macular Degeneration Treatments Trials. Ophthalmology *7*, 1037-1046.

Daniel, E., Toth, C.A., Grunwald, J.E., Jaffe, G.J., Martin, D.F., Fine, S.L., Huang, J., Ying, G.S., Hagstrom, S.A., Winter, K., and Maguire, M.G. (2014). Comparison of Age-related Macular Degeneration Treatments Trials Research Group. Risk of scar in the comparison of age-related macular degeneration treatments trials. Ophthalmology *121*, 656-666.

Doğan, M., and Kutluksaman, B. (2021). Macular pigment optical density after panretinal photocoagulation. Clin Exp Optom *104*, 187-193.

Ehlken, C., Jungmann, S., Böhringer, D., Agostini, H.T., Junker, B., and Pielen, A. (2014). Switch of anti-VEGF agents is an option for nonresponders in the treatment of AMD. Eye (Lond) *28*, 538-545.

Eichler, W., Savković-Cvijić, H., Bürger, S., Beck, M., Schmidt, M., Wiedemann, P., Reichenbach, A., and Unterlauft, J.D. (2017). Müller Cell-Derived PEDF Mediates Neuroprotection via STAT3 Activation. Cell Physiol Biochem *44*, 1411-1424.

El, Matri.L., Chebil, A., and Kort, F. (2015). Current and emerging treatment options for myopic choroidal neovascularization. Clin Ophthalmol *9*, 733-744.

Eris, E., and Vural, E. (2019). Early retinal and choroidal effect of photodynamic treatment in patients with polypoidal choroidal vasculopathy with or without anti-vascular endothelial growth factor: An optical coherence tomography angiography study. Photodiagnosis Photodyn Ther *25*, 1-6.

Falero-Perez, J., Park, S., Sorenson, C.M., and Sheibani, N. (2017). PEDF expression affects retinal endothelial cell proangiogenic properties through alterations in cell adhesive mechanisms. Am J Physiol Cell Physiol *313*, 405-420.

Farnoodian, M., Sorenson, C.M., and Sheibani, N. (2018). PEDF expression affects the oxidative and inflammatory state of choroidal endothelial cells. Am J Physiol Cell Physiol *314*, 456-472.

Farnoodian, M., Wang, S., Dietz, J., Nickells, R.W., Sorenson, C.M., and Sheibani, N. (2017). Negative regulators of angiogenesis: important targets for treatment of exudative AMD. Clin Sci (Lond) *131*, 1763-1780.

Fields, M.A., Bowrey, H.E., Gong, J., Moreira, E.F., Cai, H., Del, and Priore, L.V. (2017).

Extracellular matrix nitration alters growth factor release and activates bioactive complement in human retinal pigment epithelial cells. PLoS One *12*.

Fleckenstein, M., Keenan, T.D.L., Guymer, R.H., Chakravarthy, U., Schmitz-Valckenberg, S., Klaver, C.C., Wong, W.T., and Chew, E.Y. (2021). Age-related macular degeneration. Nat Rev Dis Primers *7*, 31.

Ford, K.M., Saint-Geniez, M., Walshe, T., Zahr, A., and D'Amore, P.A. (2011). Expression and role of VEGF in the adult retinal pigment epithelium. Invest Ophthalmol Vis Sci *52*, 9478-9487.

Fukushima, A., Maruko, I., Chujo, K., Hasegawa, T., Arakawa, H., and Iida, T. (2021). Characteristics of treatment-naïve quiescent choroidal neovascularization detected by optical coherence tomography angiography in patients with age-related macular degeneration. Graefes Arch Clin Exp Ophthalmol.

Fung, F.K., Law, B.Y., and Lo, A.C. (2016). Lutein Attenuates Both Apoptosis and Autophagy upon Cobalt (II) Chloride-Induced Hypoxia in Rat Műller Cells. PLoS One *11*.

Gao, G., Li, Y., Zhang, D., Gee, S., Crosson, C., and Ma, J. (2001). Unbalanced expression of VEGF and PEDF in ischemia-induced retinal neovascularization. FEBS Lett *489*, 270-276.

Giansanti, F., Virgili, G., Donati, M.C., Giuntoli, M., Pieretti, G., Abbruzzese, G., and Menchini, U. (2012). Long-term results of photodynamic therapy for subfoveal choroidal neovascularization with pathologic myopia. Retina *32*, 1547-1552.

Grossniklaus, H.E., Kang, S.J., and Berglin, L. (2010). Animal models of choroidal and retinal neovascularization. Prog Retin Eye Res *29*, 500-519.

Grossniklaus, H.E., Ling, J.X., Wallace, T.M., Dithmar, S., Lawson, D.H., Cohen, C., Elner, V.M., Elner, S.G., and Sternberg, P.Jr. (2002). Macrophage and retinal pigment epithelium expression of angiogenic cytokines in choroidal neovascularization. Mol Vis *8*, 119-126.

Hajdu, D., Told, R., Angeli, O., Weigert, G., Pollreisz, A., Schmidt-Erfurth, U., and Sacu, S. (2020). Identification of microvascular and morphological alterations in eyes with central retinal non-perfusion. PLoS One *15*.

Hamilton, M.M., Byrnes, G.A., Gall, J.G., Brough, D.E., King, C.R., and Wei, L.L. (2008). Alternate serotype adenovector provides long-term therapeutic gene expression in the eye. Mol Vis *14*, 2535-2546.

Hanna, R.M., Tran, N.T., Patel, S.S., Hou, J., Jhaveri, K.D., Parikh, R., Selamet, U., Ghobry, L.,

Wassef, O., Barsoum, M., Bijol, V., Kalantar-Zadeh, K., Pai, A., Amin, A., Kupperman, B., and Kurtz, I.B. (2020). Thrombotic Microangiopathy and Acute Kidney Injury Induced After Intravitreal Injection of Vascular Endothelial Growth Factor Inhibitors VEGF Blockade-Related TMA After Intravitreal Use. Front Med (Lausanne) *7*.

Hernández-Pinto, A., Polato, F., Subramanian, P., Rocha-Muñoz, A., Vitale, S., de la, Rosa, E.J., and Becerra, S.P. (2019). PEDF peptides promote photoreceptor survival in rd10 retina models. Exp Eye Res *184*, 24-29.

He, X., Cheng, R., Park, K., Benyajati, S., Moiseyev, G., Sun, C., Olson, L.E., Yang, Y., Eby, B.K., Lau, K., and Ma, J.X. (2017). Pigment epithelium-derived factor, a noninhibitory serine protease inhibitor, is renoprotective by inhibiting the Wnt pathway. Kidney Int *91*, 642-657.

Ho, T.C., Chen, S.L., Yang, Y.C., Lo, T.H., Hsieh, J.W., Cheng, H.C., and Tsao, Y.P. (2009). Cytosolic phospholipase A2-{alpha} is an early apoptotic activator in PEDF-induced endothelial cell apoptosis. Am J Physiol Cell Physiol *296*, 273-284.

Ho, T.C., Chen, S.L., Shih, S.C., Wu, J.Y., Han, W.H., Cheng, H.C., Yang, S.L., and Tsao, Y.P. (2010). Pigment epithelium-derived factor is an intrinsic antifibrosis factor targeting hepatic stellate cells. Am J Pathol *177*, 1798-1811.

Hurst, J., Mueller-Buehl, A.M., Hofmann, L., Kuehn, S., Herms, F., Schnichels, S., and Joachim, S.C. (2020). iNOS-inhibitor driven neuroprotection in a porcine retina organ culture model. J Cell Mol Med *24*, 4312-4323.

Ibuki, M., Lee, D., Shinojima, A., Miwa, Y., Tsubota, K., and Kurihara, T. (2020). Rice Bran and Vitamin B6 Suppress Pathological Neovascularization in a Murine Model of Age-Related Macular Degeneration as Novel HIF Inhibitors. Int J Mol Sci *21*, 8940.

Ingavale, S.S., Chang, Y.C., Lee, H., McClelland, C.M., Leong, M.L., and Kwon-Chung, K.J. (2008). Importance of mitochondria in survival of Cryptococcus neoformans under low oxygen conditions and tolerance to cobalt chloride. PLoS Pathog *4*.

Isola, V., Pece, A., and Parodi, M.B. (2006). Choroidal ischemia after photodynamic therapy with verteporfin for choroidal neovascularization. Am J Ophthalmol *142*, 680-683.

Jaffe, G.J., Ying, G.S., Toth, C.A., Daniel, E., Grunwald, J.E., Martin, D.F., and Maguire, M.G. (2019). Comparison of Age-related Macular Degeneration Treatments Trials Research Group. Macular Morphology and Visual Acuity in Year Five of the Comparison of Age-

related Macular Degeneration Treatments Trials. Ophthalmology *126*, 252-260.

Jalilian, E., Elkin, K., and Shin, S.R. (2020). Novel Cell-Based and Tissue Engineering Approaches for Induction of Angiogenesis as an Alternative Therapy for Diabetic Retinopathy. Int J Mol Sci *21*, 3496.

Jamali, H., Eslami, J., Kalashipour, F., and Nowroozzadeh, M.H. (2021). EFFECT OF PANRETINAL PHOTOCOAGULATION ON CORNEAL SENSATION AND TEAR FUNCTION IN PATIENTS WITH DIABETIC RETINOPATHY. Retina *41*, 338-344.

Johnen, S., Djalali-Talab, Y., Kazanskaya, O., Möller, T., Harmening, N., Kropp, M., Izsvák, Z., Walter, P., and Thumann, G. (2015). Antiangiogenic and Neurogenic Activities of Sleeping Beauty-Mediated PEDF-Transfected RPE Cells In Vitro and In Vivo. Biomed Res Int *2015*.

Johnston, E.K., Francis, M.K., and Knepper, J.E. (2015). Recombinant pigment epithelium-derived factor PEDF binds vascular endothelial growth factor receptors 1 and 2. In Vitro Cell Dev Biol Anim *51*, 730-738.

Jovanovic, J., Liu, X., Kokona, D., Zinkernagel, M.S., and Ebneter, A. (2020). Inhibition of inflammatory cells delays retinal degeneration in experimental retinal vein occlusion in mice. Glia *68*, 574-588.

Julien, S., Biesemeier, A., and Schraermeyer, U. (2013). In vitro induction of protein complexes between bevacizumab, VEGF-A^{165} and heparin: explanation for deposits observed on endothelial veins in monkey eyes. Br J Ophthalmol *97*, 511-517.

Kang, E.C., Seo, J.G., Kim, B.R., and Koh, H.J. (2017). CLINICAL OUTCOMES OF INTRAVITREAL BEVACIZUMAB VERSUS PHOTODYNAMIC THERAPY WITH OR WITHOUT BEVACIZUMAB FOR MYOPIC CHOROIDAL NEOVASCULARIZATION: A 7-Year Follow-up Study. Retina *37*, 1775-1783.

Karovic, O., Tonazzini, I., Rebola, N., Edström, E., Lövdahl, C., Fredholm, B.B., and Daré, E. (2007). Toxic effects of cobalt in primary cultures of mouse astrocytes. Similarities with hypoxia and role of HIF-1alpha. Biochem Pharmacol *73*, 694-708.

Khayat, M., Wright, D.M., Yeong, J., Xu, D., Donley, C., Lakshmipathy, G.R., Low, M.K., White, N., Williams, M., and Lois, N. (2020). IMPACT OF RETINAL ISCHEMIA ON FUNCTIONAL AND ANATOMICAL OUTCOMES AFTER ANTI-VASCULAR ENDOTHELIAL GROWTH FACTOR THERAPY IN PATIENTS WITH RETINAL VEIN

OCCLUSION. Retina *40*, 1098-1109.

Khojasteh, H., Amini, Vishte.R., Mirzajani, A., Khalili, Pour.E., Bazvand, F., Riazi-Esfahani, H., Mirghorbani, M., and Modjtahedi, B.S. (2020). Electroretinogram Changes Following Sequential Panretinal Photocoagulation for Proliferative Diabetic Retinopathy. Clin Ophthalmol *14*, 967-975.

Kim, C.S., Shin, K.S., Lee, H.J., Jo, Y.J., and Kim, J.Y. (2014). Sectoral retinal nerve fiber layer thinning in branch retinal vein occlusion. Retina *34*, 525-530.

Kim, H.W., Roh, K.H., Kim, S.W., Park, S.J., Lim, N.Y., Jung, H., Choi, I.W., and Park, S. (2019). Type I pig collagen enhances the efficacy of PEDF 34-mer peptide in a mouse model of laser-induced choroidal neovascularization. Graefes Arch Clin Exp Ophthalmol *257*, 1709-1717.

Kim, J.H., Chang, Y.S., Kim, J.W., Lee, T.G., Kim, C.G., and Lee, D.W. (2016). Radiating hemorrhage in exudative age-related macular degeneration. Jpn J Ophthalmol *6*, 466-475.

Kim, J., Kim, J.H., Do, J.Y., Lee, J.Y., Yanai, R., Lee, I.K., Suk, K., and Park, D.H. (2021). Key Role of Microglial Matrix Metalloproteinases in Choroidal Neovascularization. Front Cell Neurosci *15*.

Kim, J.T., and Park, N. (2020). Changes in choroidal vascular parameters following pan-retinal photocoagulation using swept-source optical coherence tomography. Graefes Arch Clin Exp Ophthalmol *258*, 39-47.

Kim, J.Y., Park, S., Park, S.H., Lee, D., Kim, G.H., Noh, J.E., Lee, K.J., and Kim, G.J. (2021). Overexpression of pigment epithelium-derived factor in placenta-derived mesenchymal stem cells promotes mitochondrial biogenesis in retinal cells. Lab Invest *101*, 51-69.

Koh, A., Lim, T.H., Au, Eong, K.G., Chee, C., Ong, S.G., Tan, N., Yeo, I., and Wong, D. (2011). Optimising the management of choroidal neovascularisation in Asian patients: consensus on treatment recommendations for anti-VEGF therapy. Singapore Med J *52*, 232-240.

Koizumi, H., and Hatanaka, H. (2010). Severe retinal vascular infarction after photodynamic therapy with verteporfin using the standard protocol. Arch Ophthalmol *128*, 259-262.

Krebs, I., Glittenberg, C., Ansari-Shahrezaei, S., Hagen, S., Steiner, I., and Binder, S. (2013). Non-responders to treatment with antagonists of vascular endothelial growth factor in age-related macular degeneration. Br J Ophthalmol *97*, 1443-1446.

Kurihara, T., Westenskow, P.D., Bravo, S., Aguilar, E., and Friedlander, M. (2012). Targeted deletion of Vegfa in adult mice induces vision loss. J Clin Invest *122*, 4213-4217.

Lai, T.Y., Chan, W.M., and Lam, D.S. (2004). Transient reduction in retinal function revealed by multifocal electroretinogram after photodynamic therapy. Am J Ophthalmol *137*, 826-833.

Langenfeld, A., Julien, S., and Schraermeyer, U. (2015). An improved method for the isolation and culture of retinal pigment epithelial cells from adult rats. Graefes Arch Clin Exp Ophthalmol *253*, 1493-1502.

Lee, D., Kang, H., Yoon, K.Y., Chang, Y.Y., and Song, H.B. (2020). A mouse model of retinal hypoperfusion injury induced by unilateral common carotid artery occlusion. Exp Eye Res, *201*.

Lee, D., Miwa, Y., Jeong, H., Ikeda, S.I., Katada, Y., Tsubota, K., and Kurihara, T. (2020). A Murine Model of Ischemic Retinal Injury Induced by Transient Bilateral Common Carotid Artery Occlusion. J Vis Exp *12*.

Lee, P.Y., Kim, K.S., and Lee, W.K. (2009). Severe choroidal ischemia following photodynamic therapy for pigment epithelial detachment and chronic central serous chorioretinopathy. Jpn J Ophthalmol *53*, 52-56.

Lin, C.M., Titchenell, P.M., Keil, J.M., Garcia-Ocaña, A., Bolinger, M.T., Abcouwer, S.F., and Antonetti, D.A. (2018). Inhibition of Atypical Protein Kinase C Reduces Inflammation-Induced Retinal Vascular Permeability. Am J Pathol *188*, 2392-2405.

Liu, L., Xia, F., and Hua, R. (2021). Retinal nonperfusion in optical coherence tomography angiography. Photodiagnosis Photodyn Ther *33*.

Liu, S., Biesemeier, A.K., Tschulakow, A.V., Thakkar, H.V., Julien-Schraermeyer, S., and Schraermeyer, U. (2020). A new rat model of treatment-naive quiescent choroidal neovascularization induced by human VEGF165 overexpression. Biol Open *9*, 6.

Lutty, G.A., McLeod, D.S., Bhutto, I.A., Edwards, M.M., and Seddon, J.M. (2020). Choriocapillaris dropout in early age-related macular degeneration. Exp Eye Res *192*.

Ma, B., Zhou, Y., Liu, R., Zhang, K., Yang, T., Hu, C., Gao, Y., Lan, Q., Liu, Y., Yang, X., and Qi, H. (2021). Pigment epithelium-derived factor (PEDF) plays anti-inflammatory roles in the pathogenesis of dry eye disease. Ocul Surf *20*, 70-85.

Maminishkis, A., Chen, S., Jalickee, S., Banzon, T., Shi, G., Wang, F.E., Ehalt, T., Hammer, J.A.,

and Miller, S.S. (2006). Confluent monolayers of cultured human fetal retinal pigment epithelium exhibit morphology and physiology of native tissue. Invest Ophthalmol Vis Sci *47*, 3612-3624.

Mansour, A.M., Bynoe, L.A., Welch, J.C., Pesavento, R., Mahendradas, P., Ziemssen, F., and Pai, S.A. (2010). Retinal vascular events after intravitreal bevacizumab. Acta Ophthalmol *88*, 730-735.

Marneros, A.G., Fan, J., Yokoyama, Y., Gerber, H.P., Ferrara, N., Crouch, R.K., and Olsen, B.R. (2005). Vascular endothelial growth factor expression in the retinal pigment epithelium is essential for choriocapillaris development and visual function. Am J Pathol *167*, 1451-1459.

Martinez, B., and Peplow, P.V. (2021). MicroRNAs in laser-induced choroidal neovascularization in mice and rats: their expression and potential therapeutic targets. Neural Regen Res *16*, 621-627.

Mastrodimou, N., Lambrou, G.N., and Thermos, K. (2005). Effect of somatostatin analogues on chemically induced ischaemia in the rat retina. Naunyn Schmiedebergs Arch Pharmacol *371*, 44-53.

Matysik-Woźniak, A., Loewenstein, A., Bielecka, E., and Rejdak, R. (2021). Activation of a Quiescent Choroidal Neovascularization in a Patient with Age-Related Macular Degeneration. Case Rep Ophthalmol *12*, 433-437.

Mettu, P.S., Allingham, M.J., and Cousins, S.W. (2020). Incomplete response to Anti-VEGF therapy in neovascular AMD: Exploring disease mechanisms and therapeutic opportunities. Prog Retin Eye Res *3*.

Miyazaki, M., Ikeda, Y., Yonemitsu, Y., Goto, Y., Sakamoto, T., Tabata, T., Ueda, Y., Hasegawa, M., Tobimatsu, S., Ishibashi, T., Sueishi, K. (2003). Simian lentiviral vector-mediated retinal gene transfer of pigment epithelium-derived factor protects retinal degeneration and electrical defect in Royal College of Surgeons rats. Gene Ther *10*, 1503-1511.

Mori, K., Duh, E., Gehlbach, P., Ando, A., Takahashi, K., Pearlman, J., Mori, K., Yang, H.S., Zack, D.J., Ettyreddy, D., Brough, D.E., Wei, L.L., and Campochiaro, P.A. (2001). Pigment epithelium-derived factor inhibits retinal and choroidal neovascularization. J Cell Physiol *188*, 253-263.

Mori, K., Gehlbach P, Yamamoto S, Duh E, Zack DJ, Li Q, Berns KI, Raisler BJ, Hauswirth WW,

Campochiaro PA. AAV-mediated gene transfer of pigment epithelium-derived factor inhibits choroidal neovascularization. Invest Ophthalmol Vis Sci. 2002 Jun;43(6):1994-2000.

Neo, T., Gozawa, M., Takamura, Y., Inatani, M., and Oki, M. (2020). Gene expression profile analysis of the rabbit retinal vein occlusion model. PLoS One *15*.

Nesper, P.L., Ong, J.X., and Fawzi, A.A. (2021). Exploring the Relationship Between Multilayered Choroidal Neovascularization and Choriocapillaris Flow Deficits in AMD. Invest Ophthalmol Vis Sci *62*.

Noma, H., Mimura, T., Yasuda, K., and Shimura, M. (2014). Role of soluble vascular endothelial growth factor receptors-1 and -2, their ligands, and other factors in branch retinal vein occlusion with macular edema. Invest Ophthalmol Vis Sci *55*, 3878-3885.

Noma, H., Funatsu, H., Mimura, T., Harino, S., and Hori, S. (2009). Vitreous levels of interleukin-6 and vascular endothelial growth factor in macular edema with central retinal vein occlusion. Ophthalmology *116*, 87-93.

Noma, H., Yasuda, K., and Shimura, M. (2020). Cytokines and Pathogenesis of Central Retinal Vein Occlusion. J Clin Med *9*.

Ogata, N., Wang, L., Jo, N., Tombran-Tink, J., Takahashi, K., Mrazek, D., and Matsumura, M. (2001). Pigment epithelium derived factor as a neuroprotective agent against ischemic retinal injury. Curr Eye Res *22*, 245-252.

Osborne, N.N., Casson, R.J., Wood, J.P., Chidlow, G., Graham, M., and Melena, J. (2004). Retinal ischemia: mechanisms of damage and potential therapeutic strategies. Prog Retin Eye Res *23*, 91-147.

Osaadon, P., Fagan, X.J., Lifshitz, T., and Levy, J. (2014). A review of anti-VEGF agents for proliferative diabetic retinopathy. Eye (Lond) *28*, 510-520.

Oz, O., Gürelik, G., Akyürek, N., Cinel, L., and Hondur, A. (2005). A short duration transient ischemia induces apoptosis in retinal layers: an experimental study in rabbits. Eur J Ophthalmol *15*, 233-238.

Pang, I.H., Zeng, H., Fleenor, D.L., and Clark, A.F. (2007). Pigment epithelium-derived factor protects retinal ganglion cells. BMC Neurosci *8*.

Pfau, M., Möller, P.T., Künzel, S.H., von, der, Emde, L., Lindner, M., Thiele, S., Dysli, C., Nadal, J., Schmid, M., Schmitz-Valckenberg, S., Holz, F.G., and Fleckenstein, M. (2020). Type 1

Choroidal Neovascularization Is Associated with Reduced Localized Progression of Atrophy in Age-Related Macular Degeneration. Ophthalmol Retina *4*, 238-248.

Pournaras, C.J., Rungger-Brändle, E., Riva, C.E., Hardarson, S.H., and Stefansson, E. (2008). Regulation of retinal blood flow in health and disease. Prog Retin Eye Res *27*, 284-330.

Principe, D.R., DeCant, B., Diaz, A.M., Mangan, R.J., Hwang, R., Lowy, A., Shetuni, B.B., Sreekumar, B.K., Chung, C., Bentrem, D.J., Munshi, H.G., Jung, B., Grippo, P.J., and Bishehsari, F. (2016). PEDF inhibits pancreatic tumorigenesis by attenuating the fibro-inflammatory reaction. Oncotarget *7*, 28218-28234.

Querques, G., Srour, M., Massamba, N., Georges, A., Ben, Moussa, N., Rafaeli, O., and Souied, E.H. (2013). Functional characterization and multimodal imaging of treatment-naive "quiescent" choroidal neovascularization. Invest Ophthalmol Vis Sci *54*, 6886-6892.

Rasmussen, H., Chu, KW., Campochiaro, P., Gehlbach, PL., Haller, JA., Handa, JT., Nguyen, QD., and Sung, JU. (2001). Clinical protocol. An open-label, phase I, single administration, dose-escalation study of ADGVPEDF.11D (ADPEDF) in neovascular age-related macular degeneration (AMD). Hum Gene Ther *12*, 2029-2032.

Rehak, M., Tilgner, E., Franke, A., Rauscher, F.G., Brosteanu, O., and Wiedemann, P. (2014). Early peripheral laser photocoagulation of nonperfused retina improves vision in patients with central retinal vein occlusion (Results of a proof of concept study). Graefes Arch Clin Exp Ophthalmol *252*, 745-752.

Reid, C.A., Nettesheim, E.R., Connor, T.B., and Lipinski, D.M. (2018). Development of an inducible anti-VEGF rAAV gene therapy strategy for the treatment of wet AMD. Sci Rep *8*.

Rishi, P., Rishi, E., Bhende, M., Agarwal, V., Vyas, C.H., Valiveti, M., Bhende, P., Rao, C., Susvar, P., Sen, P., Raman, R., Khetan, V., Murali, V., Ratra, D., and Sharma, T. (2016). Comparison of photodynamic therapy, ranibizumab/bevacizumab or combination in the treatment of myopic choroidal neovascularisation: a 9-year-study from a single centre. Br J Ophthalmol *100*, 1337-1340.

Rivera, J.C., Dabouz, R., Noueihed, B., Omri, S., Tahiri, H., and Chemtob, S. (2017). Ischemic Retinopathies: Oxidative Stress and Inflammation. Oxid Med Cell Longev *2017*.

Roberts, W.G., and Palade, G.E. (1995). Increased microvascular permeability and endothelial fenestration induced by vascular endothelial growth factor. J Cell Sci *108*, (Pt 6):2369-2379.

Rogers, S.L., McIntosh, R.L., Lim, L., Mitchell, P., Cheung, N., Kowalski, J.W., Nguyen, H.P., Wang, J.J., and Wong, T.Y. (2010). Natural history of branch retinal vein occlusion: an evidence-based systematic review. Ophthalmology *117*, 1094-1101.

Romdhane, K., Zola, M., Matet, A., Daruich, A., Elalouf, M., Behar-Cohen, F., and Mantel, I. (2020). Predictors of treatment response to intravitreal anti-vascular endothelial growth factor (anti-VEGF) therapy for choroidal neovascularisation secondary to chronic central serous chorioretinopathy. Br J Ophthalmol *104*, 910-916.

Russell, J.F., Al-Khersan, H., Shi, Y., Scott, N.L., Hinkle, J.W., Fan, K.C., Lyu, C., Feuer, W.J., Gregori, G., and Rosenfeld, P.J. (2020). Retinal Nonperfusion in Proliferative Diabetic Retinopathy Before and After Panretinal Photocoagulation Assessed by Widefield OCT Angiography. Am J Ophthalmol *213*, 177-185.

Ryu, G., Noh, D., van, Hemert.J., Sadda, S.R., and Sagong, M. (2021). Relationship between distribution and severity of non-perfusion and cytokine levels and macular thickness in branch retinal vein occlusion. Sci Rep *11*.

Schmitz, J.C., Protiva, P., Gattu, A.K., Utsumi, T., Iwakiri, Y., Neto, A.G., Quinn, M., Cornwell, M.L., Fitchev, P., Lugea, A., Crawford, S.E., and Chung, C. (2011). Pigment epithelium-derived factor regulates early pancreatic fibrotic responses and suppresses the profibrotic cytokine thrombospondin-1. Am J Pathol *179*, 2990-2999.

Schnichels, S., Kiebler, T., Hurst, J., Maliha, A.M., Löscher, M., Dick, H.B., Bartz-Schmidt, K.U., and Joachim, S.C. (2019). Retinal Organ Cultures as Alternative Research Models. Altern Lab Anim *47*, 19-29.

Schraermeyer, U., Julien, S., Biesemeier, A., Bartz-Schmidt, K.U., and Wolburg, H. (2015). A new kind of labyrinth- like capillary is responsible for leakage from human choroidal neovascular endothelium, as investigated by high-resolution electron microscopy. Graefes Arch Clin Exp Ophthalmol *253*, 681-689.

Seddon, J.M., McLeod, D.S., Bhutto, I.A., Villalonga, M.B., Silver, R.E., Wenick, A.S., Edwards, M.M., and Lutty, G.A. (2016). Histopathological Insights Into Choroidal Vascular Loss in Clinically Documented Cases of Age-Related Macular Degeneration. JAMA Ophthalmol *134*, 1272-1280.

Sekiya, A., Okano-Kosugi, H., Yamazaki, C.M.,and Koide, T. (2011). Pigment epithelium-derived

factor (PEDF) shares binding sites in collagen with heparin/heparan sulfate proteoglycans. J Biol Chem *286*, 26364-26374.

Sellés-Navarro, I., Villegas-Pérez, M.P., Salvador-Silva, M., Ruiz-Gómez, J.M., and Vidal-Sanz, M. (1996). Retinal ganglion cell death after different transient periods of pressure-induced ischemia and survival intervals. A quantitative in vivo study. Invest Ophthalmol Vis Sci *37*, 2002-2014.

Semeraro, F., Morescalchi, F., Duse, S., Gambicorti, E., Cancarini, A., and Costagliola, C. (2015). Pharmacokinetic and Pharmacodynamic Properties of Anti-VEGF Drugs After Intravitreal Injection. Curr Drug Metab *16*, 572-584.

Semkova, I., Kreppel, F., Welsandt, G., Luther, T., Kozlowski, J., Janicki, H., Kochanek, S., and Schraermeyer, U. (2002). Autologous transplantation of genetically modified iris pigment epithelial cells: a promising concept for the treatment of age-related macular degeneration and other disorders of the eye. Proc Natl Acad Sci U S A *99*, 13090–13095.

Serra, R., Coscas, F., Boulet, J.F., Cabral, D., Lupidi, M., Coscas, G.J., and Souied, E.H. (2020). PREDICTIVE ACTIVATION BIOMARKERS OF TREATMENT-NAIVE ASYMPTOMATIC CHOROIDAL NEOVASCULARIZATION IN AGE-RELATED MACULAR DEGENERATION. Retina *40*, 1224-1233.

Sharief, L., Chen, Y.H., Lightman, S., and Tomkins-Netzer, O. (2020). Prospective study of morphologic and functional parameter changes post intravitreal therapy for macular edema. Graefes Arch Clin Exp Ophthalmol *258*, 1941-1947.

Sheibani, N., Wang, S., Darjatmoko, S.R., Fisk, D.L., Shahi, P.K., Pattnaik, B.R., Sorenson, C.M., Bhowmick, R., Volpert, O.V., Albert, D.M., Melgar-Asensio, I., and Henkin, J. (2019). Novel anti-angiogenic PEDF-derived small peptides mitigate choroidal neovascularization. Exp Eye Res *188*.

Shimada, Y., Shibuya, M., and Shinoda, K. (2021). Transient Increase and Delay of Multifocal Electroretinograms Following Laser Photocoagulations for Diabetic Macular Edema. J Clin Med *10*, 357.

Sim, D.A., Keane, P.A., Zarranz-Ventura, J., Fung, S., Powner, M.B., Platteau, E., Bunce, C.V., Fruttiger, M., Patel, P.J., Tufail, A., and Egan, C.A. (2013). The effects of macular ischemia on visual acuity in diabetic retinopathy. Invest Ophthalmol Vis Sci *54*, 2353-2360.

Simó, R., Sundstrom, J.M., and Antonetti, D.A. (2014). Ocular Anti-VEGF therapy for diabetic retinopathy: the role of VEGF in the pathogenesis of diabetic retinopathy. Diabetes Care *37*, 893-899.

Smretschnig, E., Hagen, S., Glittenberg, C., Ristl, R., Krebs, I., Binder, S., and Ansari-Shahrezaei, S. (2016). Intravitreal anti-vascular endothelial growth factor combined with half-fluence photodynamic therapy for choroidal neovascularization in chronic central serous chorioretinopathy. Eye (Lond) *30*, 805-811.

Solecki, L., Loganadane, P., Gauthier, A.S., Simonin, M., Puyraveau, M., Delbosc, B., and Saleh, M. (2021). Predictive factors for exudation of quiescent choroidal neovessels detected by OCT angiography in the fellow eyes of eyes treated for a neovascular age-related macular degeneration. Eye (Lond) *35*, 644-650.

Spooner, K.L., Fraser-Bell, S., Cozzi, M., Staurenghi, G., Invernizzi, A., Monteduro, D., Munk, M.R., Hong, T., and Chang, A.A. (2020). Macular Atrophy Incidence and Progression in Eyes with Neovascular Age-Related Macular Degeneration Treated with Vascular Endothelial Growth Factor Inhibitors Using a Treat-and-Extend or a Pro Re Nata Regimen: Four-Year Results of the MANEX Study. Ophthalmology *127*, 1663-1673.

Subramanian, P., Locatelli-Hoops, S., Kenealey, J., DesJardin, J., Notari, L., and Becerra, S.P. (2013). Pigment epithelium-derived factor (PEDF) prevents retinal cell death via PEDF Receptor (PEDF-R): identification of a functional ligand binding site. J Biol Chem *288*, 23928-23942.

Sung, I.S., Park, S.Y., Jeong, K.Y., and Kim, H.M. (2019). Investigation of the preventive effect of calcium on inflammation-mediated choroidal neovascularization. Life Sci *233*.

Takeyama, M., Yoneda, M., Gosho, M., Iwaki, M., and Zako, M. (2015). Decreased VEGF-A and sustained PEDF expression in a human retinal pigment epithelium cell line cultured under hypothermia. Biol Res *30*, 48: 42.

Tan, X., Fujiu, K., Manabe, I., Nishida, J., Yamagishi, R., Nagai, R., and Yanagi, Y. (2015). Choroidal neovascularization is inhibited via an intraocular decrease of inflammatory cells in mice lacking complement component C3. Sci Rep *5*.

Tang, M., Yang, Y., Yu, J., Wu, N., Chen, P., Xu, L., Wang, Q., Xu, Z., Ge, J., and Yu, K., (2017). Zhuang J. Discordant mRNA and protein expression of CXCR4 under in vitro CoCl2-

induced hypoxic conditions. Biochem Biophys Res Commun *484*, 285-291.

Thulliez, M., Angoulvant, D., Pisella, P.J., and Bejan-Angoulvant, T. (2018). Overview of Systematic Reviews and Meta-analyses on Systemic Adverse Events Associated With Intravitreal Anti-Vascular Endothelial Growth Factor Medication Use. JAMA Ophthalmol *136*, 557-566.

Tian, S.W., Ren, Y., Pei, J.Z., Ren, B.C., and He, Y. (2017). Pigment epithelium-derived factor protects retinal ganglion cells from hypoxia-induced apoptosis by preventing mitochondrial dysfunction. Int J Ophthalmol *10*, 1046-1054.

Tombran-Tink, J., and Johnson, L.V. (1989). Neuronal differentiation of retinoblastoma cells induced by medium conditioned by human RPE cells. Invest Ophthalmol Vis Sci *30*, 1700-1707.

Toto, L., Di, Antonio, L., Costantino, O., and Mastropasqua, R. (2021). Anti-VEGF Therapy in Myopic CNV. Curr Drug Targets *28*.

Tsai, A.S.H., Jordan-Yu, J.M., Gan, A.T.L., Teo, K.Y.C., Tan, G.S.W., Lee, S.Y., Chong, V., and Cheung, C.M.G. (2021). Diabetic Macular Ischemia: Influence of Optical Coherence Tomography Angiography Parameters on Changes in Functional Outcomes Over One Year. Invest Ophthalmol Vis Sci *62*.

Tsai, T.H., Shih, S.C., Ho, T.C., Ma, H.I., Liu, M.Y., Chen, S.L., Tsao, Y.P. (2014). Pigment epithelium-derived factor 34-mer peptide prevents liver fibrosis and hepatic stellate cell activation through down-regulation of the PDGF receptor. PLoS One *9*.

Tsai, T., Mueller-Buehl, A.M., Satgunarajah, Y., Kuehn, S., Dick, H.B., and Joachim, S.C. (2020). Protective effect of the extremolytes ectoine and hydroxyectoine in a porcine organ culture. Graefes Arch Clin Exp Ophthalmol *258*, 2185-2203.

Udono, T., Takahashi, K., Nakayama, M., Yoshinoya, A., Totsune, K., Murakami, O., Durlu, Y.K., Tamai, M., and Shibahara, S. (2001). Induction of adrenomedullin by hypoxia in cultured retinal pigment epithelial cells. Invest Ophthalmol Vis Sci *42*, 1080-1086.

Ueda, S., Yamagishi, S., Matsui, T., Jinnouchi, Y., and Imaizumi, T. (2011). Administration of pigment epithelium-derived factor inhibits left ventricular remodeling and improves cardiac function in rats with acute myocardial infarction. Am J Pathol *178*, 591-598.

Unterlauft, J.D., Claudepierre, T., Schmidt, M., Müller, K., Yafai, Y., Wiedemann, P., Reichenbach,

A., and Eichler, W. (2014). Enhanced survival of retinal ganglion cells is mediated by Müller glial cell-derived PEDF. Exp Eye Res *127*, 206-214.

Unterlauft, J.D., Eichler, W., Kuhne, K., Yang, X.M., Yafai, Y., Wiedemann, P., Reichenbach, A., and Claudepierre, T. (2012). Pigment epithelium-derived factor released by Müller glial cells exerts neuroprotective effects on retinal ganglion cells. Neurochem Res *37*, 1524-1533.

Valiente-Soriano, F.J., Di Pierdomenico, J., García-Ayuso, D., Ortín-Martínez, A., Miralles, de Imperial-Ollero, J.A., Gallego-Ortega, A., Jiménez-López, M., Villegas-Pérez, M.P., Becerra, S.P., and Vidal-Sanz, M. (2020). Pigment Epithelium-Derived Factor (PEDF) Fragments Prevent Mouse Cone Photoreceptor Cell Loss Induced by Focal Phototoxicity In Vivo. Int J Mol Sci *21*.

Vestergaard, N., Cehofski, L.J., Honoré, B., Aasbjerg, K., and Vorum, H. (2019). Animal Models Used to Simulate Retinal Artery Occlusion: A Comprehensive Review. Transl Vis Sci Technol *8*.

Viheriälä, T., Sorvari, J., Ihalainen, T.O., Mörö, A., Grönroos, P., Schlie-Wolter, S., Chichkov, B., Skottman, H., Nymark, S., and Ilmarinen, T. (2021). Culture surface protein coatings affect the barrier properties and calcium signalling of hESC-RPE. Sci Rep *11*.

Volpert, O.V., Zaichuk, T., Zhou, W., Reiher, F., Ferguson, T.A., Stuart, P.M., Amin, M., and Bouck, N.P. (2002). Inducer-stimulated Fas targets activated endothelium for destruction by anti-angiogenic thrombospondin-1 and pigment epithelium-derived factor. Nat Med *8*, 349-357.

Wang, F.H., Sun, X.D., Zhang, X., Xu, X., Zhu, Q., Huang, J.N., Fan, Y., Gu, Q., and Liu, H.Y. (2007). Role of pigment epithelium-derived factor on proliferation and migration of choroidal capillary endothelium induced by vascular endothelial growth factor in vitro. Chin Med J (Engl) *120*, 1534-1538.

Wang, J.J., Zhang, S.X., Lu, K., Chen, Y., Mott, R., Sato, S., and Ma, J.X. (2005). Decreased expression of pigment epithelium-derived factor is involved in the pathogenesis of diabetic nephropathy. Diabetes *54*, 243-250.

Wang, J.J., Zhang, S.X., Mott, R., Knapp, R.R., Cao, W., Lau, K., and Ma, J.X. (2006). Salutary effect of pigment epithelium-derived factor in diabetic nephropathy: evidence for antifibrogenic activities. Diabetes *55*, 1678-1685.

Wang, X., Liu, X., Ren, Y., Liu, Y., Han, S., Zhao, J., Gou, X., and He, Y. (2019). PEDF protects

human retinal pigment epithelial cells against oxidative stress via upregulation of UCP2 expression. Mol Med Rep *19*, 59-74.

Wang, Y., Subramanian, P., Shen, D., Tuo, J., Becerra, S.P., and Chan, C.C. (2013). Pigment epithelium-derived factor reduces apoptosis and pro-inflammatory cytokine gene expression in a murine model of focal retinal degeneration. ASN Neuro *5*.

Weinstein, O., Abu, Tailakh, M., Lifshitz, T., Novack, V., and Levy, J. (2020). Intravitreal bevacizumab treatment for neovascular age-related macular degeneration and thromboembolic events. Eur J Ophthalmol *30*, 66-71.

Wen, X., Yuan, M., Li, C., Zeng, J., Duan, F., Lou, B., Yang, Y., Qian, X., and Lin, X. (2019). Effect of vitrectomy with intrasurgical regulation of intraocular pressure in a rabbit model of central retinal artery occlusion. Exp Eye Res *189*.

Yang, Y., Liu, F., Tang, M., Yuan, M., Hu, A., Zhan, Z., Li, Z., Li, J., Ding, X., and Lu, L. (2016). Macrophage polarization in experimental and clinical choroidal neovascularization. Sci Rep *6*.

Yu, Y.J., Mo, B., Liu, L., Yue, Y.K., Yue, C.L., and Liu, W. (2016). Inhibition of choroidal neovascularization by lentivirus-mediated PEDF gene transfer in rats. Int J Ophthalmol *9*, 1112-1120.

Zarubina, A.V., Gal-Or, O., Huisingh, C.E., Owsley, C., and Freund, K.B. (2017). Macular Atrophy Development and Subretinal Drusenoid Deposits in Anti-Vascular Endothelial Growth Factor Treated Age-Related Macular Degeneration. Invest Ophthalmol Vis Sci *58*, 6038-6045.

Zhang, S.X., Wang, J.J., Gao, G., Parke, K., and Ma, J.X. (2006). Pigment epithelium-derived factor downregulates vascular endothelial growth factor (VEGF) expression and inibits VEGF-VEGF receptor 2 binding in diabetic retinopathy. J Mol Endocrinol *37*, 1-12.

Zhao, X., Gao, M., Liang, J., Chen, Y., Wang, Y., Wang, Y., Xiao, Y., Zhao, Z., Wan, X., Jiang, M., Luo, X., Wang, F., and Sun, X. (2021). SLC7A11 Reduces Laser-Induced Choroidal Neovascularization by Inhibiting RPE Ferroptosis and VEGF Production. Front Cell Dev Biol *9*.

11 Acknowledgements

It is my great pleasure to have the opportunity to study and do research in the Division of Experimental Vitreoretinal Surgery, Center for Ophthalmology, University of Tuebingen, Germany. I would like to express my gratitude to everyone who has given me help and support during my study here.

First of all, I would like to express my deepest appreciation to my supervisor, Prof. Dr. rer. nat. Ulrich Schraermeyer for giving me the opportunity to work on the project, providing excellent working conditions, giving me guidance kindly, sharing his ideas openly, supervising me through all the time of the research and writing of this thesis. His valuable guidance helped me immensely in my research work. I also would like to thank PD Dr. Sylvie Julien-Schraermeyer, who planned the project and gave many valuable suggestions and help as well.

I am especially grateful to Dr. rer. nat. Alexander Tschulakow for his valuable help in this research work, his suggestions and timely feedback. He is also my wonderful colleague. Special thanks to Antonina Burda for her technical assistance and lab work assistance.

Special thanks should be given to Judith Birch for her excellent organizational skills, and for improving my grammar as a native English speaker. Thanks to Dr. rer. nat. Tatjana Taubitz, Dr. rer. nat. Antje Biesemeier and Dr. rer. nat. Barbara Illing for their useful advice and giving me the benefit of their experimental skills. Thanks to Liu Shan for her shared experimental experience and valuable suggestions.

Finally, I sincerely thank my parents. They have supported my entire academic career, encouraging me to keep moving forward, giving me all their help, encouragement and spiritual support. Without the hard work of my parents, there would not be the results I have achieved today.

12 Contributions

During my PhD study, I contributed to 2 studies. My detailed contributions to each study are below.

1. **The *in vivo* CNV project**

   Personal contribution: This study represents one of the main experiments I did during my PhD and the details are described in this thesis. I performed the main experiments (i.e. embedding the rat eyes by paraffin, preparing and cutting the sections and finding the induced CNV, performing immunohistochemical staining for each anti-body and taking photos, Picrosirius Red Staining and analysis of mature and immature collagen in the induced CNV) and the data analysis. Dr. Tschulakow Alexander performed the animal anesthesia and sacrifice, and I helped as an assistant. I took photos of the retinal fluorescein angiography (FA) and indocyanine green angiography (ICG) under the help of Dr. Tschulakow Alexander. PD Dr. Sylvie Julien-Schraermeyer and Dr. Tschulakow Alexander enucleated the rat eyes. The idea of the project was provided by my supervisor (Ulrich Schraermeyer). For this study, my supervisor (Ulrich Schraermeyer) helped to induce the CNV rat model by subretinal injection of AAV.VEGF^{165} vector, and intravitreal treatment. PD Dr. Sylvie Julien-Schraermeyer helped to organize the experiment. The electron microscopy experiment was performed with support from Antonina Burda.

2. **The *ex vivo* ischemic eye model project**

   Personal contribution: The idea of *ex vivo* ischemic eye model came from Professor Ulrich Schraermeyer. Both Dr. Tschulakow Alexander and me examined the intravitreal oxygen saturation in the living rats and the incubated eyes. I performed the experiments (i.e. intravitreal injection, embedding the rat eyes by paraffin, preparing and cutting the sections, performing immunohistochemical staining for each anti-body and taking photos, TUNEL staining and analysis) and the data analysis. Dr. Tschulakow Alexander sacrificed the rats. The electron microscopy of the *ex vivo* experiments were performed and alalyzed by Marina Tikhonovich and Dr. Antje K Biesemeier.